AD_____

Award Number:

W81XWH-06-1-0289

TITLE:

Scavenger Receptors and Resistance to Inhaled Allergens

PRINCIPAL INVESTIGATOR:

Lester Kobzik, M.D.

CONTRACTING ORGANIZATION:

Harvard School of Public Health

Boston, MA 02115

REPORT DATE:

February 2010

TYPE OF REPORT:

Final

PREPARED FOR: U.S. Army Medical Research and Materiel Command
Fort Detrick, Maryland 21702-5012

DISTRIBUTION STATEMENT:

XX Approved for public release; distribution unlimited

REPORT DOCUMENTATION PAGE

Form Approved
OMB No. 0704-0188

1. REPORT DATE *(DD-MM-YYYY)*	**2. REPORT TYPE**	**3. DATES COVERED** *(From - To)*
01-02-2010	Final	17 JAN 2006 - 16 JAN 2010

4. TITLE AND SUBTITLE
Scavenger Receptors and Resistance to Inhaled Allergens

5a. CONTRACT NUMBER

5b. GRANT NUMBER
W81XWH-06-1-0289

5c. PROGRAM ELEMENT NUMBER

6. AUTHOR(S)
Lester Kobzik

email: lkobzik@hsph.harvard.edu

5d. PROJECT NUMBER

5e. TASK NUMBER

5f. WORK UNIT NUMBER

7. PERFORMING ORGANIZATION NAME(S) AND ADDRESS(ES)

Harvard School of Public
Health
.
Boston, MA 02115

8. PERFORMING ORGANIZATION REPORT NUMBER

9. SPONSORING / MONITORING AGENCY NAME(S) AND ADDRESS(ES)
U.S. Army Medical Research
and Material Command Fort Detrich, MD 21702

10. SPONSOR/MONITOR'S ACRONYM(S)

11. SPONSOR/MONITOR'S REPORT NUMBER(S)

12. DISTRIBUTION / AVAILABILITY STATEMENT

Approved for public release; distribution unlimited

13. SUPPLEMENTARY NOTES

14. ABSTRACT
Our central hypothesis was that lung macrophage scavenger receptors normally function to bind and clear inhaled allergens and pathogens, thereby preventing allergic responses and infections. The purpose of the project was to determine whether 1) decreased levels of SRAs (mediated by environmental stresses) increase susceptibility to asthma; and 2) modulating levels of scavenger receptors will affect resistance to asthma. The results indicate that scavenger receptors modulate the allergic response, primarily by modifying dendritic cell trafficking to thoracic lymph nodes in the setting of asthma. Dendritic cells deficient in the scavenger receptors SRA I/II or MARCO traveled to the lymph nodes faster, and generated a more robust asthmatic response when allergen was delivered into the lungs. Scavenger receptors are linked to oxidant air pollution responses in a complex manner. Oxidant air pollution increases expression of MARCO which serves to scavenge oxidized pro-inflammatory lipids, thereby dampening, but not eradicating, acute inflammatory responses.

15. SUBJECT TERMS
asthma, allergy, scavenger receptors, dendritic cells

16. SECURITY CLASSIFICATION OF:			**17. LIMITATION OF ABSTRACT**	**18. NUMBER OF PAGES**	**19a. NAME OF RESPONSIBLE PERSON**
a. REPORT	**b. ABSTRACT**	**c. THIS PAGE**			USAMRMC
U	U	U	UU	50	**19b. TELEPHONE NUMBER** *(include area code)*

Table of Contents

INTRODUCTION:

Our central hypothesis is that lung macrophage scavenger receptors normally function to bind and clear inhaled allergens and pathogens, thereby preventing allergic responses and infections. The purpose of the project is to determine whether 1) decreased levels of SRAs (mediated by environmental stresses) increase susceptibility to asthma or pneumonia; and 2) therapy to increase or maintain normal levels of scavenger receptors will increase resistance to asthma and pneumonia. The scope of the research includes studies using in vivo mouse models (Aim 1), studies of the specific role of alveolar macrophages (Aim 2) and dendritic cells (Aim 3) and studies of the effects of pollutants on scavenger receptors (Aim 4).

BODY:

Task 1: Determine susceptibility of SRA 'knockout' (KO) mice to asthma.

In this work we report that the class A scavenger receptors (SRAs) MARCO and SR-AI/II are expressed on lung macrophages (MΦ) and dendritic cells (DC) and function in innate defenses against inhaled pathogens and particles. Increased expression of SRAs in the lungs of mice in an OVA-asthma model suggested an additional role in modulating responses to inhaled allergen. After OVA sensitization and aerosol challenge, SR-AI/II and MARCO-deficient mice exhibited greater eosinophilic airway inflammation and airway hyperresponsiveness compared to wild-type mice. A role for simple SRA-mediated antigen clearance ('scavenging') by lung macrophages was excluded by observation of comparable uptake of fluorescent OVA by wild-type and SRA-deficient lung MΦs and DCs. In contrast, airway instillation of fluorescent antigen revealed significantly higher traffic of labelled DCs to thoracic lymph nodes in SRA-deficient mice than in controls. The increased migration of SRA-deficient DCs was accompanied by enhanced proliferation in thoracic lymph nodes of adoptively transferred OVA-specific T cells after airway OVA challenge. The data identify a novel role for SRAs expressed on lung DCs in down-regulation of specific immune responses to aero-allergens by reduction of DC migration from the site of antigen uptake to the draining lymph nodes. This studied is detailed in the publication which is Appendix 1.

Task 2: Determine role of SRAs on DCs in responses to inhaled allergen:

This work sought to test the hypothesis that DC SRAs act to down-regulate allergic immune responses. While we made good progress in some areas, we must also report some disappointing results in other areas, despite considerable effort.

To study dendritic cells, we learned and optimized in vitro culture protocols to grow bone-marrow derived dendritic cells from both wild-type and SRA knockout mice. This produces a large number of cells suitable for easy analysis of phenotype and function.

We have confirmed purity of the cultured dendritic cells by immunolabeling with CD11c marker (>95% +).

Initial results with functional assays to compare DCs from wild-type and knockout mice were promising, as indicated in an earlier annual report. However, as we repeated and expanded these analyses, we have consistently observed an absence of significant differences in the wild-type vs. knockout groups. For example, to test whether scavenger receptors reduce cell motility (as observed in vivo as increased DC accumulation in lymph nodes in our asthma model), we have developed microscopic and live cell imaging assays to quantitate cell movement. The first assay uses modified Boyden migration chambers and results in counting of cells that move from an upper chamber to the lower chamber. The second assay measures random migration by tracing cell movement over 12-24 hours in a live cell system. The details of these assays and the results are presented next, followed by conclusions and discussion.

Dendritic cell isolation and differentiation:
Bone marrow progenitor cells were isolated from normal female wild-type or MARCO$^{-/-}$ adult (8-12 wk) Balb/c mice and cultured in 6-well tissue culture plates at 3e6/well in RPMI-10 (RPMI 1640 + 10% FBS + 1 mM l-glutamine + penicillin/streptomycin) with 20 ng/ml rGM-CSF (Peprotech) at 37° C, 5% CO_2. Media was changed every 2-3 d without disturbing the cells for 7 d. For motility and chemotaxis assays, on day 7-8 of culture, immature DC were replenished with media with or without maturation for 24 h using 1 µg/ml LPS, then harvested by pipetting and replated in assay dishes or wells. For surface receptor expression assays, immature cells were removed from plates by pipetting, replated in fresh media in low-adherence tissue culture dishes, and matured for 24-48 h with 20 ng/ml TNFα or 1 µg/ml LPS; cells were then removed by pipetting and stained for flow cytometry.

Random motility assay:
Immature and mature DC were harvested on day 8-9 of culture as indicated and stained with Hoescht (Molecular Probes) in normal saline + 10 mM HEPES + 0.5% BSA for 5 min at 37° C. Cells were then washed and adhered to glass-bottom tissue culture plates (MatTek) coated with 50 µg/ml fibronectin (Sigma) for 4 h at 37° C, 5% CO_2 in RPMI-10 + 10 mM HEPES + 20 ng/ml rGM-CSF. Cells were then imaged at 5 min intervals for 16 h using a Nikon confocal microscope fitted with an environmental chamber at 37° C. Cell tracks were generated by tracking nuclei positions using the MTrackJ plugin (Erik Meijering, University Medical Center, Rotterdam, Netherlands) for ImageJ (NIH). Graphs and analysis were performed using the Chemotaxis Tool plugin (Ibid) for ImageJ.

Chemotaxis:
Immature and mature DC were harvested on day 8-9 of culture as indicated and resuspended in RPMI-10 at 1e7/ml, then 100 µl cell suspension was placed into the top well of 8 µm pore transwells (BD Falcon) in 24-well tissue culture plates (BD Falcon) containing 0.5 ml RPMI-10 ± 0.1-100 nM CCL21, 50 ng/ml MIP-1α, or 100 ng/ml MCP-1 (all chemokines obtained from Peprotech) in triplicate wells per condition. Cells were allowed to migrate for 4 h at 37° C, 5% CO_2; transwells were then removed and cells

that had migrated to the lower well were harvested using 2 mM EDTA. Migrated cells were counted using flow cytometric cell counting, and percent migrated cells was determined for each well using cell counts obtained from parallel wells containing cells without the transwell inserts. Chemotactic indices were calculated by normalizing all data relative to the percentage of migrated cells (matched type and maturation state) in wells with no chemokine.

Results:

No significant differences were observed in DC migration, either in random movement in the absence of stimulation or in chemotaxis in response to CCL21 or MIP-1α. This suggests that MARCO does not act as a molecular “brake” on DC movement from the lung to the lymph nodes.

A

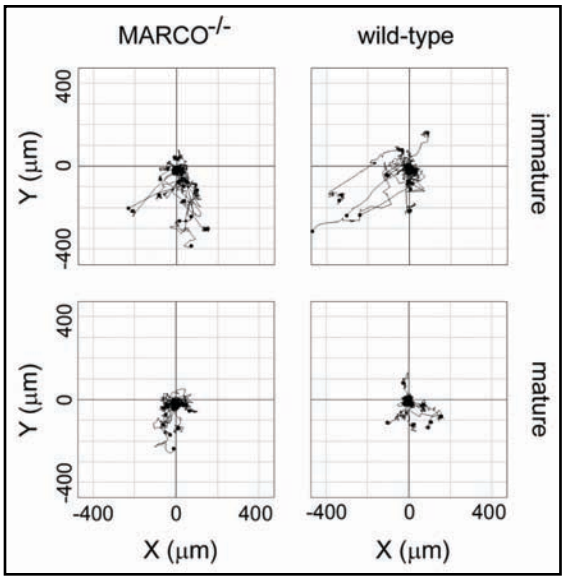

Figure 1: Random migration by BMD-DC. Bone marrow progenitor cells were isolated from normal adult Balb/c mice and cultured in RPMI-10 with rGM-CSF. Cells were cultured 7-8 d, matured for 24 h with LPS, and then labeled with Hoescht and plated on fibronectin-coated, glass-bottom dishes. Cell movement was tracked for 16 h by tracing nuclei using time-lapse microscopy. Data were analyzed using ImageJ. Representative data from n = 4 experiments. A, Cell tracks over time. B, Total distance traveled. C,

B

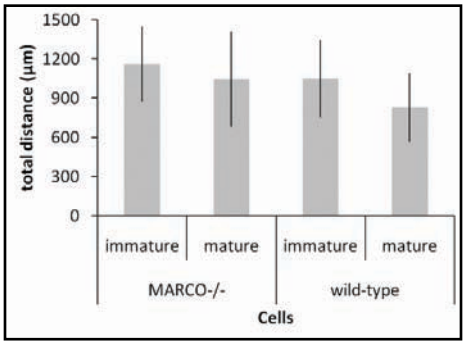

C

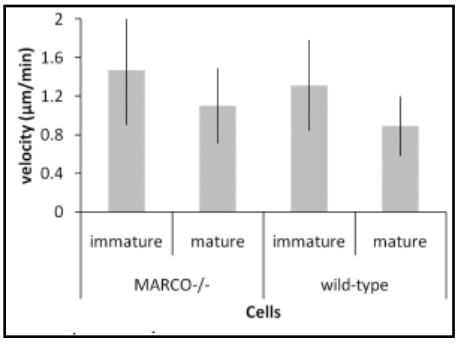

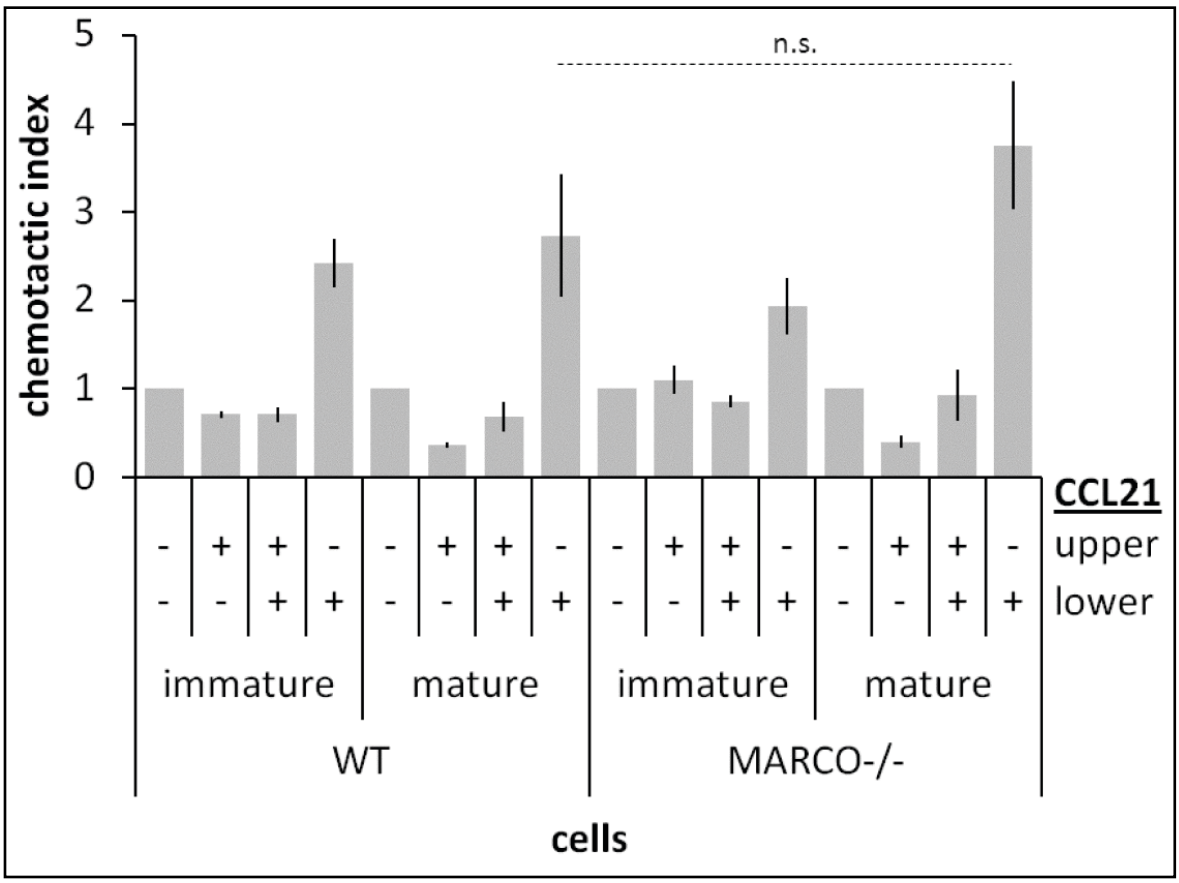

Figure 2: Chemotaxis by BMD-DC. Bone marrow progenitor cells were isolated from normal adult Balb/c mice and cultured in RPMI-10 with rGM-CSF. Cells were cultured 7-8 d, matured for 24 h with LPS, then placed in the upper well of 8 μm transwells with (+) or without (-) 100 nM CCL21 in the upper and lower wells as indicated, and allowed to migrate for 4 h at 37° C. Transwells were then removed and cells that had migrated to the lower well were harvested and counted using flow cytometric cell counting. The percent migrated cells were determined using cell counts obtained from parallel wells containing cells without the transwell inserts, and chemotactic indices were calculated by normalizing all data relative to the percentage of migrated cells in wells with no chemokine. Cumulative data are mean ± standard error of n = 8 experiments. All values obtained from wells with CCL21 in the lower well only were significant compared to wells with no chemokine. N.S., not significant ($p > 0.3$).

We hypothesized that MARCO alters DC migration by affecting DC motility, DC maturation, or both. In parallel to the evaluation of migration, results of which reported above, we examined the effects of MARCO on DC maturation in response to two maturation stimuli, TNFα and LPS, using flow cytometry to measure changes in surface marker expression prior to and following maturation caused by these agents.

Although surface expression of key DC maturation markers (CD80, CD86, MHC-II), adhesion molecules (CD11b, CD11c, CD54), and antigen presentation/costimulation

proteins (CD40, CD80, CD86, MHC-I, MHC-II) was increased in LPS- and TNFα-matured DC, no significant differences were observed in their expression on MARCO$^{-/-}$ versus wild-type DC. We next report the methods used and the results of these studies.

Cell surface receptor expression by flow cytometry:

Immature or mature DC were harvested on day 9 of culture, resuspended in Facs Buffer (PBS + 10 mM HEPES + 2 mM EDTA + 0.5% BSA), and stained for surface markers using specific labeled antibodies against CD11c, CD11b, CD19, CD40, CD54, CD80, CD83, CD86, MARCO, MHC-I, and MHC-II, or isotype controls (all antibodies obtained from eBioscience). Cells were then washed, fixed, and cellular fluorescence measured using a FACSCalibur flow cytometer (BD Biosciences). Data were analyzed using FlowJo software (TreeStar).

24h LPS

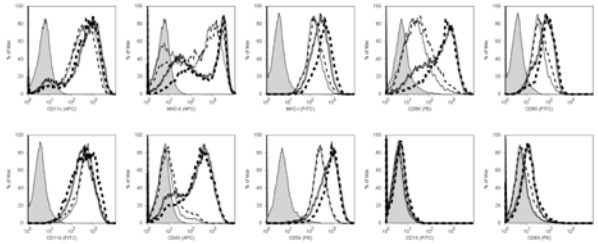

24h TNFα

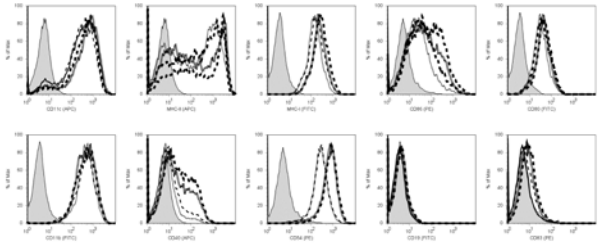

48h LPS

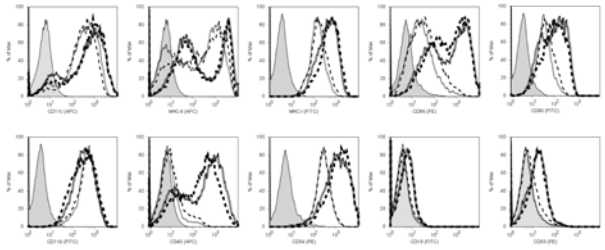

48h TNF

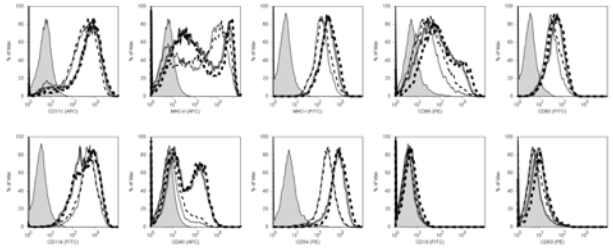

Figure 3: Surface receptor expression by BMD-DC. Bone marrow progenitor cells were isolated from normal adult Balb/c mice and cultured in RPMI-10 with rGM-CSF. Cells were cultured 7 d, matured for 24-48 h with TNFα or LPS, and then stained for surface markers using specific labeled antibodies against CD11c, MHC-II, MHC-I, CD86, CD80, CD11b, CD40, CD54, CD19, CD83, or isotype controls. Representative data from n = 4 experiments. Shaded line, isotype staining of BMD-DC. Thin dotted or dashed lines, immature cells. Thick dotted or dashed lines, LPS- or TNFα-matured cells. Dotted lines, MARCO$^{-/-}$ DC. Dashed lines, wild-type DC.

In vivo component of task 2-4. We made reasonable progress in a number of experimental areas related to the in vivo components of tasks 2-4. First, we have established effective adoptive transfer protocols using either primary DCs harvested from spleen or bone-marrow derived DCs. These protocols show clear acquisition of asthma susceptibility in otherwise normal recipients of DCs harvested from 'asthmatic' donor mice, but not from normal non-asthmatic DCs. The development of these protocols is a key step, especially the ability to cause increased asthma susceptibility using bone-marrow derived DCs. The latter allows us to more easily prepare the large number of DCs from wild-type and knockout mice needed for the adoptive transfer into sufficient replicate animals. A second area of good progress has been in the analysis of environmental exposures on airway responses and the role of MARCO and SRA in this response (Task 4). We have begun the LPS exposures with promising results, and have also observed relevant differences in responses to oxidant air pollutant exposure in MARCO/SRA knockout mice exposed to ozone. These methods and results are presented next.

Adoptive Transfer of Primary DCs

We used magnetic beads (Miltenyi) to isolate splenic DCs from female mice sensitized with OVA and aerosol challenged (asthmatic) or normal controls. The purified CD11c+ DCs were injected i.p. (2 X 10^5) into normal non-allergic mice. The next day, recipient mice were then subjected to the 'intentionally suboptimal' protocol using OVA (single ip injection rather than two, followed by 3 days of aerosol challenge 10 days after injection). As shown in Fig 4, the main finding is that an asthma phenotype developed after the adoptive transfer of DCs purified from 'asthma-susceptible' mice, but not after adoptive transfer of DCs from normal pups. Important negative controls include lack of effect by injection of splenic CD4+ T cells, macrophages or other cells that flow through the isolation column (Figure 4C).

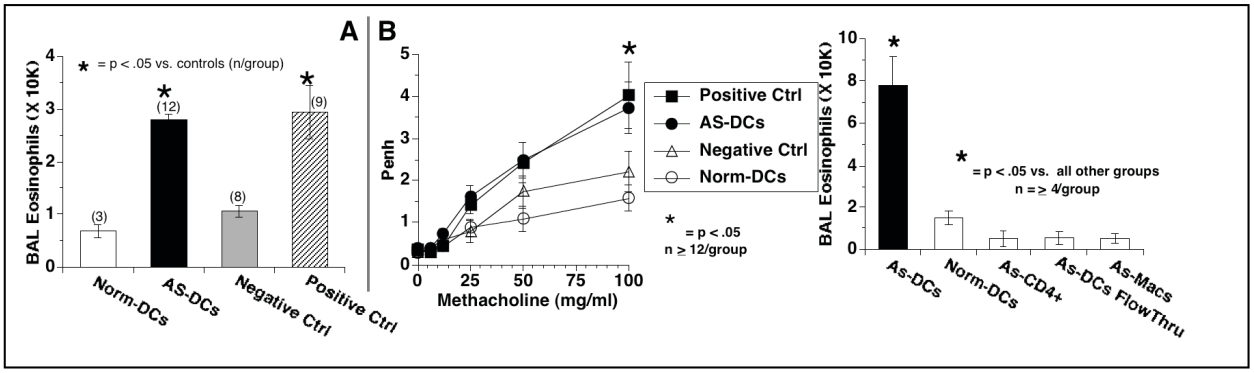

Figure 4: Adoptive transfer of DCs. Normal mice received splenic CD11c+ DCs from asthmatic (AS-DCs) or normal (Norm-DCs) donors, followed by an 'intentionally suboptimal' protocol. Recipients of AS-DCs, but not Norm-DCs, showed allergic inflammation (A) and Penh responses (B) comparable to the positive control (standard OVA sensitization). Adoptive transfer of other splenocytes or flow-through non-DC cells

had minimal effect (C).

Immunophenotyping of DCs. To evaluate the surface expression of MHC-II and relevant co-stimulatory molecules and subpopulation markers in the DCs from two groups, flow cytometric analysis was performed using a FACSCanto II (Beckton-Dickinson) flow cytometer with dedicated data acquisition system and software for analysis. Labelling was performed at 4 ^{0}C for 40 minutes, in presence of 20% normal mouse serum to block non-specific binding. Concentration of labelling antibody depended on the manufacturer's instructions (Miltenyi Biotec, Auburn, CA; or eBioscience, San Diego, CA). Specificity of labeling was verified using isotype controls.We found no significant differences in surface expression of these markers: both for NoBa and AsBa the CD11c+ cells were about 95 % positive for MHC-II, 83% positive for CD86 and 25% positive for CD8a. A summary of these data is shown in Figure 5.

Figure 5

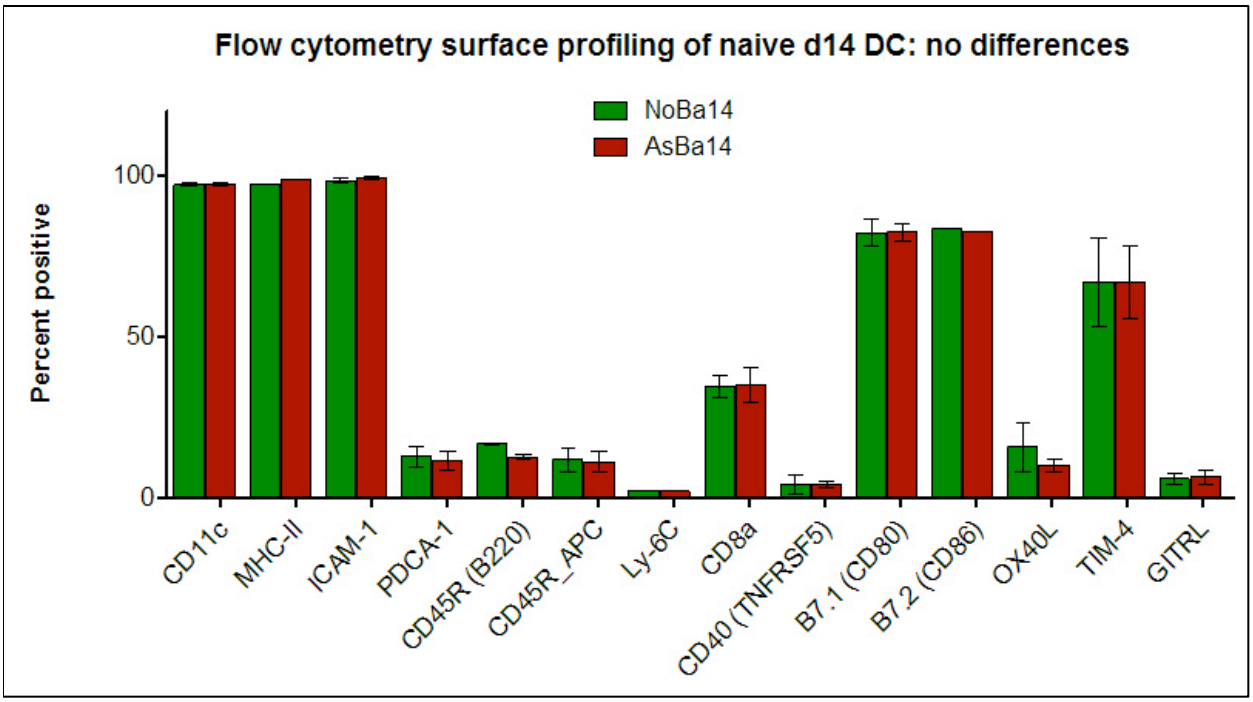

Adoptive Transfer of Cultured DCs.

To facilitate adoptive transfer of DCs from SRA knockout mice, we sought to develop a source from bone-marrow derived DCs. Moreover, since cytokine skewing of DC towards Th1- versus Th2-inducing DC (DC1 and DC2, respectively) has been studied by many laboratories, we also investigated this protocol to increase our chances of testing the influence of SRA receptors in a DC2 type population.

Dendritic cell isolation and differentiation:
We followed a protocol designed to produce DC0, DC1, and DC2 subtypes of DCs. Bone marrow progenitor cells were isolated from normal adult (8-12 wk) Balb/c mice and cultured in 6-well tissue culture plates at 3e6/well in RPMI-10 (RPMI 1640 + 10%

FBS + 1 mM l-glutamine + penicillin/streptomycin) with 20 ng/ml rGM-CSF + 20 ng/ml rIL-3 (Peprotech) at 37° C, 5% CO_2. To these cultures were added no cytokines (DC0), 20 ng/ml IFNγ + 20 U/ml rIL-12 (DC1), or 20 ng/ml rIL-4 (DC2). Media was changed every 2 d without disturbing the cells. On day 4 of culture, loosely adherent cells were removed by pipetting, washed twice in PBS, and counted. DC were resuspended in PBS at 2e6 live cells/ml (by trypan blue exclusion), where dead cells typically constituted less than 20% of total cells. DC were adoptively transferred to normal P4 Balb/c pups by i.p. injection of 100 µl cells (2e5 DC). Remaining DC were resuspended in Facs Buffer (PBS + 10 mM HEPES + 2 mM EDTA + 0.5% BSA) and stained for surface markers using specific labeled antibodies against CD11c, CD11b, CD40, CD80, CD86, MHC-I, and MHC-II, or isotype controls (all antibodies obtained from eBioscience).

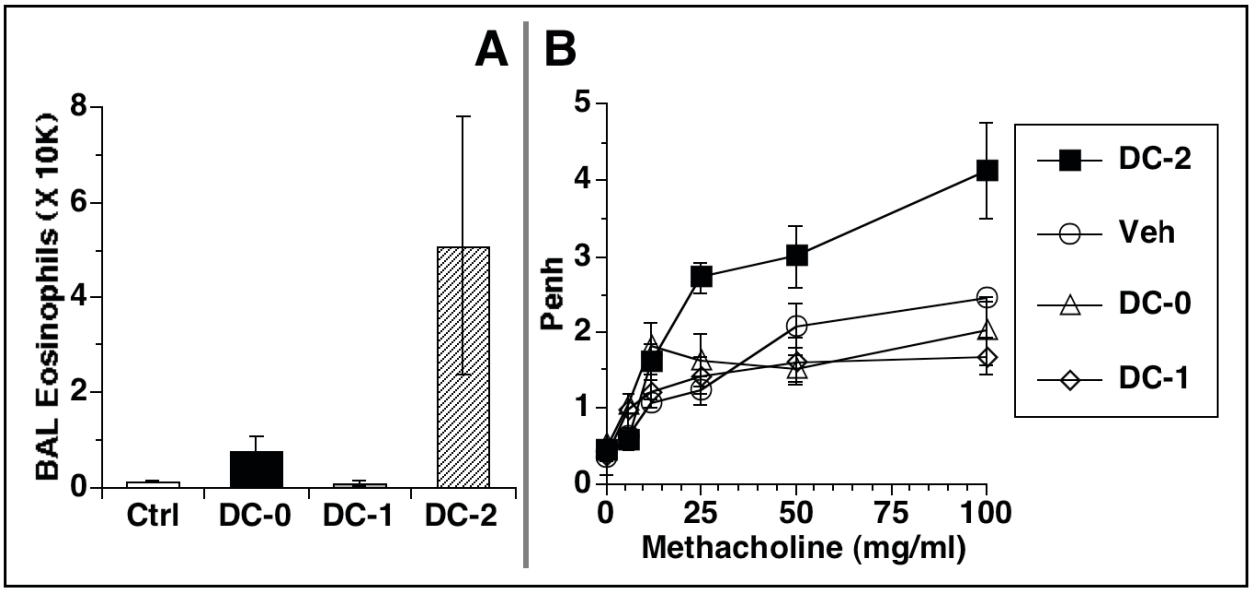

Figure 6: Adoptive transfer of in vitro bone marrow-derived dendritic cells. Normal mice received DCs differentiated to favor DC0, DC1 or DC2 phenotypes, and were subjected to the 'intentionally suboptimal' protocol. Recipients of DC2, but not DC0 or DC1 cells, showed enhanced AI (A) and Penh responses (B), consistent with re-creation of the 'asthma-susceptible' DC phenotype.

Gene expression and Epigenomic profiling of asthma-susceptible vs normal DCs. To determine if pro-allergic DCs were linked to increased expression of SRAs and other related genes, we performed microarray analysis of total cell RNA isolated from asthma-susceptible or control DCs. Repeated trials using two different platforms (Illumina, Affymetrix) did not reveal any substantial or reproducible changes. Most fold-changes for genes were small e.g (1.3X) and the list of genes showing these small differences (~20-200 depending on stringency) was completely different in the datasets produced by the two platforms. (data not shown). We concluded that there was no difference in expression and that the small differences observed were 'noise'.

To determine if epigenetic differences in regulation of genes could contribute to the different phenotype of the pro-asthmatic vs. normal DCs. we conducted genome-wide DNA methylation analysis.

Epigenome-wide DNA methylation scanning was performed by Switchgear Genomics (Menlo Park, CA). This method exploits sensitivity to restriction endonucleases conferred by the absence of methylation on cytosine residues. A cocktail of methylation-sensitive nucleases (with 99.9% efficiency and specificity fo unmethylated DNA) is used to digest half of each genomic DNA sample, prior to differential fluorescent labeling (Cy3 green for the treated sample; Cy5 red for the untreated). Competitive hybridization is performed onto tiled arrays that cover the human genome, resulting in changes in the ratio of fluorescence depending on methylation-driven nuclease sensitivity. (Decreased methylation leads to increased binding of the red-labeled fragments). The competitive hybridization uses a 400,000 oligo probe array which measures methylation status at ~42,000 unique regions in the mouse genome; 92% of the ~22,000 predicted CpG islands are covered, and 20,000 additional CpG-rich regions that are not annotated as CpG islands are also covered. The array includes 1,000 negative control regions (absent of CpGs) to build an error model for analysis.

For epigenomic data, the Switchgear Genomics company provides a normalized data matrix containing zscores. The data transformation was done as follows. The log2 ratio (untreated-cy5/treated-cy3) was calculated for each probe. The sample treatment decreases the signal from unmethylated DNA but does not change the signal from methylated DNA. Therefore a large ratio means the target is unmethylated in the sample whereas a log2 ratio of 0 means the target is methylated. The median log2 ratio of the negative control probes was subtracted from the experimental and control ratios to center the data. The data were then smoothed by averaging across a sliding window of 3 neighboring probes shifting 1 probe at a time. This helps to minimize noise from single probes. The negative control probes (designed to regions that are not affected by the treatment) serve as a background distribution to assign a confidence limit to each experimental probe. The mean and standard deviation were calculated from the negative control probes for each sample. These statistical measures were then used to calculate a z-score for each experimental probe within that experiment. The z-score was calculated as: [(exp log2 ratio)-(mean log2 ratio of negs)] / (stdev log2 ratio of negs). This statistical measure takes into account and normalizes for the variation in each individual sample, thus making comparisons between samples more reliable. Each z-score measure is the number of stdev units from the mean of the negative control distribution. Based on the area under the curve of a standard distribution, a z-score of 1.6 means that there is 95% chance that the measurement lies outside of the negative control distribution and therefore is unmethylated.

Expression or methylation data values from experimental groups were further compared in TM4 package via several high-level methods, including Significance Analysis for Microarrays (SAM) and/or Analysis of Variance (ANOVA). SAM is initially performed at false discovery rate (FDR) rate of 0% for maximum stringency; p-value stringency for ANOVA-based comparisons will include several levels (e.g. 0.05, 0.01, 0.005) depending on the size of the output list of sites and the desired flexibility of downstream functional enrichment analysis. Additionally cluster analysis (hierarchical

clustering, HCL) was performed to identify interrelated traits of expression or methylation changes across the groups.

Entire outputs and raw data of the DNA methylation arrays are publicly available as NCBI's Gene Expression Omnibus (GEO) database record # GSE13380, which includes information on approximately 450,000 50-mer probes. This is the first submission of such genome-wide methylation data to our knowledge.

Genomic DNA from the pro-asthmatic vs. normal DCs showed remarkable differences in the degree of methylation at a number of CpG sites throughout the genome, including both annotated CpG islands and other locations. These findings are illustrated in Figure 7, which shows a subset of a larger hierarchical clustering data set, presented as a heatmap comparing the methylation status of DC DNA from pro-asthmatic vs. normal DCs. Panel 7B (right) illustrates the fold difference in normalized fluorescence of the top 40 di ferentially methylated sites.

Figure 7:

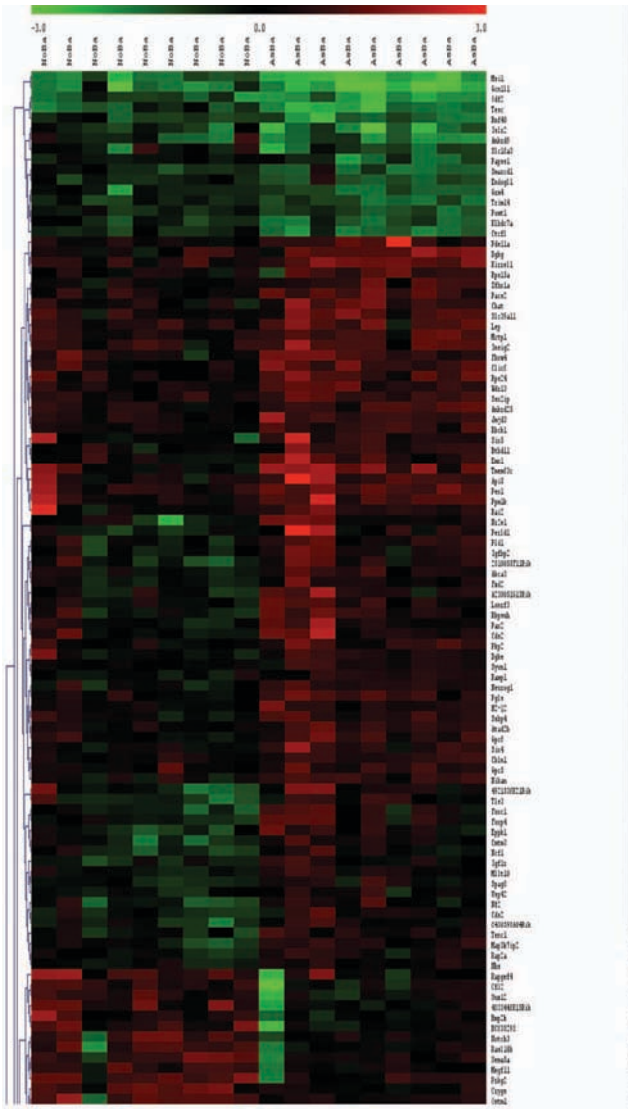

REGION	CLOSEST REFSEQ GENE	Fold	Raw p value
chr1:141238365-141239162	Zbtb41	716.7	0.003
chr4:119784314-119785823	Foxo6	204.1	0.006
chr17:56121704-56122067	Ptprs	154.0	0.008
chr6:99485789-99487833	Eif4e3	130.6	0.006
chr4:55553276-55554728	Klf4	122.4	0.009
chr4:150838544-150840848	Phf13	62.6	0.010
chr11:43524990-43526412	Ttc1	54.9	0.009
chr15:82999482-83000160	Cyb5r3	47.9	0.002
chr16:18040701-18041827	Rtn4r	42.6	0.007
chr4:44254201-44255665	Rnf38	32.7	0.002
chr14:29847853-29848653	Gnl3	32.1	0.005
chr12:25161036-25161826	Grhl1	30.9	0.007
chr11:102111951-102113537	Atxn7l3	28.5	0.007
chr7:25104070-25104898	Lipe	27.8	0.002
chr9:71909183-71910831	Tcf12	26.8	0.006
chr5:20566978-20568275	Ptpn12	25.0	0.007
chr1:71585915-71586639	Fn1	23.5	0.002
chr10:94845090-94846749	Socs2	22.3	0.001
chr17:28496658-28497186	Mapk13	21.9	0.006
chr3:137801351-137802825	H2afz	21.7	0.002
chr10:80749241-80750235	Gipc3	20.9	0.005
chr7:34362376-34364521	Kctd15	20.1	0.004
chr8:129308243-129309088	1810063B05Rik	19.3	0.003
chr19:4439170-4439677	Rhod	18.0	0.006
chr8:3587354-3588037	2310057J16Rik	16.9	0.003
chr5:125480773-125481067	Ncor2	15.8	0.010
chr6:72118509-72118920	Atoh8	15.6	0.000
chr15:82999482-83000160	Cyb5r3	15.4	0.010
chr4:153827585-153828214	Pank4	13.8	0.008
chr5:122371639-122372196	Myl2	12.8	0.009
chr5:100304231-100304534	Enoph1	12.3	0.006
chr10:120713372-120714293	Gns	12.2	0.010
chr5:129159750-129160102	Rimbp2	11.8	0.009
chr17:65850084-65851009	Twsg1	11.4	0.003
chr8:129831577-129832204	Tomm20	11.0	0.007
chr12:74916322-74916824	Syt16	10.6	0.005
chr7:79899739-79900210	Zfp710	9.3	0.007
chr8:64175856-64176127	Sh3rf1	9.2	0.005
chr10:127861440-127862801	Smarcc2	8.9	0.000
chr18:16951167-16952628	Cdh2	8.9	0.009

We next evaluated the overall level of methylation or demethylation, using the sites identified as significantly d ferent between the two groups. This list can be larger or smaller depending on the stringency of statistic criteria (p-value cutoff 0.05 vs 0.005, etc). However independent of the stringency we found that overall there was a higher level of methylation in the DCs of asthma-susceptible neonates compared to that of controls (which were, respectively, more demethylated; Figure 8A). As shown in Figure 8D, each of the samples in the 'asthma-susceptible' group had higher level of methylation; concordantly, the overall number of demethylated sites in all 9 samples was higher in the normal group (not shown)

Figure 8A

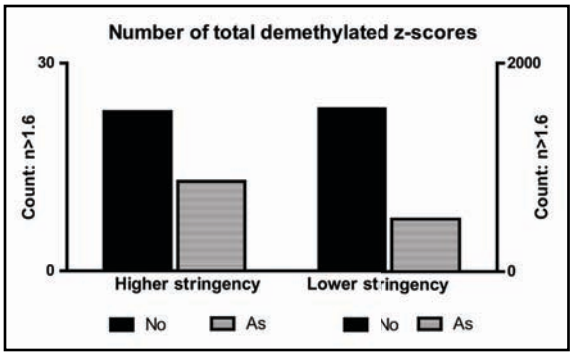

Figure 8B

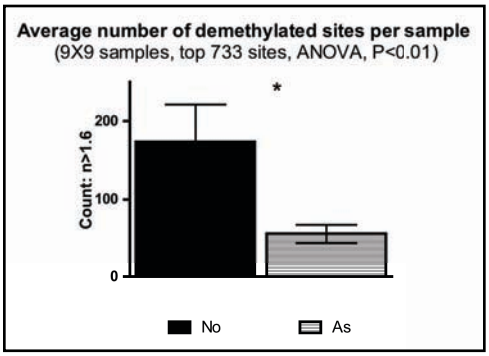

The exciting part of these findings is the novel observation that di ferences in how dendritic cells behave in terms of allergic predisposition can be linked to epigenetic control mechanisms. Although many differences were observed, none were found in the area of the genes for the SRAs. This does not exclude a regulatory role but additional studies are needed to sort this out. One limitation of these studies is that the gene expression analyses used resting dendritic cells. It is possible and worthy of investigation that activated DCs would in fact show a distinct profile in the pro-asthmati vs. normal groups.

Task 3: Determine role of SRAs on AMs in responses to inhaled allergen:
This work sought to test the hypothesis that AM SRAs also mediate down-regulation of immune responses to allergens by use of adoptive transfer experiments. Pilot experiments failed to show any effect of wild type or knockout AMs at the doses used. We put these unpromising studies on hold to concentrate on the dendritic cell work, which did allow the productive results shown above. Because the work for in vitro with dendritic cells took more time and effort than anticipated, we were not able to make further progress on this aim.

Task 4: Modulation of SRAs and Air Pollution Responses

Our goal in these experiments was to expose allergic mice to inhaled air pollutants to investigate how pollutant-generated oxidant stress modulates SRAs and how that, in turn, could affect asthma severity.

For air pollution studies, we made significant progress using ozone as a model oxidant. The data obtained using ozone support the hypothesis that down-regulation of SRAs will lead to harmful increased acute inflammation.

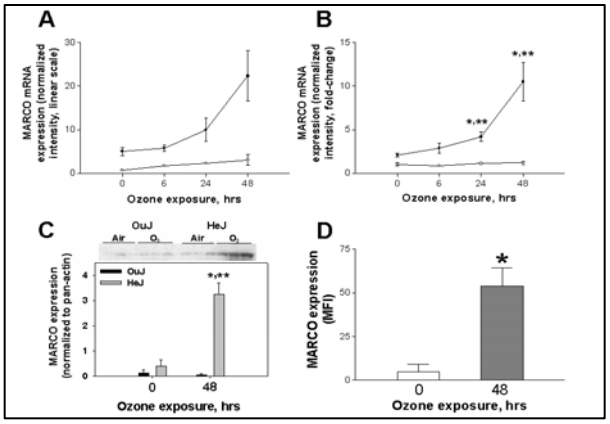

As shown in Fig. 9, oxidant pollutant exposure increased MARCO expression at the mRNA level, using both array and PCR analysis, and at the protein level (Western blot and cell surface analysis). Additional experimentation has shown that both MARCO and SRA KO mice demonstrate increased acute inflammation in response to the mild ozone challenge used here, linked to defective clearance of pro-inflammatory oxidized phospholipids, such cholesterol epoxide or oxidized surfactant phospholipids (PON-GPC) in the absence of the scavenger receptors Fig. 10 below.

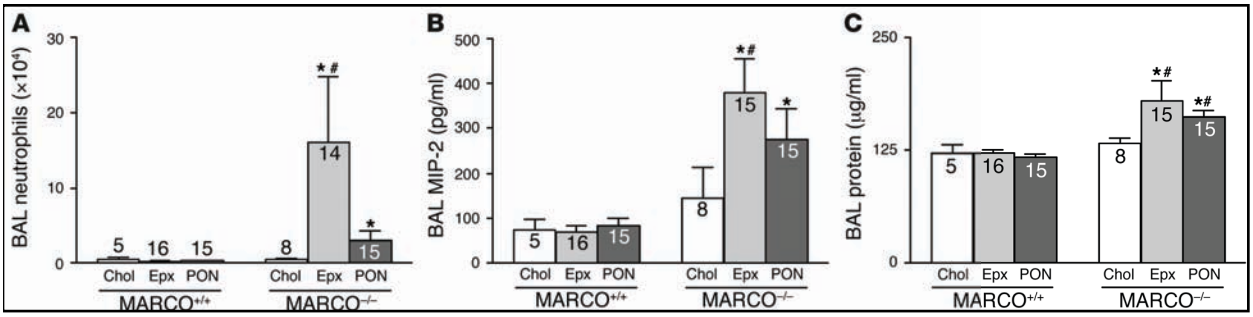

Figure 10: MARCO decreases inflammation in lungs of mice exposed to β-epoxide or PON-GPC i.t. BAL samples obtained from MARCO$_{-/-}$ mice 7 hours after i.t. instillation of 1 μg β-epoxide (Exp) or PON-GPC (PON) showed higher levels of neutrophils (**A**), MIP-2 (**B**), and total protein (**C**) compared with controls. Number of mice per group is shown for each bar. *P < 0.05 versus respective treated MARCO$_{+/+}$ group; #P < 0.05 versus

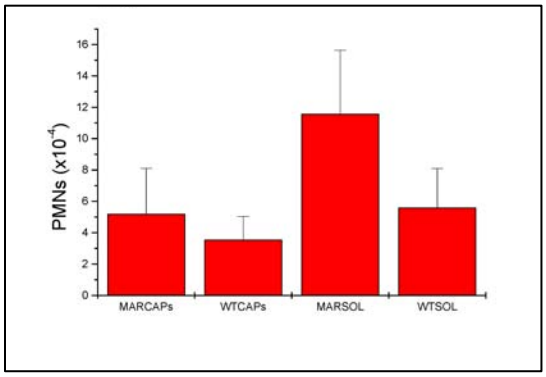

We have begun studies using exposure to solid air pollutants. As shown in Fig. 11 (left), we find similar enhanced acute inflammation in MARCO deficient mice exposed to air pollution samples. However, this difference is only evident when the soluble component of the air pollution particles is instilled, a finding that is under current further investigation. Many of these findings are detailed in the publication which is Appendix 2.

Key Research Accomplishments:

- Completed experiments to compare random migration and directed chemotaxis in dendritic cells from wild-type and MARCO-deficient mice
- Completed experiments to compare cell surface immunophenotype before and after in vitro maturation with TNF and LPS in dendritic cells from wild-type and MARCO-deficient mice
- Established system for adoptive transfer experiments in vivo to test ability of wild-type vs. knockout dendritic cells to alter susceptibility to asthma
- Established in vitro system to generate TH2 vs TH1 skewing dendritic cells to more efficiently test ability of wild-type vs. knockout dendritic cells to alter susceptibility to asthma in adoptive transfer experiments
- Identified novel epigenetic differences in pro-asthmatic dendritic cells vs. normal dendritic cells
- Confirmed predicted increased sensitivity of SRA deficient mice (MARCO and SRA) to inflammation caused by oxidant pollutants with gaseaous ozone and identified mechanism as delayed clearance of pro-inflammatory oxidized lipids.

Reportable Outcomes:

Three publications related to this research are:

1 Arredouani MS, Franco F, Imrich A, Fedulov A, Lu X, Perkins D, et al. Scavenger Receptors SR-AI/II and MARCO limit pulmonary dendritic cell migration and allergic airway inflammation. J Immunol. 2007;178(9):5912-2

2. Dahl M, Bauer AK, Arredouani M, Soininen R, Tryggvason K, Kleeberger SR, et al. Protection against inhaled oxidants through scavenging of oxidized lipids by macrophage receptors MARCO and SR-AI/II. J Clin Invest. 2007;117(3):757-64

3. Sulahian TH, Imrich A, Deloid G, Winkler AR, Kobzik L. Signaling pathways required for macrophage scavenger receptor-mediated phagocytosis: analysis by scanning cytometry. Respir Res. 2008;9:59

Abstract related to this work

1. Scavenger receptors and resistance to allergies L. Kobzik. presented at Military Health Research Forum, Aug/Sept 2009, Kansas City, MO

15 The results of our studies indicate that scavenger receptors modulate the allergic response, primarily by modifying dendritic cell trafficking to thoracic lymph nodes in the setting of asthma. We found that dendritic cells deficient in the scavenger receptors SRA I/II or MARCO traveled to the lymph nodes faster, and generated a more robust and intense asthmatic response when allergen was delivered into the lungs. We also observed that scavenger receptors are linked to oxidant air pollution responses in a complex manner. Oxidant air pollution increases expression of MARCO which serves to scavenge oxidized pro-inflammatory lipids, thereby dampening, but not eradicating, acute inflammatory responses. e also developed scanning cytometry methods for measuring macrophage phenotype in a high-throughput manner which will enable future studies.

We plan to continue two especially interesting aspects of these studies. First, the epigenetic control of dendritic cell and macrophage function, and how this might impact lung host defense against allergens, merits further investigation. We are continuing these studies, stimulated by the findings above. Second, the ability of modulation of SRAs by oxidants suggests that discovery of other drugs or agents to modulate these receptors could be of therapeutic value. We are pursuing screening platforms, such as those illustrated in Appendix 3, to search for increased SRA expression after drug modulation.

Appendices:

Three publications related to this research are attached as appendices:

1 Arredouani MS, Franco F, Imrich A, Fedulov A, Lu X, Perkins D, et al. Scavenger Receptors SR-AI/II and MARCO limit pulmonary dendritic cell migration and allergic airway inflammation. J Immunol. 2007;178(9):5912-2

2. Dahl M, Bauer AK, Arredouani M, Soininen R, Tryggvason K, Kleeberger SR, et al. Protection against inhaled oxidants through scavenging of oxidized lipids by macrophage receptors MARCO and SR-AI/II. J Clin Invest. 2007;117(3):757-64

3. Sulahian TH, Imrich A, Deloid G, Winkler AR, Kobzik L. Signaling pathways required for macrophage scavenger receptor-mediated phagocytosis: analysis by scanning cytometry. Respir Res. 2008;9:59

Personnel supported by this grant:

Lester Kobzik, P.I.
M. Arredouani
T. Sulahian
R. Lim
A. Fedulov
A. Bedugnis

Scavenger Receptors SR-AI/II and MARCO Limit Pulmonary Dendritic Cell Migration and Allergic Airway Inflammation[1]

Mohamed S. Arredouani,[2,3]* Francesca Franco,[3†‡] Amy Imrich,* Alexey Fedulov,* Xin Lu,[§] David Perkins,[¶] Raija Soininen,[‖] Karl Tryggvason,[#] Steven D. Shapiro,[†] and Lester Kobzik[4]*

The class A scavenger receptors (SR-A) MARCO and SR-AI/II are expressed on lung macrophages (MΦs) and dendritic cells (DCs) and function in innate defenses against inhaled pathogens and particles. Increased expression of SR-As in the lungs of mice in an OVA-asthma model suggested an additional role in modulating responses to an inhaled allergen. After OVA sensitization and aerosol challenge, SR-AI/II and MARCO-deficient mice exhibited greater eosinophilic airway inflammation and airway hyperresponsiveness compared with wild-type mice. A role for simple SR-A-mediated Ag clearance ("scavenging") by lung MΦs was excluded by the observation of a comparable uptake of fluorescent OVA by wild-type and SR-A-deficient lung MΦs and DCs. In contrast, airway instillation of fluorescent Ag revealed a significantly higher traffic of labeled DCs to thoracic lymph nodes in SR-A-deficient mice than in controls. The increased migration of SR-A-deficient DCs was accompanied by the enhanced proliferation in thoracic lymph nodes of adoptively transferred OVA-specific T cells after airway OVA challenge. The data identify a novel role for SR-As expressed on lung DCs in the down-regulation of specific immune responses to aeroallergens by the reduction of DC migration from the site of Ag uptake to the draining lymph nodes. ***The Journal of Immunology*****, 2007, 178: 5912–5920.**

The lung is constantly exposed to numerous inhaled particles and pathogens and relies on the broad ligand specificity of scavengers and other pattern recognition receptors for innate immune defense (1–3). The scavenger receptor (SR)[5] family includes two members in the SR-A subclass that are expressed on lung macrophages (MΦs) and dendritic cells (DCs), MARCO (MΦ receptor with collagenous structure), and SR-AI/II (SR-A, types I and II) (1, 2, 4). MARCO, like SR-AI/II, binds acetylated low-density lipoprotein and bacteria but not yeast (5–7). MARCO and SR-AI/II expressed on alveolar macrophages function to promote the uptake and clearance of inhaled particles and bacteria (7–10).

Aeroallergens constitute another common inhaled challenge to the lung's immune cells. Stimulated in part by gene expression profiling that shows increased expression of MARCO and SR-AI/II in the lungs of mice in an OVA-asthma model, we sought to determine whether SR-As contributed to defense of the lung against inhaled allergens using receptor-deficient mice and a model of allergic asthma. We found that sensitized mice lacking SR-A develop more severe airway inflammation and airway hyperresponsiveness (AHR) in response to inhaled aeroallergen. Because SR-As mediate macrophage binding and clearance of modified proteins, we initially expected that decreased clearance of Ag (OVA) by SR-A-deficient alveolar macrophages (AMs) would be a mechanism for increased allergic responses, but this postulate proved incorrect. We next evaluated the effect of SR-A-deficiency on the ability of Ag-loaded pulmonary DCs to migrate to the draining lymph nodes (LNs) and generate specific T cell responses. The data indicate that MARCO and SR-AI/II function in a novel mechanism to down-regulate migration of pulmonary DCs to thoracic LNs and thereby diminish T cell responses to specific aeroallergens.

Materials and Methods

Animals

Six- to eight-week-old mice genetically deficient in MARCO ($MARCO^{-/-}$) or SR-AI/II ($SR\text{-}AI/II^{-/-}$) were used in all experiments. Age- and sex-matched wild-type (WT) (C57BL/6 and BALB/c) mice purchased from Charles River Laboratories were used as controls. $MARCO^{-/-}$ mice were generated using targeted homologous recombination (9) and were backcrossed for at least 10 generations to the C57BL/6 background. $SR\text{-}AI/II^{-/-}$ mice were generated by disrupting exon 4 of the SR-A gene, which is essential for the formation of functional trimeric

*Department of Environmental Health, Harvard School of Public Health, Boston, MA 02115; †Pulmonary and Critical Care Medicine, Brigham and Women's Hospital, Harvard Medical School, Boston, MA 02115; ‡Clinica di Malattie dell'Apparato Respiratorio, Dipartimento Integrato di Oncologia ed Ematologia, Università degli Studi di Modena e Reggio Emilia, Modena, Italy; §Department of Family and Preventive Medicine, University of California San Diego, CA 92101; ¶Department of Medicine, University of California San Diego, CA 92101; ‖Department of Medical Biochemistry and Molecular Biology, Biocenter Oulu, University of Oulu, Oulu, Finland; and #Department of Medical Biochemistry and Biophysics, Karolinska Institutet, Stockholm, Sweden

Received for publication September 5, 2006. Accepted for publication February 9, 2007.

The costs of publication of this article were defrayed in part by the payment of page charges. This article must therefore be hereby marked *advertisement* in accordance with 18 U.S.C. Section 1734 solely to indicate this fact.

[1] This work was supported by National Institutes of Health Grants ES0002 and ES11008, and by Department of Defense Grant W81XWH-06-1-0289. M.S.A. is a recipient of the Jere Mead fellowship.

[2] Current address: Beth Israel Deaconess Medical Center, Harvard Medical School, 77 Avenue Louis Pasteur, HIM-1039, Boston, MA 02115.

[3] M.S.A. and F.F. contributed equally to this work.

[4] Address correspondence and reprint requests to Dr. Lester Kobzik, Department of Environmental Health, Harvard School of Public Health, 665 Huntington Avenue, Boston, MA 02115. E-mail address: lkobzik@hsph.harvard.edu

[5] Abbreviations used in this paper: SR, scavenger receptor; SR-AI/II, SR class A, type I and type II; AHR, airway hyperresponsiveness; AM, alveolar macrophage; BAL, bronchoalveolar lavage; BALF, BAL fluid; Ct, threshold cycle; C3H, C3H/HeJ; DC, dendritic cell; i.t., intratracheal; KO, knockout; LN, lymph node; MARCO, macrophage receptor with collagenous structure; MΦ, macrophage; $P_{enh,}$ enhanced pause; WT, wild type.

receptors (11). Double knockout (KO) mice were obtained in our laboratory by intercross of single KO mice.

Both single KO mice were backcrossed in our laboratory to the BALB/c background for eight generations. DO11.10 mice, which are transgenic for the TCR recognizing OVA peptide 323–339, A/J, C3H/HeJ (C3H), and C3H/HeOuJ mice were from The Jackson Laboratory. All animals were housed in sterile microisolator cages and had no evidence of spontaneous infection. Approval before all experimentation was obtained from Harvard School of Public Health institutional animal use review committee.

Mouse model of airway allergic inflammation1

To compare allergic responses in SR-A and normal mice, groups of MARCO$^{-/-}$, SR-AI/II$^{-/-}$, and C57BL/6 WT control mice were sensitized i.p. with 8 μg OVA in 1 mg of alum gel in 0.5 ml of PBS on days 0 and 7. On day 14 the sensitized mice were challenged with aerosolized 0.5% OVA or PBS for 1 h. Mice were sacrificed 72 h postchallenge, blood was collected through heart puncture, and the lungs were lavaged with PBS before they were harvested, inflated with formalin, and processed for histologic analysis.

In BALB/c mice, 10 μg OVA in 2 mg of Alum powder were administered i.p. at days 0 and 7 followed by aerosol challenge with either PBS or 1% OVA for 30 min on days 14 and 15.

Microarray data analysis

Microarray data was acquired from the Public Expression Profiling Resource (http://pepr.cnmcresearch.org; see project 108). Gene expression data were calculated by using the GeneChip-Robust Multiarray Analysis algorithm (12) from the Bioconductor project (http://www.bioconductor.org/). The fold change in MARCO and SR-A gene expression was calculated as the ratio of the level in the OVA/control sample.

The raw p values were adjusted by false discovery rate correction and an adjusted p value <0.05 was interpreted as significant.

RT and real-time PCR

Total lung RNA was extracted from normal and OVA-sensitized and challenged BALB/c mice using a Qiagen RNAeasy kit according to manufacturer's instructions. RNA purity was controlled by OD measurement. RNA concentrations were adjusted and the samples were reverse transcribed to cDNA using the novel SuperScript III first-strand cDNA synthesis kit (Invitrogen Life Technologies). cDNA samples were analyzed in duplicate in a quantitative real-time PCR using the SYBR Green Supermix (Bio-Rad) for MARCO and SR-A message with the following primer sequences (Integrated DNA Technologies): SR-A sense (5′-AGAATTTCAGCATGGC AACTG-3′) and SR antisense (5′-ACGGACTCTGACATGCAGTG-3′); and MARCO sense (5′-GAAACAAAGGGGACATGGG-3′) and MARCO antisense (5′-TTCACACCTGCAATCCCTG-3′). Murine β-actin was used as housekeeping control and a no-template sample was used as a negative control. Data are represented as ΔCt (threshold cycle) values, with the lower values indicating a greater abundance of mRNA in the sample.

Measurement of airway hyperresponsiveness

AHR was measured in MARCO$^{-/-}$, SR-AI/II$^{-/-}$, and BALB/c WT mice using whole body plethysmography (Buxco; EMKA Technologies) 24h after the last of two daily OVA or PBS aerosol challenges. The response of the airways to inhaled methacholine (Sigma-Aldrich) at concentrations ranging from 6.25 to 100 mg/ml (13) was recorded. AHR was expressed as enhanced pause (P_{enh}), a calculated value that correlates with airway resistance.

Bronchoalveolar lavage (BAL)

BAL was performed in situ with a 20-gauge catheter inserted into the proximal trachea, flushing the lower airways six times with 0.8 ml of PBS. The fluid retrieved from the first flushing was kept for ELISA. The BAL fluid cells were separated from the BAL fluid by centrifugation, resuspended in PBS, and counted and a fraction was cytospun on microscopic slides for staining with Diff-Quick (Baxter Scientific Products) for subsequent leukocyte differential counts.

OVA uptake studies

To prepare the OVA-FITC conjugate, OVA was dissolved in carbonate buffer (pH 9.2). Freshly prepared FITC in DMSO (10 mg/ml) was added at a ratio of 10 mg per 200 mg of OVA and the mixture was incubated at room temperature in the dark for 1 h. To remove free FITC, the mixture was dialyzed for 24 h against PBS. MARCO$^{-/-}$, SR-AI/II$^{-/-}$, and C57BL/6 mice were given a 15-min aerosol treatment with a 10 mg/ml solution of OVA-FITC. BALs were performed 1 h later and cells were analyzed by flow cytometry. To test the binding of OVA to AMs in vitro, BAL fluid (BALF) cells (200×10^3/well) from C57BL/6 WT and double KO mice were pretreated for 5 min with 5 μM cytochalasin D and then incubated with 5 μg/ml OVA-Alexa Fluor 488 for 40 min at 37°C and analyzed by flow cytometry.

Instillation of macromolecule solutions into the trachea

Mice were anesthetized by i.p. injection of 2.5% Avertin and received an intratracheal (i.t.) injection of 600 μg of OVA-FITC in a volume of 60 μl of sterile PBS. The trachea was carefully exposed via a small midline incision and the solution was inoculated. The incision was then closed with sterile silk and the mice were allowed to fully recover before being returned to the cages.

Preparation of single-cell suspensions and immunofluorescent labeling

Lung digestion medium consisted of RPMI 1640 (from Invitrogen Life Technologies) supplemented with 1 mg/ml collagenase type IV (Sigma-Aldrich) and 0.5 mg/ml DNase (deoxyribonuclease I from a bovine pancreas; Sigma-Aldrich). LN digestion medium consisted of 1 $\times$ HBSS (Cellgro; Mediatech) and 2% EDTA-treated FBS (HyClone) supplemented with 2.5 mg/ml collagenase type IV (Sigma-Aldrich). EDTA-treated FBS was prepared by adding 20 μl of 0.5 M EDTA per ml of FBS. FACS staining buffer consisted of PBS (free of Ca^{2+} or Mg^{2+}) supplemented with 5% FBS, 0.1% sodium azide, and 5 mM EDTA.

Preparation of lung and LN single-cell suspensions

Lung. Animals were euthanized by CO_2 narcosis. Following a thoracotomy, right heart catheterization was performed using a 21-gauge, 0.75-inch siliconized needle (SURFLO winged infusion set; Terumo) and the pulmonary circulation was perfused with at least 20 ml of sterile PBS to remove the intravascular pool of cells. Two milliliters of digestion medium were then injected in the trachea using a 22-gauge catheter and the trachea was quickly sealed with silk suture after the catheter was removed. The trachea and lungs were then removed and the lungs were carefully separated from the heart, thymus, and trachea and incubated at 37°C in additional 3 ml of digestion medium for 30 min. Incubation was then prolonged for an additional 30 min with vigorous pipetting of the samples at 10-min intervals with a 5-ml serological pipet. Subsequently, samples were passed through a 70-μm nylon cell strainer, subjected to RBC lysis, incubated in calcium- and magnesium-free PBS containing 10 mM EDTA for 5 min at room temperature on a shaker, and finally resuspended in FACS staining buffer and kept on ice until immunofluorescent labeling.

Lymph nodes. For migration studies, animals were euthanized by CO_2 narcosis 24 h after an i.t. injection of OVA-FITC. For T cell proliferation studies, animals were euthanized by CO_2 narcosis 96 h after the injection of OVA. Following a thoracotomy, paratracheal and parathymic intrathoracic LNs were removed under a stereo microscope (Olympus SZ 60) and incubated at 37°C in 3 ml of LN digestion medium. After 10 min of incubation, LNs were minced with 20-gauge, 1.5-inch and 25-gauge, 0.625-inch needles (BD Biosciences) and incubation was prolonged for another 10 min. Subsequently, samples were passed through a 7-μm nylon cell strainer, incubated in calcium- and magnesium-free PBS containing 10 mM EDTA for 5 min at room temperature on a shaker, and finally resuspended in FACS staining buffer and kept on ice until immunofluorescent labeling.

Labeling of single cell suspensions for flow cytometry

All staining procedures were performed at 4°C. Cells were preincubated for 20 min with a Fc receptor blocking Ab (anti-CD16/CD32; BD Biosciences) to reduce nonspecific binding. For lung studies, cells were subsequently stained with a PE-Cy5.5-conjugated hamster anti-mouse CD11c mAb (Caltag Laboratories) and data acquisition was performed using the FL1/FL3 template to allow assessment of the distribution of CD11c-bright cells with regard to autofluorescence. A PE-Cy 5.5-conjugated hamster IgG isotype control was used to determine background staining (Caltag Laboratories). Rat anti-F4/80 (IgG2a; clone 6F12) and rat anti Mac-3 (IgG1; clone M3/84) were from BD Biosciences. For migration studies, cells were stained with a PE-Cy5.5-conjugated hamster anti-mouse CD11c mAb (Caltag Laboratories). For T cell proliferation studies, cells were stained

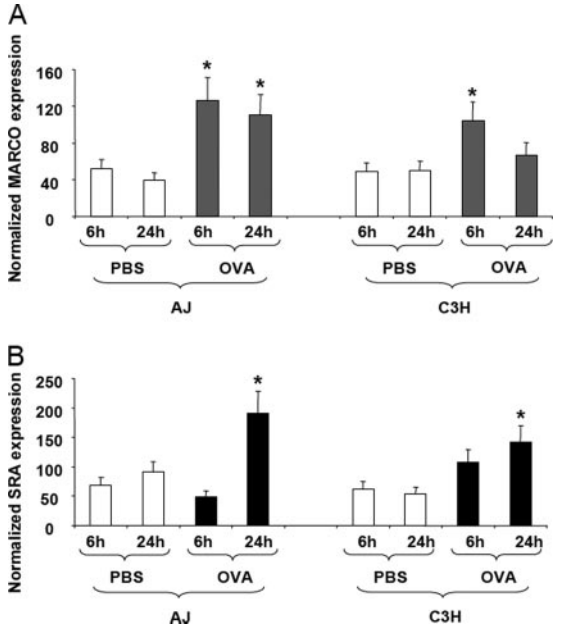

FIGURE 1. Augmented expression of MARCO and SR-AI/II in allergic asthma. Microarray analysis of RNA transcripts for MARCO (*A*) and SR-AI/II (SRA) (*B*) was performed on asthmatic and control A/J (AJ) and C3H mice at 6 h and 24 h after allergen or PBS challenge. Data are expressed as mean ± SD of normalized gene expression obtained from five mice. *, $p < 0.05$ vs same time point after PBS challenge.

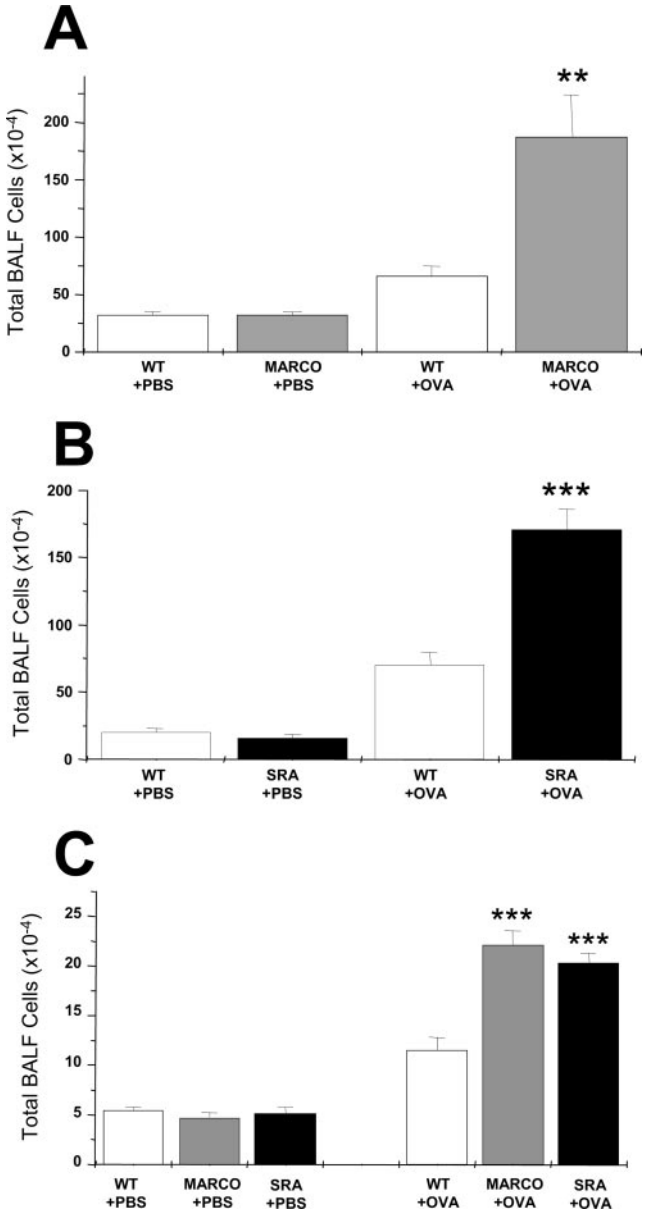

FIGURE 2. BAL cell yields after OVA-sensitization and challenge. Control (C57BL/6 or BALB/c), MARCO$^{-/-}$ and SR-AI/II$^{-/-}$ (SRA) mice were sensitized twice with OVA in alum and exposed once to 1% aerosolized OVA (+OVA). As a negative control, mice were immunized with OVA and challenged with PBS aerosol (+PBS). Seventy-two hours after aerosol exposure, lungs were lavaged and then fixed in formalin for H&E staining. Total leukocyte counts were determined in BALF of MARCO$^{-/-}$, SR-AI/II$^{-/-}$, and their WT counterparts in both C57BL/6 (*A* and *B*) and BALB/c (*C*) backgrounds. Data shown here are representative of 18 (*A*), 12 (*B*), and 6 mice (*C*) per group. **, $p < 0.01$; ***, $p < 0.001$; for OVA vs PBS challenge.

with PE mouse anti-mouse DO11.10 TCR mAb (clone KJ1-26) (Caltag Laboratories). A PE-conjugated mouse IgG2a isotype control was used to determine background staining (Caltag Laboratories). Flow cytometry data acquisition was performed on a BD FACScan running CellQuest software (BD Biosciences). Flow Jo software (Tree Star) was used for data analysis. For lung and migration studies 50,000 total events were acquired for each sample. For T cell proliferation studies 500,000 total events were acquired for each sample. Dead cells were gated out based on light scatter properties.

In vivo assessment of T cell proliferation

CD4$^+$ T cells were enriched from the spleens of DO11.10 mice by magnetic bead separation under sterile conditions using a mixture of biotin-conjugated mAbs against CD8a (rat IgG2a; Ly-2), CD11b (rat IgG2b; Mac-1), CD45R (rat IgG2a; B220), CD49b (rat IgM; DX5), and Ter-119 (rat IgG2b), followed by anti-biotin microbeads (colloidal superparamagnetic microbeads conjugated to a monoclonal anti-biotin Ab, mouse IgG1; clone Bio3-18E7.2) (Miltenyi Biotec). CD4$^+$ DO11.10 T cells were subsequently labeled with 10 μM CFSE (Sigma-Aldrich) at 37°C for 10 min as described by Lyons et al. (14) and then resuspended in sterile PBS. Mice received an i.v. injection of 10×10^6 CFSE-labeled DO11.10 T cells 24 h before an i.t. injection of 600 μg of OVA in a volume of 60 μl of PBS. Four days later T cell responses were analyzed in the draining mediastinal LNs by observing the CFSE division profiles of live KJ1-26$^+$ CD4$^+$ T cells. The number of transgenic T cells in each LN was calculated as percentage of KJ1-26$^+$CFSE$^+$ cells among the total cell number.

Statistical analysis

Student's *t* test (unpaired, two-tailed) was used to calculate significance levels for all measurements. Data are presented as mean ± SEM or SD. Differences were considered significant when $p < 0.05$.

Results

Increased MARCO and SR-AI/II gene expression in a murine model of asthma

To identify genes modulated in asthma, we analyzed public databases of microarray expression profiling in experimental murine asthma models. In a project conducted by M. Wills-Karp (Cincinnati Children's Hospital Medical Center, Cincinnati, OH; data openly available online at the Public Expression Profiling Resource (http://pepr.cnmcresearch.org/)), the response to OVA exposure at 6 and 24 h following allergen challenge in both the A/J and C3H strains was determined by using five replicates of whole lung RNA from each experimental group. We processed the data as described in *Materials and Methods*. A comparison of allergen-challenged mice to saline-challenged mice revealed a significant up-regulation of MARCO and SR-AI/II after exposure to OVA in both strains (Fig. 1, *A* and *B*). A

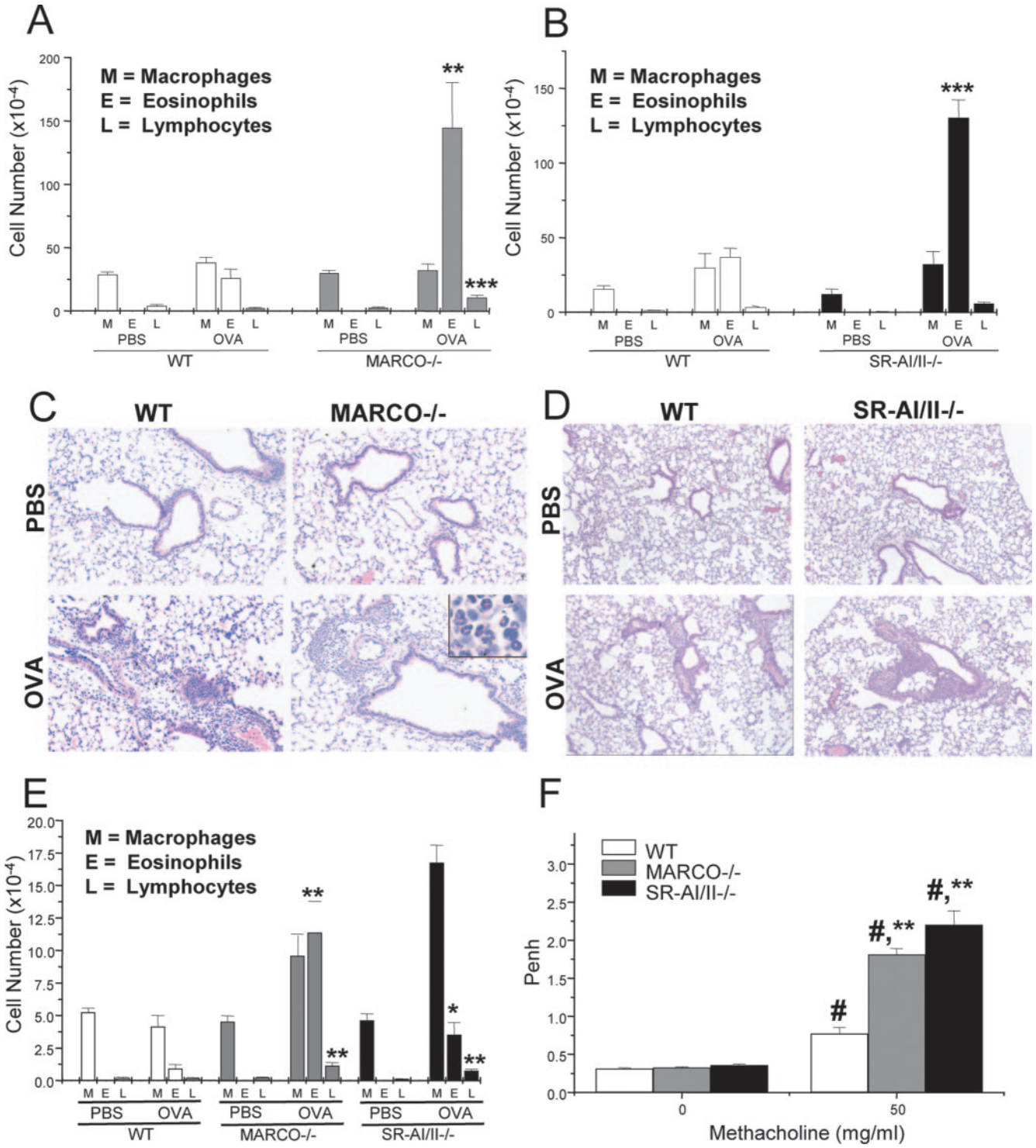

FIGURE 3. Response to OVA challenge in WT vs SR-A-deficient mice. Differential counts showing the amounts of BALF macrophages, eosinophils, and lymphocytes were determined on stained cytospin slides from MARCO$^{-/-}$, SR-AI/II$^{-/-}$, and their WT counterparts in both C57BL/6 (*A* and *B*) and BALB/c backgrounds (*E*). Data shown here are representative of 18 mice per group (*A*), 12 mice per group (*B*), and 6 mice per group (*E*). *, $p < 0.05$; **, $p < 0.01$; and ***, $p < 0.001$; for OVA vs PBS challenge. Representative photomicrographs of tissue histopathology are shown from WT (*C* and *D*), MARCO$^{-/-}$ (*C*), and SR-AI/II$^{-/-}$ (*D*) mice challenged with either PBS or OVA. *Inset* (*C*, *lower right panel*) shows higher magnification (×600) of eosinophils and mononuclear cells comprising the inflammatory infiltrates. Images are shown at a ×200 original magnification for MARCO$^{-/-}$ and ×100 for SR-AI/II$^{-/-}$ mice. SR-A-deficient mice also show enhanced airway hyperreactivity (*F*) as measured by whole body plethysmography in conscious OVA-sensitized and challenged BALB/c mice. P_{enh}, an index of airway obstruction, was recorded after aerosolization of either PBS or 50 mg/ml methacholine. Data represent mean P_{enh} values ± SEM (six mice per group for OVA/OVA and three mice per group for OVA/PBS). #, $p < 0.05$ vs PBS challenge; **, $p < 0.01$ vs WT mice.

similar trend was found in studies using the C57BL/6 strain (search for GDS348 on the Gene Expression Omnibus DataSets site: http://www.ncbi.nlm.nih.gov/entrez/query.fcgi?db=gds). We also observed increased MARCO and SR-A gene expression in RT-PCR analysis of lung samples from OVA-sensitized and exposed mice compared with controls (e.g., ΔCT values for

OVA vs controls were 5.3 ± 0.6 vs 6.6 ± 0.4 (SR-A) and 7.2 ± 1.1 vs 9.2 ± 1.5 (MARCO); lower ΔCT values indicate a greater abundance of mRNA targets).

Increased severity of airway inflammation in SR-A deficient mice during allergic asthma

We next directly analyzed the physiologic relevance of the two SR-A receptors, MARCO and SR-AI/II, in vivo in a murine model of allergic airway inflammation caused by OVA sensitization and aerosol challenge. Due to the unavailability of SR-A KO mice in the susceptible A/J and resistant C3H backgrounds used in the microarray studies, we used the C57BL/6 and BALB/c strains, both known to show pulmonary expression of SR-As (8, 9) and to be prone to OVA-induced airway inflammation (15, 16). Seventy-two hours after the aerosol challenge, sham-challenged mice (OVA/PBS groups) showed no sign of inflammation, whereas all OVA/OVA groups showed a remarkable increase in the total number of leukocytes recruited to the airways (Fig. 2, *A* and *B*). Notably, the total number of eosinophils and lymphocytes in the BAL samples from OVA/OVA groups was substantially greater in the SR-A-deficient mice relative to their control counterparts (Fig. 3, *A* and *B*). OVA/PBS mice, in contrast, did not show any recruitment of eosinophils into their airways. Consistent with the increased leukocyte numbers in lavage samples of OVA-challenged SR-A-deficient mice, histologic analysis of lungs harvested from these mice showed allergic inflammation consisting of peribronchial and perivascular cell infiltrates of eosinophils and mononuclear cells (Fig. 3, *C* and *D*).

Unlike C57BL/6 mice, allergen-sensitized BALB/c mice develop easily detectable AHR following exposure to inhaled allergen (15, 16). MARCO$^{-/-}$ and SR-AI/II$^{-/-}$ mice on the BALB/c background also showed a significant increase in eosinophils and macrophages (Fig. 3*E*) and total cell number (Fig. 2*C*) in the BALF following OVA challenge, compared with their WT counterparts. The basis for the increased macrophage number in the KO mice on the BALB/c background is unknown. It is also worth mentioning that the discrepancy in both the intensity and the nature of cellular inflammatory responses between C57BL/6 and BALB/c strains after exposure to inhaled OVA is an expected result of the different induction protocols we have used to achieve significant eosinophilic recruitment and the Ag dose-dependent response in these strains. Whole body plethysmography was used to evaluate pulmonary function changes after OVA challenge in WT vs MARCO$^{-/-}$ and SR-AI/II$^{-/-}$ mice. Following aerosolized bronchoconstrictor (methacholine) challenge, WT mice showed a slight, but significant, increase in AHR relative to the baseline ($p < 0.05$). In contrast, MARCO$^{-/-}$ and SR-AI/II$^{-/-}$ mice showed a much more robust response ($p < 0.01$; Fig. 3*F*), consistent with their greater allergic inflammatory response.

WT and SR-A-deficient lung MΦs show normal uptake of inhaled OVA allergen

AMs can efficiently bind and internalize unopsonized particles and bacteria through SR-As, leading to the clearance of inhaled matter from the airways and the reduction of the resulting inflammation (7–9) and are known to similarly bind modified proteins (17–19). To determine whether SR-As could reduce allergic inflammation by simply "scavenging" aeroallergen with a resulting decrease in allergen dose, we measured their ability to internalize inhaled allergens using FITC-OVA. WT and KO mice were exposed to inhaled fluorescent OVA, the airways were lavaged 1 h later, and the total fluorescence of AMs was evaluated by flow cytometry.

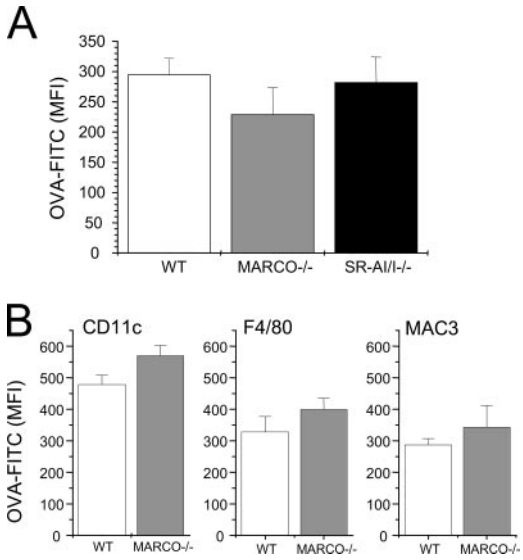

FIGURE 4. Absence of SR-As on AMs does not affect the clearance of inhaled allergen. *A*, Control (C57BL/6), MARCO$^{-/-}$, and SR-AI/II$^{-/-}$ mice were challenged with aerosolized OVA-FITC (10 mg/ml) for 15 min. The lungs were lavaged 1 h later with PBS and cells were analyzed by flow cytometry to compare the uptake of fluorescent OVA. Data shown represent the mean ± SEM of four mice per group. *B*, In separate experiments, three WT and three MARCO$^{-/-}$ mice received 600 μg of OVA-FITC i.t. The lungs were harvested 4 h later and cell suspensions prepared by homogenization were labeled with Abs to either CD11c, F4/80, or MAC3 Ags and the mean green fluorescence intensity (MFI) of the double positive cells was determined.

Similar amounts of FITC-OVA were found associated with AMs in WT, MARCO$^{-/-}$, and SR-AI/II$^{-/-}$ mice ($p > 0.05$), indicating essentially identical uptake in vivo (Fig. 4*A*). In parallel experiments, FITC-OVA was administered i.t. to the mice and the amount of OVA associated with the MΦ population was determined on the cells isolated from whole lung homogenates. The total amount of FITC-OVA on MΦs, as discriminated by gating of the CD11c^{+}, F4/80^{+}, or MAC3^{+} populations, was similar in both WT and MARCO$^{-/-}$ mice ($p > 0.05$; Fig. 4*B*). In vitro assays confirmed that the absence of receptors did not affect AM binding of OVA, as double-deficient AMs bound Alexa Fluor 488-OVA to nearly the same extent as did control AMs (data not shown). These findings are consistent with previous reports indicating that, unlike chemically modified albumin, native albumin binding to MΦs is not mediated through SR-As (17–19), and they also indicate that nebulization does not per se denature the allergenic proteins sufficiently to create SR-A binding domains.

Allergen-loaded SR-A-deficient DCs show increased migration from the lungs to the draining LNs

We next sought to investigate whether another SR-A-expressing cell type, the lung DC, was involved in the increased asthmatic phenotype seen in SR-A-deficient mice. Airway DCs capture Ags in the lungs and migrate to the regional LNs where they present the Ag to the specific T cells. To track DC migration from the lungs to the draining LNs, we administered OVA-FITC i.t. and analyzed cell suspensions prepared from mediastinal LNs 24 h later. DCs were labeled with anti-CD11c Ab and the number of cells expressing the CD11c and also carrying FITC was determined by flow cytometry. Although there are no significant differences in LN cellularity under basal conditions (Fig. 5*A*), OVA challenge of the airways resulted in an increase in LN cellularity, an increase which

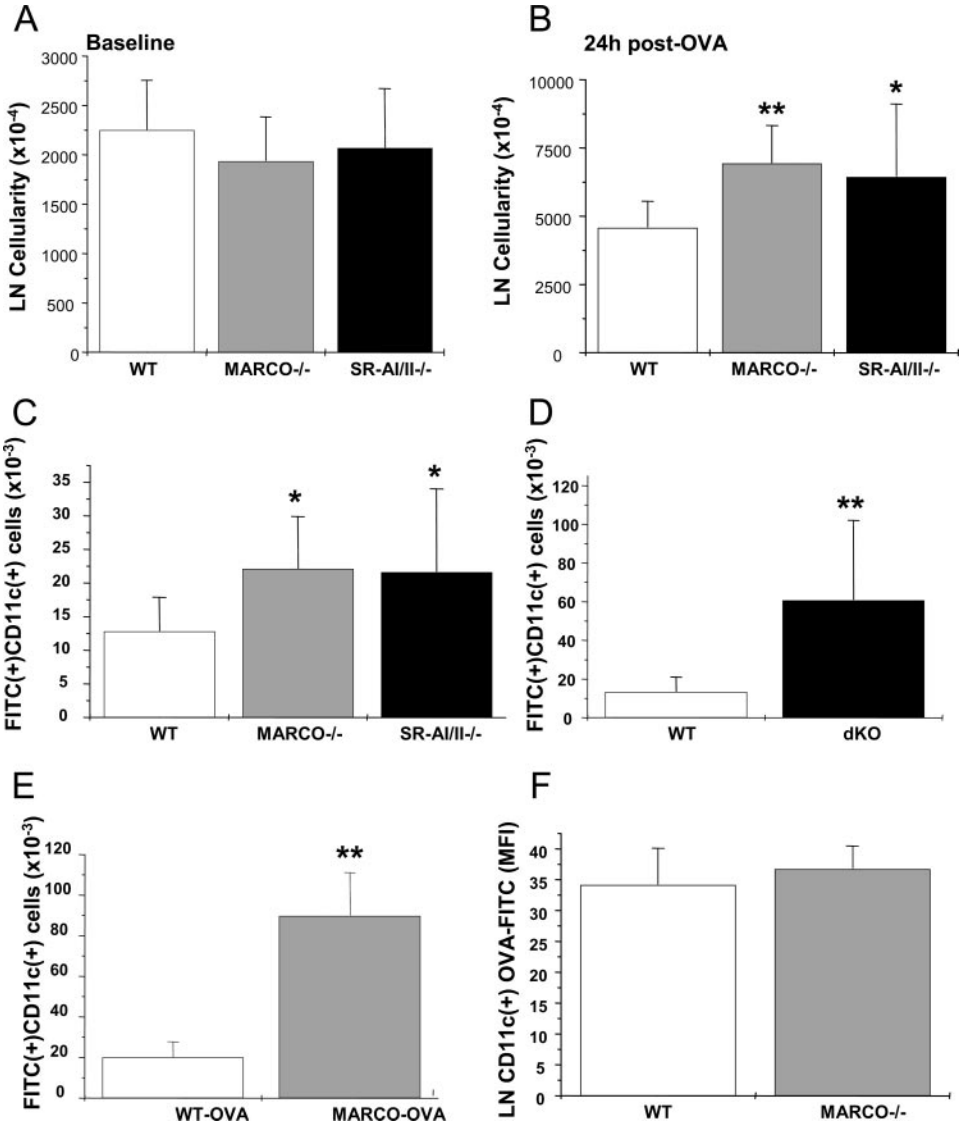

FIGURE 5. Increased migration of MARCO$^{-/-}$ and SR-AI/II$^{-/-}$ pulmonary DCs in response to an inhaled Ag challenge. *A* and *B*, The total cell content of homogenized mediastinal LNs from C57BL/6, MARCO$^{-/-}$, and SR-AI/II$^{-/-}$ mice was determined before (*A*) or 24 h after (*B*) they received 600 μg of OVA-FITC i.t. *C–F*, LN suspensions from OVA-FITC-challenged mice were stained for CD11c and the fraction of FITC^{+} DCs was determined by flow cytometry (*C*). A similar protocol was applied to double KO (dKO) mice (*D*) and OVA-sensitized C57BL/6 and MARCO$^{-/-}$ mice (*E*). Also, the amount of green fluorescence associated with the DCs was determined (*F*). Data represent the mean ± SD from two or more separate experiments with at least six mice per genotype, *, $p < 0.05$; **, $p < 0.01$.

is greater in the SR-A-deficient mice (Fig. 5*B*). A striking finding was that SR-A-deficient mice showed a significantly greater number of Ag-loaded DCs in the thoracic LNs (Fig. 5*C*), indicating that DC migration is more efficient in the KO mice. Double KO mice showed an even greater migration of airway DCs after OVA challenge compared with control mice and single deficient mice (Fig. 5*D*). These studies were performed in unimmunized mice. We next assessed DC migration in OVA-sensitized WT and MARCO$^{-/-}$ mice. Notably, although the sensitized WT mice showed an elevated migration of airway DCs to the LNs after OVA exposure (note the expanded range of the *y*-axis), the increase was even more marked in the MARCO$^{-/-}$ mice (Fig. 5*E*). To determine whether differences in Ag (OVA) uptake by WT or SR-A-deficient DCs could mediate the enhanced allergic responses in SR-A-deficient mice, we also evaluated the OVA-FITC content of the DCs that reach the LNs after Ag challenge (measured as green fluorescence). We observed the same amounts of Ag in the DCs reaching the LNs in both WT and MARCO$^{-/-}$ mice (Fig. 5*F*). This indicates that SR-A-deficiency does not alter the uptake of OVA-FITC Ag by DCs, a finding similar to data obtained with macrophages (Fig. 4). To evaluate the potential of trace endotoxin in the OVA preparation to modulate DC migration, we performed OVA-FITC instillation into endotoxin-sensitive and resistant (C3H/Ouj and C3H/HeJ respectively). No differences were observed in the numbers of migrated FITC^{+}CD11C^{+} DCs found in thoracic LNs in the two strains of mice (data not shown).

To evaluate the possibility that the enhanced DC migration in KO mice was due to a higher basal number of DCs in the lungs, we quantified the lung DC population in naive MARCO$^{-/-}$ and control mice. Lung DCs were defined as bright CD11c^{+} cells with low autofluorescence, as described by Vermaelen and Pauwels (20). We found that the number of lung DCs was not statistically different between MARCO$^{-/-}$ and their control WT mice (data not shown).

Allergen challenged SR-A deficient mice show enhanced T cell priming in the draining LNs

To more directly test the functional significance of augmented Ag-loaded DC migration in SR-A-deficient mice, we used an adoptive transfer model to assess T cell proliferation in the draining LNs after Ag challenge. BALB/c WT, MARCO$^{-/-}$, and SR-AI/II$^{-/-}$ mice were injected i.v. with CFSE-labeled OVA-specific CD4^{+} T lymphocytes from DO11.10 transgenic mice. Recipient mice were challenged i.t. with OVA 24 h later. The mediastinal LNs were

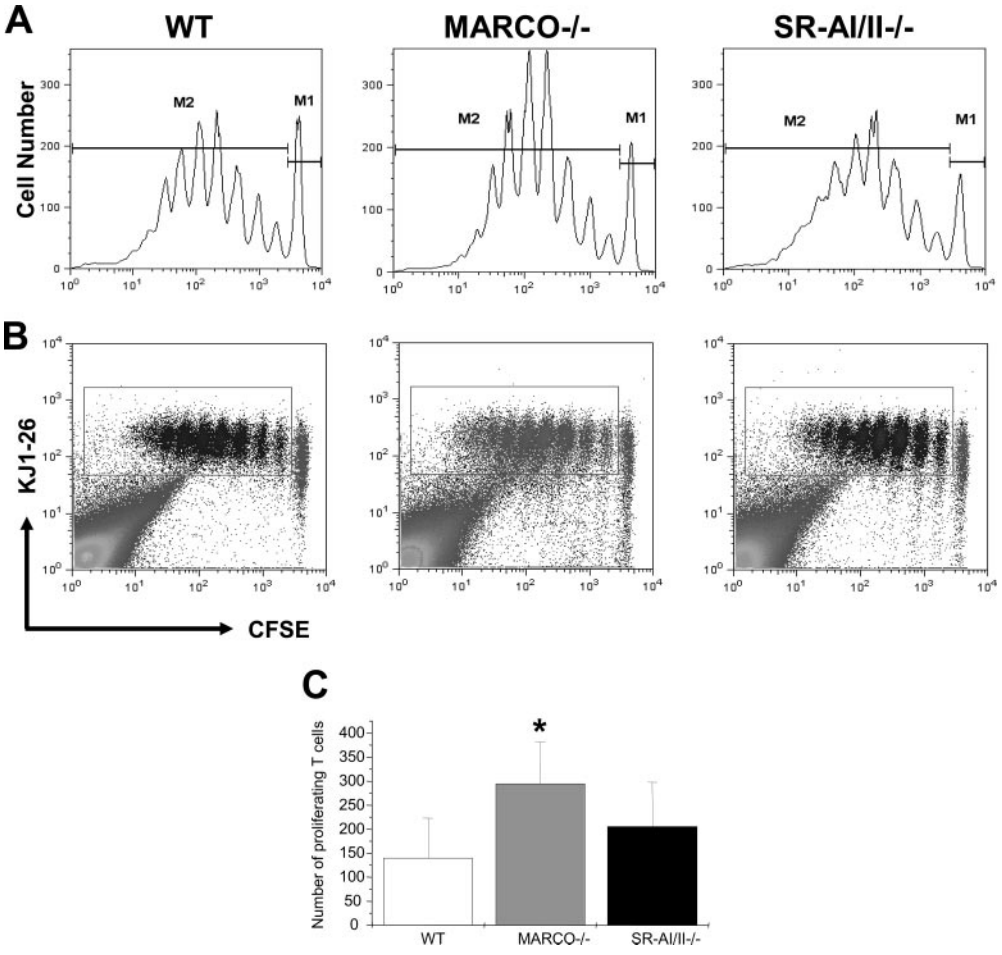

FIGURE 6. Enhanced Ag-induced T lymphocyte proliferation in mediastinal LNs of SR-A-deficient mice. CFSE-labeled spleen $CD4^+$ T cells from DO11.10 mice were transferred i.v. into BALB/c, $MARCO^{-/-}$, and $SR\text{-}AI/II^{-/-}$ mice 24 h before i.t. administration of OVA. Ninety-six hours later, cell suspensions were prepared from draining LNs and stained with KJ-126-PE Ab. Representative histograms (*A*; cells in the M2 zone have undergone at least one division) and dot plots (*B*; cells in the rectangles have undergone at least one division) are shown for control, $MARCO^{-/-}$, and $SR\text{-}AI/II^{-/-}$ mouse groups. The deduced absolute number of cells that underwent at least one division is shown in *C*. Data represent the mean ± SD from eight ($MARCO^{-/-}$) and 12 mice ($SR\text{-}AI/II^{-/-}$). *, $p < 0.05$.

harvested 96 h after OVA challenge for an analysis of dye dilution as a function of cell division.

Comparable numbers of adoptively transferred DO11.10 T cells reached the mediastinal LNs in all three groups of mice (data not shown) and, similarly, comparable fractions underwent at least one division (percentage of cells showing decreased CFSE was 91, 93.5, and 92%, respectively, in WT, $MARCO^{-/-}$, and $SR\text{-}AI/II^{-/-}$ mice). However, there was a greater proliferative response in the LNs of $MARCO^{-/-}$ mice ($295 \pm 83 \times 10^3$; mean ± SD) compared with WT mice ($140 \pm 83 \times 10^3$), indicating that a higher absolute number of T cells had undergone a greater number of divisions in the $MARCO^{-/-}$ mice (Fig. 6). This indicates that the larger numbers of Ag-loaded DCs that migrate to the draining LNs of the $MARCO^{-/-}$ mice result in a greater proliferative response by Ag-specific T lymphocytes. $SR\text{-}AI/II^{-/-}$ mice showed a similar trend that did not reach statistical significance in T cell proliferation ($206 \pm 92 \times 10^3$) compared with control mice.

Discussion

The data presented identify a novel role for SR-As expressed on lung DCs in modulating pulmonary responses to aeroallergens. The context for our findings includes the recognition of the important role of DCs in the pathogenesis of asthma (21) and as professional APCs that bridge innate and adaptive immunity (22, 23). DCs express SR-AI/II, which functions in Ag presentation and adaptive immunity (17, 19, 24–28). For example, $SR\text{-}AI/II^{-/-}$ mice are deficient in mounting an efficient T cell response to maleylated murine serum albumin, a known SR-AI/II ligand (29). In contrast, the role of MARCO receptors in modulating adaptive immunity has not been examined.

It has been postulated that MARCO expression is induced upon DC maturation (30, 31). Although we did not directly address the maturation state of pulmonary DCs in naive WT mice, we know the following: 1) only immature DCs can take up and process Ag (32); 2) immunohistochemical studies show the expression of MARCO only on MΦs in the normal lung (8) with an absence of MARCO labeling in normal airways that contain $CD11c^+$ airway DCs; and 3) mediastinal LN DCs express MARCO after OVA challenge (data not shown). This suggests that pulmonary DCs start to express MARCO after allergen encounter, consistent with the increased MARCO gene expression observed after OVA challenge in microarray studies.

Some limitations of the study merit discussion. For some control experiments, only MARCO-deficient mice were analyzed (e.g., the migration of DCs in OVA-sensitized mice; Fig. 5*E*). Hence, the full extent to which SR-AI/II deficiency mirrors the findings with MARCO-deficient mice requires further characterization. One potential problem to be considered is the confounding effects of trace endotoxin in the OVA allergen. Two lines of evidence argue against this possibility. First, no differences were observed in the numbers of migrated $FITC^+CD11C^+$ DCs found in either endotoxin-sensitive or endotoxin-resistant thoracic LNs (C3H/Ouj and C3H/HeJ respectively). Second, we have previously reported similar levels of cytokine release (TNF-α and MIP-2) by AMs from WT and KO mice in response to LPS in vitro (9), arguing against differential responses on this basis.

In peripheral tissues such as the lungs, DCs exist normally in an immature state and provide a sentinel function for foreign Ags (32). Upon Ag encounter, DCs undergo a process of maturation that triggers their migration to draining LNs and enhances their Ag-presenting capacity (23). The migration of Ag-loaded DCs from peripheral tissues to the LNs is a critical step in generating an optimal immune response (33, 34) and, hence, a potential regulatory point.

SR-As may inhibit DC migration through a number of mechanisms. SR-As have been shown to promote adhesion to matrix molecules (35, 36) and to other cells, e.g., marginal zone macrophages to B cells (37), and either of these interactions could potentially reduce cell migration. Pikkarainen et al. (38) have previously shown that fibroblastic cell lines transfected with MARCO undergo significant morphologic changes through the induction of dendritic plasma membrane processes. These processes include the appearance of large lamellipodia-like structures and long plasma membrane extensions. Moreover, a clear correlation exists between MARCO expression and the rearranged actin cytoskeleton of mature DCs (30), although in this study MARCO expression upon maturation was associated with a decrease in filopodia and a round phenotype. The morphologic changes induced by simple MARCO expression do not require its interaction with any given ligand. The rearrangements induced by MARCO in fibroblastic cell lines were shown to be partially dependent on Rac1 (38). Rac, together with Rho and Cdc42, represent a group of small GTPases involved in the formation of filopodia and podosomes in immature DCs (39), structural changes that could increase adhesion and reduce migration. To test the speculation that adhesion to a matrix might mediate some of the observed effects, studies of the kinetics of induction of MARCO expression on airway and LN DCs after allergen challenge are warranted, as well as a comparison of the migration capacity of MARCO-deficient and WT DCs. Additional mechanisms are suggested by data indicating the ability of scavenger receptors, when present, to skew the cytokine milieu and immune response toward Th1-type immunity (40). Indeed, one of the mechanisms leading to increased AHR in allergic asthma is the enhanced recruitment of eosinophils into the allergen-challenged airways as we observed in the lungs of SR-A deficient mice. This may be a consequence of the increased recruitment of Th lymphocytes and an altered cytokine milieu.

Innate immune responses are increasingly recognized as critical modifiers of adaptive immunity (41, 42). In the example presented here, the innate pattern recognition receptors, the SR-As, mediate reduced amounts of total Ag delivery to LNs (through decreased numbers of DCs carrying similar amounts of Ag per cell). SR-A-mediated down-regulation of lung immune responses likely contributes to the reduction of unwanted immune responses to commonly encountered environmental aeroallergens.

Disclosures

The authors have no financial conflict of interest.

References

1. Pearson, A. M. 1996. Scavenger receptors in innate immunity. *Curr. Opin. Immunol.* 8: 20–28.
2. Krieger, M., and J. Herz. 1994. Structures and functions of multiligand lipoprotein receptors: macrophage scavenger receptors and LDL receptor-related protein (LRP). *Annu. Rev. Biochem.* 63: 601–637.
3. Gough, P. J., and S. Gordon. 2000. The role of scavenger receptors in the innate immune system. *Microbes Infect.* 2: 305–311.
4. Arredouani, M., and L. Kobzik. 2004. The structure and function of MARCO, a macrophage class a scavenger receptor. *Cell. Mol. Biol.* 50: OL657–OL665.
5. van der Laan, L. J., M. Kangas, E. A. Dopp, E. Broug-Holub, O. Elomaa, K. Tryggvason, and G. Kraal. 1997. Macrophage scavenger receptor MARCO: in vitro and in vivo regulation and involvement in the anti-bacterial host defense. *Immunol. Lett.* 57: 203–208.
6. Gough, P. J., D. R. Greaves, and S. Gordon. 1998. A naturally occurring isoform of the human macrophage scavenger receptor (SR-A) gene generated by alternative splicing blocks modified LDL uptake. *J. Lipid Res.* 39: 531–543.
7. Arredouani, M. S., A. Palecanda, H. Koziel, Y. C. Huang, A. Imrich, T. H. Sulahian, Y. Y. Ning, Z. Yang, T. Pikkarainen, M. Sankala, et al. 2005. MARCO is the major binding receptor for unopsonized particles and bacteria on human alveolar macrophages. *J. Immunol.* 175: 6058–6064.
8. Palecanda, A., J. Paulauskis, E. Al-Mutairi, A. Imrich, G. Qin, H. Suzuki, T. Kodama, K. Tryggvason, H. Koziel, and L. Kobzik. 1999. Role of the scavenger receptor MARCO in alveolar macrophage binding of unopsonized environmental particles. *J. Exp. Med.* 189: 1497–1506.
9. Arredouani, M., Z. Yang, Y. Y. Ning, G. Qin, R. Soininen, K. Tryggvason, and L. Kobzik. 2004. The scavenger receptor MARCO is required for normal lung defense against pneumococcal pneumonia and inhaled particles. *J. Exp. Med.* 200: 267–272.
10. Arredouani, M. S., Z. Yang, A. Imrich, Y. Ning, G. Qin, and L. Kobzik. 2006. The macrophage scavenger receptor SR-AI/II and lung defense against pneumococci and particles. *Am. J. Respir. Cell Mol. Biol.* 35: 474–478.
11. Suzuki, H., Y. Kurihara, M. Takeya, N. Kamada, M. Kataoka, K. Jishage, O. Ueda, H. Sakaguchi, T. Higashi, T. Suzuki, et al. 1997. A role for macrophage scavenger receptors in atherosclerosis and susceptibility to infection. *Nature* 386: 292–296.
12. Wu, Z., and R. A. Irizarry. 2004. Preprocessing of oligonucleotide array data. *Nat. Biotechnol.* 22: 656–658.
13. Hamada, K., Y. Suzaki, A. Goldman, Y. Y. Ning, C. Goldsmith, A. Palecanda, B. Coull, C. Hubeau, and L. Kobzik. 2003. Allergen-independent maternal transmission of asthma susceptibility. *J. Immunol.* 170: 1683–1689.
14. Lyons, A. B., J. Hasbold, and P. D. Hodgkin. 2001. Flow cytometric analysis of cell division history using dilution of carboxyfluorescein diacetate succinimidyl ester, a stably integrated fluorescent probe. *Methods Cell Biol.* 63: 375–398.
15. Takeda, K., A. Haczku, J. J. Lee, C. G. Irvin, and E. W. Gelfand. 2001. Strain dependence of airway hyperresponsiveness reflects differences in eosinophil localization in the lung. *Am. J. Physiol.* 281: L394–L402.
16. Shinagawa, K., and M. Kojima. 2003. Mouse model of airway remodeling: strain differences. *Am. J. Respir. Crit. Care Med.* 168: 959–967.
17. Shakushiro, K., Y. Yamasaki, M. Nishikawa, and Y. Takakura. 2004. Efficient scavenger receptor-mediated uptake and cross-presentation of negatively charged soluble antigens by dendritic cells. *Immunology* 112: 211–218.
18. Haberland, M. E., and A. M. Fogelman. 1985. Scavenger receptor-mediated recognition of maleyl bovine plasma albumin and the demaleylated protein in human monocyte macrophages. *Proc. Natl. Acad. Sci. USA* 82: 2693–2697.
19. Abraham, R., N. Singh, A. Mukhopadhyay, S. K. Basu, V. Bal, and S. Rath. 1995. Modulation of immunogenicity and antigenicity of proteins by maleylation to target scavenger receptors on macrophages. *J. Immunol.* 154: 1–8.
20. Vermaelen, K., and R. Pauwels. 2004. Accurate and simple discrimination of mouse pulmonary dendritic cell and macrophage populations by flow cytometry: methodology and new insights. *Cytometry A.* 61: 170–177.
21. Lambrecht, B. N., M. De Veerman, A. J. Coyle, J. C. Gutierrez-Ramos, K. Thielemans, and R. A. Pauwels. 2000. Myeloid dendritic cells induce Th2 responses to inhaled antigen, leading to eosinophilic airway inflammation. *J. Clin. Invest.* 106: 551–559.
22. Banchereau, J., and R. M. Steinman. 1998. Dendritic cells and the control of immunity. *Nature* 392: 245–252.
23. Banchereau, J., F. Briere, C. Caux, J. Davoust, S. Lebecque, Y. J. Liu, B. Pulendran, and K. Palucka. 2000. Immunobiology of dendritic cells. *Annu. Rev. Immunol.* 18: 767–811.
24. Geng, Y. J., and G. K. Hansson. 1995. High endothelial cells of postcapillary venules express the scavenger receptor in human peripheral lymph nodes. *Scand. J. Immunol.* 42: 289–296.
25. Abraham, R., A. Choudhury, S. K. Basu, V. Bal, and S. Rath. 1997. Disruption of T cell tolerance by directing a self antigen to macrophage-specific scavenger receptors. *J. Immunol.* 158: 4029–4035.
26. Bansal, P., P. Mukherjee, S. K. Basu, A. George, V. Bal, and S. Rath. 1999. MHC class I-restricted presentation of maleylated protein binding to scavenger receptors. *J. Immunol.* 162: 4430–4437.
27. Singh, N., S. Bhatia, R. Abraham, S. K. Basu, A. George, V. Bal, and S. Rath. 1998. Modulation of T cell cytokine profiles and peptide-MHC complex availability in vivo by delivery to scavenger receptors via antigen maleylation. *J. Immunol.* 160: 4869–4880.
28. Yang, G., J. Addai, W. H. Tian, A. Frolov, T. M. Wheeler, and T. C. Thompson. 2004. Reduced infiltration of class A scavenger receptor positive antigen-presenting cells is associated with prostate cancer progression. *Cancer Res.* 64: 2076–2082.
29. Nicoletti, A., G. Caligiuri, I. Tornberg, T. Kodama, S. Stemme, and G. K. Hansson. 1999. The macrophage scavenger receptor type A directs modified proteins to antigen presentation. *Eur. J. Immunol.* 29: 512–521.
30. Granucci, F., F. Petralia, M. Urbano, S. Citterio, F. Di Tota, L. Santambrogio, and P. Ricciardi-Castagnoli. 2003. The scavenger receptor MARCO mediates cytoskeleton rearrangements in dendritic cells and microglia. *Blood* 102: 2940–2947.
31. Re, F., S. L. Belyanskaya, R. J. Riese, B. Cipriani, F. R. Fischer, F. Granucci, P. Ricciardi-Castagnoli, C. Brosnan, L. J. Stern, J. L. Strominger, and

L. Santambrogio. 2002. Granulocyte-macrophage colony-stimulating factor induces an expression program in neonatal microglia that primes them for antigen presentation. *J. Immunol.* 169: 2264–2273.
32. Cella, M., F. Sallusto, and A. Lanzavecchia. 1997. Origin, maturation and antigen presenting function of dendritic cells. *Curr. Opin. Immunol.* 9: 10–16.
33. Vermaelen, K. Y., I. Carro-Muino, B. N. Lambrecht, and R. A. Pauwels. 2001. Specific migratory dendritic cells rapidly transport antigen from the airways to the thoracic lymph nodes. *J. Exp. Med.* 193: 51–60.
34. Gunn, M. D., S. Kyuwa, C. Tam, T. Kakiuchi, A. Matsuzawa, L. T. Williams, and H. Nakano. 1999. Mice lacking expression of secondary lymphoid organ chemokine have defects in lymphocyte homing and dendritic cell localization. *J. Exp. Med.* 189: 451–460.
35. el Khoury, J., C. A. Thomas, J. D. Loike, S. E. Hickman, L. Cao, and S. C. Silverstein. 1994. Macrophages adhere to glucose-modified basement membrane collagen IV via their scavenger receptors. *J. Biol. Chem.* 269: 10197–10200.
36. Gowen, B. B., T. K. Borg, A. Ghaffar, and E. P. Mayer. 2000. Selective adhesion of macrophages to denatured forms of type I collagen is mediated by scavenger receptors. *Matrix Biol.* 19: 61–71.
37. Karlsson, M. C., R. Guinamard, S. Bolland, M. Sankala, R. M. Steinman, and J. V. Ravetch. 2003. Macrophages control the retention and trafficking of B lymphocytes in the splenic marginal zone. *J. Exp. Med.* 198: 333–340.
38. Pikkarainen, T., A. Brannstrom, and K. Tryggvason. 1999. Expression of macrophage MARCO receptor induces formation of dendritic plasma membrane processes. *J. Biol. Chem.* 274: 10975–10982.
39. Burns, S., A. J. Thrasher, M. P. Blundell, L. Machesky, and G. E. Jones. 2001. Configuration of human dendritic cell cytoskeleton by Rho GTPases, the WAS protein, and differentiation. *Blood* 98: 1142–1149.
40. Bhatia, S., S. Mukhopadhyay, E. Jarman, G. Hall, A. George, S. K. Basu, S. Rath, J. R. Lamb, and V. Bal. 2002. Scavenger receptor-specific allergen delivery elicits IFN-γ-dominated immunity and directs established TH2-dominated responses to a nonallergic phenotype. *J. Allergy Clin. Immunol.* 109: 321–328.
41. Janeway, C. A., Jr., and R. Medzhitov. 2002. Innate immune recognition. *Annu. Rev. Immunol.* 20: 197–216.
42. Reis e Sousa, C. 2004. Toll-like receptors and dendritic cells: for whom the bug tolls. *Semin. Immunol.* 16: 27–34.

Protection against inhaled oxidants through scavenging of oxidized lipids by macrophage receptors MARCO and SR-AI/II

Morten Dahl,[1] Alison K. Bauer,[2] Mohamed Arredouani,[1] Raija Soininen,[3] Karl Tryggvason,[4] Steven R. Kleeberger,[2] and Lester Kobzik[1]

[1]Department of Environmental Health, Harvard School of Public Health, Harvard Medical School, Boston, Massachusetts, USA.
[2]Laboratory of Respiratory Biology, National Institute of Environmental Health Sciences, NIH, Research Triangle Park, North Carolina, USA.
[3]Department of Medical Biochemistry and Molecular Biology, Biocenter Oulu, University of Oulu, Oulu, Finland.
[4]Division of Matrix Biology, Department of Medical Biochemistry and Biophysics, Karolinska Institutet, Stockholm, Sweden.

Alveolar macrophages (AMs) express the class A scavenger receptors (SRAs) macrophage receptor with collagenous structure (MARCO) and scavenger receptor AI/II (SRA-I/II), which recognize oxidized lipids and provide innate defense against inhaled pathogens and particles. Increased MARCO expression in lungs of ozone-resistant mice suggested an additional role protecting against inhaled oxidants. After ozone exposure, MARCO$^{-/-}$ mice showed greater lung injury than did MARCO$^{+/+}$ mice. Ozone is known to generate oxidized, proinflammatory lipids in lung lining fluid, such as 5β,6β-epoxycholesterol (β-epoxide) and 1-palmitoyl-2-(9′-oxo-nonanoyl)-glycerophosphocholine (PON-GPC). Intratracheal instillation of either lipid caused substantial neutrophil influx in MARCO$^{-/-}$ mice, but had no effect in MARCO$^{+/+}$ mice. Normal AMs showed greater uptake in vitro of β-epoxide compared with MARCO$^{-/-}$ AMs, consistent with SRA function in binding oxidized lipids. SR-AI/II$^{-/-}$ mice showed similar enhanced acute lung inflammation after β-epoxide or another inhaled oxidant (aerosolized leachate of residual oil fly ash). In contrast, subacute ozone exposure did not enhance inflammation in SR-AI/II$^{-/-}$ versus SR-AI/II$^{+/+}$ mice, reflecting increased AM expression of MARCO. These data identify what we believe to be a novel function for AM SRAs in decreasing pulmonary inflammation after oxidant inhalation by scavenging proinflammatory oxidized lipids from lung lining fluids.

Introduction

Inhaled oxidants are important causes of environmental lung injury, and the oxidative stress caused by air pollution and tobacco smoke can contribute to the pathogenesis of chronic obstructive pulmonary disease (COPD) and asthma (1, 2). The first point of contact between lung tissue and inhaled oxidants is the epithelial lining fluid. If levels of antioxidants in the lining fluid are inadequate to control activities of the inhaled oxidants, secondary oxidation products arise, which can pass on the oxidative stress to the surrounding milieu and underlying epithelium (3). By exposing bovine surfactant to ozone, Murphy and colleagues identified 5β,6β-epoxycholesterol (β-epoxide) and 1-palmitoyl-2-(9′-oxo-nonanoyl)-glycerophosphocholine (PON-GPC) as 2 major surfactant-derived oxidation products (4, 5). Both lipids are proinflammatory and may contribute to lung inflammation after ozone inhalation (4, 5). As surfactant covers a large fraction of the pulmonary epithelium, β-epoxide and PON-GPC can reach relatively high concentrations on the surface and be widely distributed during conditions of oxidative stress. Rapid clearance of oxidized surfactant lipids from the lung lining fluid therefore seems critical for a successful host response against inhaled oxidants.

Macrophage receptor with collagenous structure (MARCO) and scavenger receptor AI/II (SR-AI/II) are class A scavenger receptors (SRAs) on macrophages with potential functions in host defense against modified lipids (6). MARCO and SR-AI share the same overall domain structure, but differ in that MARCO has a longer extracellular domain and lacks an α–helical coiled coil domain (7). SR-AI and SR-AII are 2 similar receptors generated through alternative splicing of a single gene. Macrophage scavenger receptors have long been known to clear modified lipids and contribute to foam cell formation during atherogenesis (8). They also function as part of innate defense systems in the lung, as scavenger receptors on alveolar macrophages (AMs) have been shown to bind environmental particles and bacteria (9–11). However, their role in protecting the lung against oxidized surfactant lipids generated by inhaled oxidants has not to our knowledge been examined previously.

Gene expression profiling identified increased MARCO expression in lungs of ozone-resistant mice, suggesting a protective role for this receptor. Using mice with genetic deletion of MARCO or SR-AI/II, we analyzed their specific in vivo roles in regulating lung inflammation in response to 2 inhaled oxidants, ozone and residual oil fly ash (ROFA). We also examined the in vivo role of MARCO and SR-AI/II in lungs exposed to oxidized surfactant lipids such as β-epoxide and PON-GPC. Absence of MARCO increased BAL markers of lung inflammation and injury after inhalation of ozone or ROFA leachate and after instillation of B-epoxie or PON-GPC. In vitro studies confirmed diminished uptake of oxidized lipids by MARCO-deficient AMs. Our data identify what we believe to be a novel role for MARCO

Nonstandard abbreviations used: AM, alveolar macrophage; BAL, bronchoalveolar lavage; COPD, chronic obstructive pulmonary disease; β-epoxide, 5β,6β-epoxycholesterol; i.t., intratracheal(ly); MARCO, macrophage receptor with collagenous structure; MIP-2, macrophage inflammatory protein–2; PMN, polymorphonuclear leukocyte; PON-GPC, 1-palmitoyl-2-(9′-oxo-nonanoyl)-glycerophosphocholine; ROFA, residual oil fly ash; SRA, scavenger receptor class A; SR-AI/II, scavenger receptor AI/II.

Conflict of interest: The authors have declared that no conflict of interest exists.

Citation for this article: *J. Clin. Invest.* **117**:757–764 (2007). doi:10.1172/JCI29968.

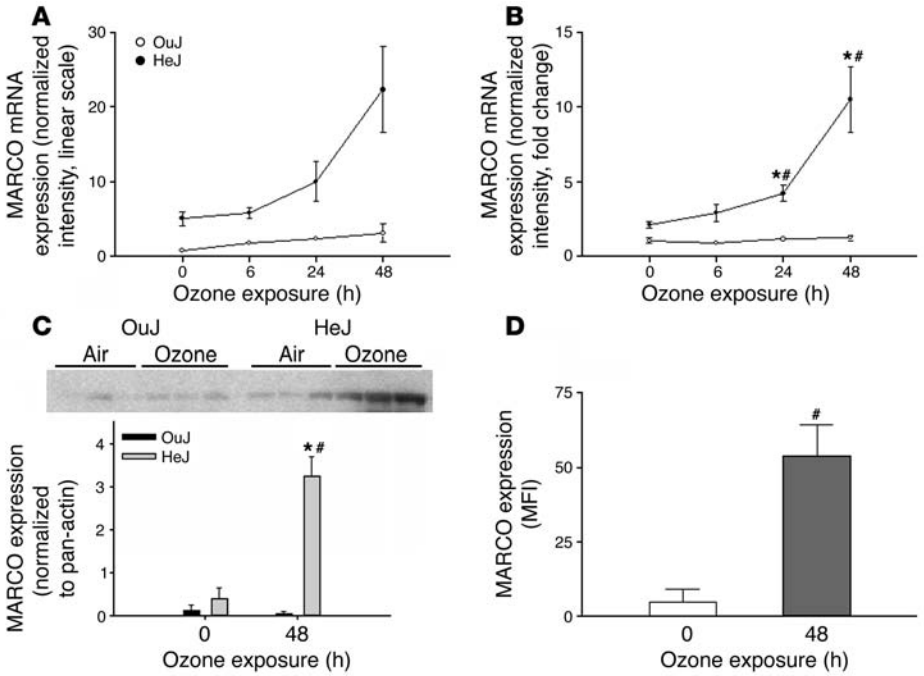

Figure 1
Ozone upregulates MARCO in lungs from ozone-resistant HeJ mice. HeJ or congenic ozone-sensitive OuJ mice were exposed to 0.3 ppm ozone for up to 48 hours. Microarray analysis (**A**) and RT-PCR (**B**) were performed on total RNA isolated from lung samples and showed increased MARCO mRNA expression in HeJ mice (filled symbols) compared with OuJ mice (open symbols). (**C**) Western blot analysis of lung tissue obtained after 48 hours of ozone exposure also showed increased MARCO protein expression. (**D**) Ozone upregulates MARCO on the surface of AMs of C57BL/6 mice exposed to 0.3 ppm ozone for 48 hours, as shown by increased fluorescence after flow cytometric analysis. Results shown are representative of 3 independent experiments. MFI, mean fluorescence intensity. $^{*}P < 0.05$ versus ozone-treated OuJ; $^{\#}P < 0.05$ versus air-exposed control.

and SR-AI/II in innate defenses against inhaled oxidants: beneficial scavenging of oxidized surfactant lipids from damaged lung lining fluids.

Results

Increased expression of MARCO after ozone exposure in vivo. In order to identify potential mediators of the ozone resistance previously observed in C3H/HeJ mice (12), we used microarray profiling and RT-PCR to analyze gene expression in lungs of ozone-resistant (C3H/HeJ) and consomic, ozone-sensitive (C3H/OuJ) mice. Analysis after exposure to 0.3 ppm ozone for 48 hours showed increased MARCO mRNA expression at 24 and 48 hours in C3H/HeJ compared with C3H/OuJ mice (Figure 1, A and B). Western blot analysis of lung tissue from C3H/HeJ mice after 48 hours of 0.3-ppm ozone exposure confirmed the increased MARCO expression at the protein level (Figure 1C).

Because the increased MARCO expression in whole-lung homogenate samples could be caused by increased lung macrophage numbers after ozone inhalation, we next isolated AMs from C57BL/6 mice also exposed to 0.3 ppm ozone for 48 hours and immunostained them for cell surface MARCO. We found that MARCO was significantly upregulated on the surface of AMs from C57BL/6 mice in response to ozone exposure (Figure 1D), facilitating further analysis using C57BL/6 mice with a specific deletion of the *MARCO* gene (9, 13).

MARCO decreases inflammation in the lungs of mice exposed to ozone. To examine whether MARCO deficiency modulates lung inflammation in response to ozone, we exposed $MARCO^{+/+}$ and $MARCO^{-/-}$ mice to 0.3 ppm ozone for 48 hours and performed bronchoalveolar lavage (BAL). As expected, ozone caused increased neutrophil numbers in BAL fluid from $MARCO^{+/+}$ mice; however, the increase was 2-fold higher in $MARCO^{-/-}$ than in $MARCO^{+/+}$ mice (20×10^4 versus 8×10^4; $P = 0.003$; Figure 2A). Ozone mediates oxidative damage to the alveolocapillary membrane, and proteins leak from plasma into alveoli. Ozone caused increased BAL protein levels in $MARCO^{+/+}$ mice, but the ozone-associated increase in BAL protein was slightly higher in $MARCO^{-/-}$ than $MARCO^{+/+}$ mice (Figure 2B). Ozone exposure also cause increased oxidative stress, which may result in the formation of 8-isoprostane from arachidonic acid phospholipids (14, 15). The relatively low concentration of ozone used in our exposures (0.3 ppm) had no detectable effect on the level of 8-isoprostane in BAL samples from $MARCO^{+/+}$ mice, but increased BAL 8-isoprostane levels in $MARCO^{-/-}$ mice (Figure 2C). Hence, the presence of MARCO reduced the intensity of injury in lungs of $MARCO^{+/+}$ mice exposed to ozone, as measured by levels of neutrophils, protein, and 8-isoprostane.

MARCO decreases neutrophil accumulation in the lungs of mice exposed to aerosolized ROFA. To examine whether MARCO inhibits inflammation in lungs exposed to other inhaled oxidants besides ozone, we next exposed $MARCO^{-/-}$ mice to aerosolized leachate from ROFA, a surrogate for air pollution particulates (100 mg/ml for 1 hour). The soluble metals present in dissolved ROFA (leachate) constitute most of the mass of ROFA samples and provide a useful model of acute lung injury following aerosol exposure (16). As expected, brief exposure to ROFA aerosol (1 hour) caused increased neutrophilia in $MARCO^{+/+}$ mice upon BAL analysis 18 hours later. Strikingly, the increase was 5-fold higher in $MARCO^{-/-}$ than in $MARCO^{+/+}$ mice (5×10^4 versus 1×10^4; $P < 0.001$; Figure 2D). BAL isoprostane levels were minimal and not different between the 2 groups after these ROFA exposures which cause a lower absolute level of BAL neutrophilia than seen after ozone exposures (data not shown). After exposure to a higher concentration of ROFA (leachate of 300 mg/ml for 1.5 hours), $MARCO^{-/-}$ mice showed increased levels — similar to those following ozone exposure — of BAL polymorphonuclear leukocytes (PMNs) compared with $MARCO^{+/+}$ mice (20×10^4 versus 14×10^4, average of 5 mice per group) and a corresponding trend for increased BAL isoprostanes (8.2 pg/ml versus 5.5 pg/ml).

MARCO decreases inflammation in the lungs of mice exposed to oxidized lipids in vivo. Ozone exposure of lung lining fluid cholesterol creates β-epoxide, an oxidized surfactant lipid that is cytotoxic in vitro

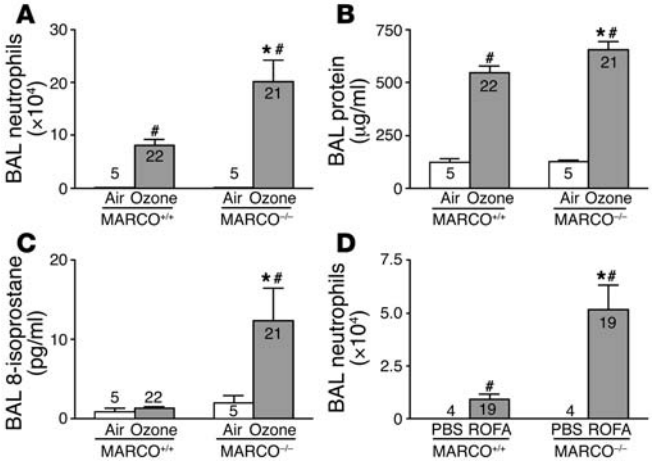

Figure 2
MARCO decreases inflammation in lungs of mice exposed to ozone and ROFA. (**A**–**C**) BAL samples obtained from MARCO$^{-/-}$ mice after exposure to 0.3 ppm ozone for 48 hours showed higher levels of neutrophils (**A**), total protein (**B**), and 8-isoprostane (**C**) compared with controls. (**D**) BAL samples obtained from MARCO$^{-/-}$ mice 18 hours after exposure to aerosolized leachate from ROFA (100 mg/ml, 1 hour) showed higher levels of neutrophils compared with controls. Number of mice per group is shown for each bar. *P < 0.05 versus treated MARCO$^{+/+}$ group; #P < 0.05 versus untreated.

and may contribute to lung inflammation after ozone inhalation (4, 17). Also, ozonolysis of unsaturated surfactant glycerophosphocholines creates PON-GPC (5). To determine whether MARCO protects against these oxidized surfactant lipids, we instilled 1 μg β-epoxide or PON-GPC intratracheally (i.t.) into MARCO$^{-/-}$ mice. We found that i.t. instillation of either β-epoxide or PON-GPC into MARCO$^{-/-}$ mice caused substantial neutrophil influx, whereas these agents had no effect in MARCO$^{+/+}$ mice at this dose (Figure 3A). Instillation of a 100-fold greater dose of either β-epoxide or PON-GPC into MARCO$^{+/+}$ mice did cause BAL neutrophilia ($2.3 \pm 2.8 \times 10^4$ and $17 \pm 21 \times 10^4$, n = 5 and 2, respectively), confirming the proinflammatory potential of these agents when present in sufficient concentration. Instillation of β-epoxide and PON-GPC i.t. into MARCO$^{-/-}$ mice also caused increased levels of the neutrophil chemoattractant macrophage inflammatory protein–2 (MIP-2) and total protein in BAL fluid, while no such effects were observed in MARCO$^{+/+}$ mice (Figure 3, B and C).

MARCO promotes lipid accumulation in AMs exposed to β-epoxide in vitro. To examine the role of MARCO in scavenging β-epoxide, we incubated MARCO$^{-/-}$ and MARCO$^{+/+}$ AMs with β-epoxide for 24 hours and quantitated cellular lipid content by flow cytometry after labeling with the fluorescent dye Nile Red. We found that MARCO$^{-/-}$ AMs exhibited diminished uptake compared with MARCO$^{+/+}$ AMs, as evidenced by lower staining for cellular lipids after β-epoxide incubation (relative fluorescence, MARCO$^{+/+}$, 30.8 ± 10.7; MARCO$^{-/-}$, 10.3 ± 10.3). Viability of MARCO$^{-/-}$ and MARCO$^{+/+}$ AMs were similar at 95% and 94%, respectively, after 18 hours of β-epoxide incubation.

SR-AI/II decreases neutrophil accumulation in the lungs of mice exposed to ROFA and β-epoxide in vivo. In order to determine whether the other major macrophage SRA, SRA-I/II, also protects against inhaled oxidants, we exposed SR-AI/II$^{+/+}$ and SR-AI/II$^{-/-}$ mice to ROFA aerosols or β-epoxide by i.t. instillation and measured acute lung inflammatory responses by BAL analysis 7 hours later. While the ROFA aerosol caused a small increase in BAL neutrophils in SR-AI/II$^{+/+}$ mice, the increase was substantially higher in SR-AI/II$^{-/-}$ mice (9.9×10^4 versus 0.8×10^4; P = 0.002; Figure 4A). Similarly, i.t. instillation of β-epoxide into SR-AI/II$^{-/-}$ mice caused substantial neutrophil influx, whereas it had no effect in SR-AI/II$^{+/+}$ mice (11×10^4 versus 0.2×10^4; P < 0.001; Figure 4B).

We also evaluated responses after the longer exposures to inhaled ozone (0.3 ppm for 48 hours). In contrast to findings with MARCO$^{-/-}$ mice, ozone caused similar small increases in neutrophils in SR-AI/II$^{+/+}$ and SR-AI/II$^{-/-}$ mice (Figure 4C). Because ozone exposure was associated with increased expression of MARCO in normal or wild-type mice (Figure 1), we sought to determine whether increased expression of MARCO also occurs in SR-AI/II$^{-/-}$ mice. We isolated AMs from SR-AI/II$^{-/-}$ mice exposed to 0.3 ppm ozone for 48 hours, immunostained for cell surface MARCO, and quantified the expression using flow cytometry. We found that SR-AI/II$^{-/-}$ AMs exhibited substantially higher staining for MARCO after ozone exposure compared with air-exposed controls (Figure 5).

Discussion

Our interest in the role of the macrophage SRAs MARCO and SR-AI/II in regulating lung inflammation after ozone inhalation began with microarray data showing increased pulmonary

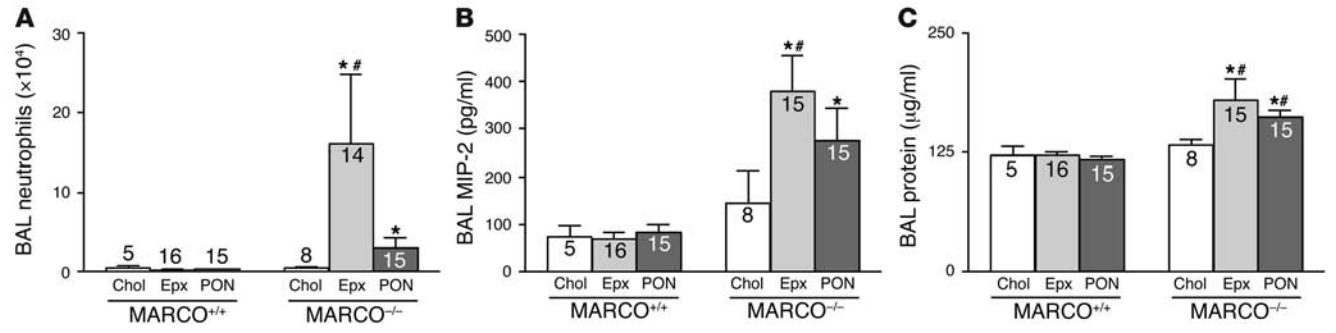

Figure 3
MARCO decreases inflammation in lungs of mice exposed to β-epoxide or PON-GPC i.t. BAL samples obtained from MARCO$^{-/-}$ mice 7 hours after i.t. instillation of 1 μg β-epoxide (Exp) or PON-GPC (PON) showed higher levels of neutrophils (**A**), MIP-2 (**B**), and total protein (**C**) compared with controls. Number of mice per group is shown for each bar. *P < 0.05 versus respective treated MARCO$^{+/+}$ group; #P < 0.05 versus cholesterol (Chol) control.

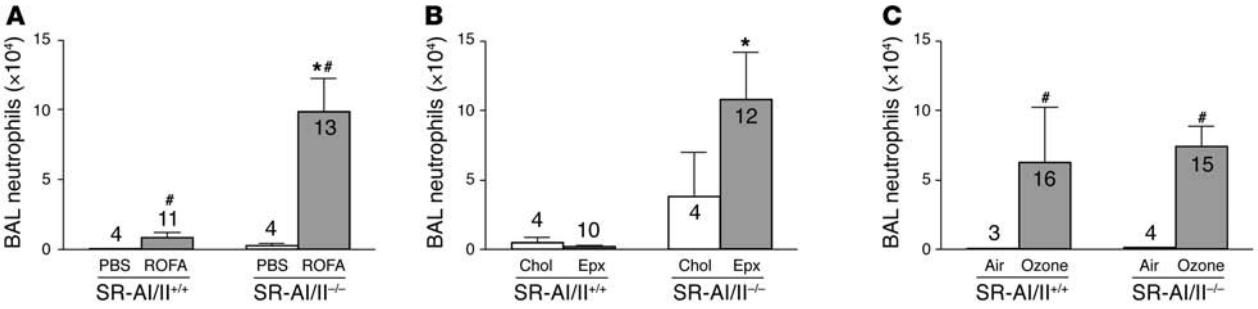

Figure 4
SR-AI/II decreases neutrophil accumulation in lungs of mice exposed to ROFA and i.t. β-epoxide, but not ozone. SR-AI/II$^{-/-}$ mice received aerosolized leachate from ROFA (100 mg/ml for 1 hour; **A**), 1 μg i.t. β-epoxide (**B**), or 0.3 ppm ozone (**C**) for 48 hours. Number of mice per group is shown for each bar. *$P < 0.05$ versus treated SR-AI/II$^{+/+}$ group; #$P < 0.05$ versus untreated control.

MARCO mRNA expression in ozone-resistant HeJ mice, but not in ozone-sensitive OuJ mice (Figure 1). While this initial hypothesis-generating data came from HeJ and OuJ mice, we subsequently determined that ozone inhalation also increased MARCO expression on AMs from C57BL/6 mice, allowing more detailed analyses using mice deficient in MARCO (available on a C57BL/6 background). We found that absence of MARCO increased lung inflammation after inhalation of ozone and another inhaled oxidant, aerosolized ROFA leachate. These findings prompted further examination of the role of lung macrophage MARCO in uptake and removal of oxidized surfactant lipids such as β-epoxide and PON-GPC. Our analyses showed that MARCO mediated intracellular lipid accumulation after incubation of lung macrophages with β-epoxide in vitro. MARCO acted to protect lungs against inflammation after β-epoxide and PON-GPC instillation in vivo, as shown by increased inflammatory responses in MARCO$^{-/-}$ mice. Taken together, these data suggest what we believe to be a previously unrecognized role for lung macrophage SRAs in lung defense against inhaled oxidants through clearance of otherwise proinflammatory oxidized surfactant lipids from damaged lung lining fluids.

Our data show similar, but not identical, functions for the 2 receptors studied, MARCO and SR-AI/II. We found that SR-AI/II, also contributed to protection of the lungs against acute inflammation, as determined by the number of BAL neutrophils after ROFA and β-epoxide exposure. In contrast to MARCO$^{-/-}$ mice, however, SR-AI/II$^{-/-}$ mice did not show increased inflammation in experiments using 48 hours of exposure to ozone. After such ozone exposure, we observed increased expression of MARCO on AMs from both SR-AI/II$^{+/+}$ and SR-AI/II$^{-/-}$ mice, suggesting a protective effect of MARCO in both groups. Moreover, it is noteworthy that ozone exposure did not cause increased expression of the gene encoding SR-AI/II in the same microarray analyses that revealed increased MARCO expression in the ozone-resistant HeJ mice (data not shown). One interpretation is that basal levels of SR-AI/II contribute to clearance of proinflammatory oxidized lipids generated by the acute challenges of ROFA aerosols or direct instillation of β-epoxide. Comparison of data from these more acute exposures with those of the 48-hour ozone experiments suggest that the basal and unchanged level of SR-AI/II is insufficient for optimal clearance of oxidized lipids generated during the longer exposure to ozone, a task mediated by the increased MARCO expression we observed in the ozone model. It is also possible that during repair of inflammation, scavenger receptors may be involved in binding and clearing cellular debris, thereby hampering further amplification of the inflammation in the lung. Hence, to the extent that such repair processes are initiated at the 48-hour time point of the ozone exposure, MARCO and SR-AI/II may limit inflammation through mechanisms beyond the proposed binding of oxidized lipids.

It is worth noting that ozone and ROFA generate different lipid oxidation products. Ozone produces specific lipid ozonation products plus nonspecific lipid autoxidation from both ozone-initiated reactions within the epithelial lining fluid and after the onset of the inflammatory response. On the other hand, ROFA likely generates oxidized lipids via transition metal redox cycling as well as inflammation. Production of β-epoxide occurs in both scenarios, while PON-GCP should be relatively specific to ozone reactions. To facilitate comparison of ROFA to ozone exposures, we also analyzed BAL PMNs and isoprostanes using a higher ROFA concentration, which caused levels of PMNs comparable to those seen with ozone. Under these conditions, MARCO$^{-/-}$ mice showed a higher number of BAL PMNs and a trend toward higher 8-isoprostane levels. These data further support the conclusion that MARCO can scavenge a range of oxidatively modified lipids rather than being strictly specific for autoxidation-derived lipids.

When β-epoxide and PON-GCP were administered to MARCO$^{+/+}$ mice, MARCO appeared to inhibit the inflammatory response to the oxidized lipids in full. When MARCO$^{+/+}$ mice were exposed to ROFA or ozone, MARCO only partly decreased the inflammatory

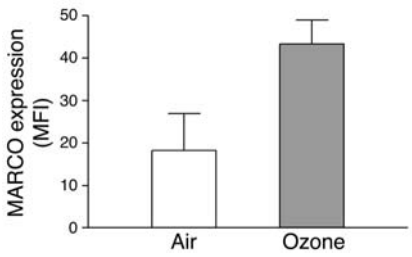

Figure 5
Ozone upregulates MARCO on the surface of SR-AI/II$^{-/-}$ AMs. SR-AI/II$^{-/-}$ mice were exposed to 0.3 ppm ozone for 48 hours, after which the AMs were isolated, labeled for MARCO, and analyzed by flow cytometry. Results shown are representative of 2 independent experiments.

response, indicating that other oxidized products are capable of inducing inflammation in MARCO$^{+/+}$ mice. At 100-fold greater doses, both β-epoxide and PON-GCP caused neutrophil influx in MARCO$^{+/+}$ mice 7 hours after instillation (2.3×10^4 and 17×10^4, respectively). At lower doses, the oxidized surfactant lipids did not seem critical to the inflammatory response in MARCO$^{+/+}$ mice, probably because MARCO and other scavenger receptors were capable of clearing the lipids sufficiently from the lung surface.

We have previously shown important functions for MARCO and SR-AI/II in innate immune responses against bacteria and environmental particles (9–11). The current data indicate that MARCO and SR-AI/II are also involved in clearing oxidized surfactant lipids in the lung. In atherosclerosis, scavenger receptors have long been known to take up oxidized lipids and contribute to foam cell formation (8, 18, 19). While SR-AI/II is implicated in lipid loading of macrophage-derived foam cells during atherogenesis (18, 20–22), the receptor is also expressed on AMs, indicating that it may be engaged in metabolism of modified lipids in the lung. MARCO is upregulated on human foam cells (23) and on foam cells in atherosclerotic lesions from mice (24, 25), and a high-fat diet causes increased MARCO mRNA expression in the lungs and livers of C57BL/6 mice (25), further supporting a role for MARCO in lipid uptake in the lung.

Lipid ozonation products from surfactant are essential for the transmission of toxic signals to the pulmonary epithelium after ozone inhalation (3, 26, 27). The oxidized surfactant lipids β-epoxide and PON-GPC are important lipid ozonation products implicated in this process. They are created from cholesterol and oleate- and palmitoyl-containing glycerophosphocholines, which constitute about 5% and 20%, respectively, of the lung surfactant (28, 29). Also, β-epoxide is created from cholesterol in cell membranes. Both lipids are detected in vitro after exposing bovine surfactant to ozone (4, 5), and β-epoxide and nonanals are detected in vivo in BALs after exposing rodents to ozone (17, 30). We are not aware of previous studies measuring β-epoxide and PON-GPC using the 48-hour exposure conditions of the present study. However, exposing C57BL/6 mice to 0.5 ppm ozone for 3 hours creates 2.5 ng β-epoxide per ml BAL, and unexposed lungs from C57BL/6 mice have β-epoxide levels of approximately 95 ng per lung (17). Our data using bolus instillation of 1 μg β-epoxide and PON-GPC provide a proof-of-principle, but future studies would benefit by more detailed measurement of the BAL levels of oxidized lipids during the 48-hour exposure to ozone.

Macrophages have previously been shown to take up β-epoxide (31), whereas PON-GPC uptake by macrophages is less well described. Lipid ozonation products regulate several proinflammatory cytokines, chemokines, and adhesion molecules (5, 32–37). Both β-epoxide and PON-GPC have specifically been associated with cytotoxic activities and expression of IL-8 (5, 32), an important neutrophil chemoattractant after ozone exposure (3, 38, 39). In the present study, viability of AMs was relatively unaffected by β-epoxide incubation (16 μg/ml), in contrast to previous studies of cell lines in which this dose has been shown to have cytotoxic effects (4, 32, 40). One explanation might be that the primary cells used in our assay resist the cytotoxic effect better than cell lines do. Alternatively, differences in our assay compared with previous studies may also account for the better cell survival we observed. Consistent with prior observations of β-epoxide and PON-GPC as potential stimulators of IL-8 release (5, 32), MIP-2, a rodent homolog of human IL-8, was markedly increased after i.t. instillation of β-epoxide or PON-GPC into MARCO$^{-/-}$ mice.

Both lung epithelial cells and macrophages express CXC chemokine mRNA and protein after ozone exposure in vivo (38, 41). MIP-2 expression after oxidant exposure has been localized immunohistochemically to both AMs and alveolar epithelial cells (38, 42). However, these data do not allow quantitation of the relative contribution of epithelial cells versus macrophages to MIP-2 release. One mechanism suggested by our present data is protection of lung epithelial cells from oxidized lipids by AM scavenging. Another possibility is that AM scavenger receptors divert oxidized lipids away from other, more proinflammatory receptors on the same cell and thereby reduce AM-derived MIP-2 and the inflammatory response that follows. In order to begin to address this question, we compared the capacity of AMs from MARCO$^{+/+}$ and MARCO$^{-/-}$ mice to respond to oxidants by secretion of MIP-2. We observed similar fold increases in MIP-2 release in AMs exposed in vitro to H_2O_2 generated by a glucose oxidase–glucose system (43) (fold increase at 50 μg/ml glucose oxidase, MARCO$^{+/+}$, 1.9 ± 0.6; MARCO$^{-/-}$, 1.8 ± 0.4; $n = 3$; our unpublished observations). These data suggest that MARCO$^{-/-}$ AMs retain the ability to respond to oxidants with proinflammatory cytokines, similar to previous observations using LPS (9). The question of the relative contribution of epithelial versus macrophage cytokine release when AM scavenger receptors are absent could be further analyzed in vitro. However, extrapolation to in vivo biology will remain difficult, as previous coculture experiments show enhanced release of CXC chemokines in response to environmental oxidants when AMs and lung epithelial cells are in contact (44).

Oxidants are present in air pollution and tobacco smoke or are released from activated leukocytes during lung inflammation. Increased oxidative stress in terms of increased BAL 8-isoprostane levels has been detected in lungs of smokers, patients with asthma, and patients with COPD (45). Therefore, we exposed MARCO$^{-/-}$ and MARCO$^{+/+}$ mice to the smoke from 4 unfiltered cigarettes and after 6 hours found higher BAL neutrophils in MARCO$^{-/-}$ than in MARCO$^{+/+}$ mice (0.51 versus 0.07×10^4; $n = 8$ and $n = 11$, respectively; $P = 0.02$; our unpublished observations). These data indicate that MARCO protects the lung from acute cigarette smoke exposure. However, because cigarette smoke contains both particulate and gaseous proinflammatory components, whether MARCO protects by scavenging particles, smoke-generated oxidized lipids, or both, remains to be determined in future studies. When the lung lining fluid is under oxidative attack in injuries other than ozone-induced lung disease, significant concentrations of β-epoxide and PON-GPC may be produced and contribute to inflammation. In support of this idea, genetic studies show that the reduced activity of microsomal epoxide hydrolase, an enzyme that metabolizes β-epoxide (46), is associated with a higher risk of COPD and emphysema (47, 48). Other members of the epoxide hydrolase family besides microsomal epoxide hydrolase are also expressed in the lung (49–51), but their relation to the risk of lung disease is less well described.

In conclusion, our data indicate what we believe to be a previously unrecognized role for MARCO and SR-AI/II in innate defenses against inhaled oxidants, scavenging oxidized surfactant lipids from damaged lung lining fluids. This mechanism may apply to proinflammatory oxidized surfactant lipids other than the β-epoxide and PON-GPC we studied. We also speculate that MARCO and SR-AI/II could be involved in a general mechanism to dampen inflammation caused by the oxidized surfactant lipids generated during many forms of pulmonary inflammation and

injury. Similar to the role for scavenger receptors in atherosclerosis (8, 52), SRAs internalize potentially proinflammatory oxidized lipids without engaging the typical phlogistic response in the lungs.

Methods

Animals. Mice (8–12 weeks old) genetically deficient in MARCO or SR-AI/AII on the C57BL/6 background were used in all experiments but the initial gene expression profiling experiments, in which C3H/OuJ and C3H/HeJ mice were used. Age- and sex-matched MARCO$^{+/+}$ and SR-AI/II$^{+/+}$ C57BL/6 mice were used as controls. MARCO$^{-/-}$ mice were developed using homologous recombination and were backcrossed for at least 8 generations to the C57BL/6 background (9, 13). SR-AI/II$^{-/-}$ C57BL/6 mice were generated by disrupting exon 4 of the gene encoding SR-AI/II (also known as macrophage scavenger receptor 1; *Msr1*) as previously described (18) and were kindly provided by T. Kodama (University of Tokyo, Tokyo, Japan). All animals were housed in sterile microisolator cages and had no evidence of spontaneous infection. Ethical approval before all experimentation was obtained from the Harvard Medical Area Animal Use Committee, Boston, Massachusetts, USA.

Ozone exposure. Mice were placed in cages in a 145-l stainless steel chamber with a Plexiglass door and then exposed to 0.3 ppm ozone for 48 hours. As a control, mice were exposed to atmospheric air in a neighboring chamber in the same room. During exposures, mice had continuous access to food and water. Ozone was generated by passing oxygen (Airgas East) through UV light, which was subsequently mixed with room air in the chamber. By the constant drawing of a sample of the chamber atmosphere through a sampling port, the ozone concentration within the chamber was monitored constantly by a UV photometric ozone analyzer (model 49; Thermo Electron Corp.), which was calibrated by a UV photometric ozone calibrator (model 49PS; Thermo Electron Corp.). In this ozone-induced lung disease model, there is acute lung inflammation with primary influx of neutrophils and production of proinflammatory mediators similar to ozone-induced lung injury in humans. BAL was performed within 1 hour after cessation of ozone exposure.

Aerosol exposure to ROFA leachate. A single sample (1 kg) of ROFA, obtained from the precipitator unit of a local power plant, was generously provided by J. Godleski (Harvard School of Public Health, Boston, Massachusetts, USA). ROFA was suspended at 100 mg/ml in PBS, pH 7.4, and sonicated for 10 minutes. After sitting for 30 minutes at room temperature, the ROFA suspension was incubated at 37°C with rotation for 4 hours and then centrifuged at 3,000 *g* for 10 minutes. The supernatant (leachate) was removed and used for aerosol exposures. Mice were exposed to a nebulized aerosol of ROFA leachate for 1 hour within individual compartments of a mouse "pie" chamber (Braintree Scientific) using a Pari IS2 nebulizer (SUN Medical Supply) connected to an air compressor (PulmoAID; DeVilbiss). BAL was performed 18 hours after the aerosol exposure, a time point previously determined to be most representative of maximal neutrophil accumulation and airway hyperresponsiveness in normal or Balb/C mice (16).

Lipid i.t. instillation. Mice were anesthetized by injecting 100–200 μl of 20 mg/ml ketamine hydrochloride (Fort Dodge Laboratories Inc.) intramuscularly into the right thigh. For each mouse, 50 μl of 20 μg/ml β-epoxide (C2648; Sigma-Aldrich), 50 μl of 20 μg/ml PON-GPC (870605; Avanti Polar Lipids), or 50 μl of 20 μg/ml cholesterol (C8667; Sigma-Aldrich) was instilled i.t. BAL was performed 7 hours after i.t. lipid installation.

Affymetrix GeneChip array analysis. The left lungs of C3H/OuJ and C3H/HeJ mice exposed to 0.3 ppm ozone or air (n = 3 per group) for 6, 24, or 48 hours of continuous exposure were processed for Affymetrix microarray analysis. Total RNA was isolated using TRIzol reagent (Invitrogen). cDNA was synthesized using SuperScript choice system (Invitrogen), followed by purification via phenol/chloroform extraction and labeling using an ENZO BioArray RNA transcript labeling kit. Purified biotin-labeled cRNA was then generated with QIAGEN's RNeasy kit and fragmented randomly to about 200 bp (200 mM Tris-acetate, pH 8.2; 500 mM KOAc; and 150 mM MgOAc). Each fragmented cRNA sample was hybridized to Affymetrix Murine Genome U74Av2 oligonucleotide arrays according to the manufacturer's instructions. Fluorescent images were read using a Hewlett-Packard G2500A Gene Array Scanner. Each GeneChip underwent a stringent quality-control regime using Microarray Analysis Software (version 5; Affymetrix) and the following parameters: cRNA fold changes (amount of cRNA obtained from starting RNA); scaling factor; percentage of "Present" calls; signal intensity; housekeeping genes; internal probe set controls; and visual inspection of the .dat files for hybridization artifacts. The expression value (mean difference) for each gene was determined by calculating the mean of differences of intensity (perfect match intensity minus mismatch intensity) between its probe pairs. The expression analysis files created by Microarray Analysis Software (version 5) were transferred to GeneSpring 7.0 (Silicon Genetics) for statistical analyses and characterization of data. All samples were normalized in GeneSpring to OuJ air-exposed controls, similar to previous studies (53). After a stringent filtering of genes, including elimination of absent flags in all groups and inclusion of only those genes with significant interactions for strain and time ($P < 0.05$, 2-way ANOVA), we then identified changes in MARCO expression in OuJ versus HeJ mice at each time point.

RT-PCR. The same total RNA used for the microarray analysis (1 μg) was reverse transcribed into cDNA in a volume of 50 μl. We then used 2.0 μl of cDNA for quantitative PCR using a purchased probe set for MARCO according to the manufacturer's instructions (Mm00440265_m1; PerkinElmer). MARCO expression was normalized to 18S (Hs99999901_s1; PerkinElmer).

Western blotting. A piece of the right lung from the same mice as in the microarray analysis was homogenized in RIPA buffer, and supernatants containing total lung protein were obtained. Total protein (100 μg) was denatured, fractionated by a 10% SDS-PAGE gel, and transferred onto PVDF membranes. After blocking with 5% nonfat dried milk in Tris-buffered saline, pH 7.4, the membrane was incubated with rat anti-MARCO antibody (diluted 1:100; Cell Sciences). The membranes were then incubated with an anti-rat HRP-labeled secondary antibody (Santa Cruz Biotechnology Inc.), and protein signals were visualized with a chemiluminescent reagent (ECL Plus Western blotting detection system; Amersham Biosciences).

Cell isolation and BAL analyses. Mice were euthanized by an overdose of pentobarbital, and their lungs were lavaged 6 times with 0.8 ml ice-cold PBS. Total cell yield was determined by hemocytometer, and differential counts were determined by microscopic evaluation of cytocentrifuge preparations stained with modified Wright-Giemsa. BAL protein levels were determined using the Bio-Rad protein assay, BAL 8-isoprostane was determined by competitive enzyme immunoassay (Cayman Chemical), and BAL MIP-2 was determined by ELISA assay (R&D Systems) according to the manufacturers' instructions.

Flow cytometry. Lavaged AMs from nonexposed MARCO$^{+/+}$ and MARCO$^{-/-}$ mice were plated at 160×10^3/well in cell culture medium, 50 μg/ml cholesterol, or 16 μg/ml β-epoxide in 1% heat-inactivated fetal bovine serum/penicillin/streptomycin/RPMI. After 24 hours, cells were washed 2 times in PBS, resuspended in 200 μl PBS, and incubated on ice with 200–400 ng/ml Nile Red for 20–30 minutes. At least 90% of the cells were viable, as determined by Trypan Blue staining. After incubation, yellow-gold fluorescence emission was collected at 530–560 nm on a Coulter Epics Elite flow cytometer (Beckman Coulter). LPS level in the β-epoxide stock solution (20 μg/ml) was found to be below detection limit (less than 6.25 pg/ml) using the Limulus amebocyte lysate assay (QCL-1000; BioWhittaker).

Lavaged AMs from SR-AI/II$^{+/+}$ and SR-AI/II$^{-/-}$ mice exposed to air or 0.3 ppm ozone for 48 hours were suspended at 2×10^6 per ml and incubated in 20 μg/ml rat anti-mouse CD16/CD32 (catalog no. 553140; BD Biosciences — Pharmingen) for 45 minutes on ice. After 45 minutes, 10 μg FITC-conjugated rat anti-mouse MARCO antibody (catalog no. MCA1849FA; Serotec), 10 μg FITC-conjugated rat anti-mouse IgG antibody (catalog no. MCA1211F; Serotec), or medium was added to each 400-μl cell suspension. After 55 minutes of incubation on ice, cells were washed 2 times in 1.2 ml PBS and resuspended in 5 μg/ml propidium iodine, 1% BSA, and PBS, after which fluorescence emission was collected at 530 nm on the flow cytometer using propidium iodine gating for live cells.

Statistics. Statistical analysis was performed with SPSS version 12. Mann-Whitney *U* test or 2-tailed Student's *t* test was used for comparisons of 2 groups. Results are reported as mean ± SEM. A *P* value less than 0.05 was considered significant.

Acknowledgments

This study was supported by NIH grants ES011008 and ES 00002 (to L. Kobzik) as well as by the Danish Medical Research Council (22-02-0549) to M. Dahl.

Received for publication August 4, 2006, and accepted in revised form December 12, 2006.

Address correspondence to: Lester Kobzik, Department of Environmental Health, Harvard School of Public Health, 665 Huntington Avenue, Boston, Massachusetts 02115, USA. Phone: (617) 432-2247; Fax: (617) 432-0014; E-mail: lkobzik@hsph.harvard.edu.

Morten Dahl and Alison K. Bauer contributed equally to this work.

1. MacNee, W., and Rahman, I. 2001. Is oxidative stress central to the pathogenesis of chronic obstructive pulmonary disease? *Trends Mol. Med.* **7**:55–62.
2. Bowler, R.P. 2004. Oxidative stress in the pathogenesis of asthma. *Curr. Allergy Asthma Rep.* **4**:116–122.
3. Mudway, I.S., and Kelly, F.J. 2000. Ozone and the lung: a sensitive issue. *Mol. Aspects Med.* **21**:1–48.
4. Pulfer, M.K., and Murphy, R.C. 2004. Formation of biologically active oxysterols during ozonolysis of cholesterol present in lung surfactant. *J. Biol. Chem.* **279**:26331–26338.
5. Uhlson, C., et al. 2002. Oxidized phospholipids derived from ozone-treated lung surfactant extract reduce macrophage and epithelial cell viability. *Chem. Res. Toxicol.* **15**:896–906.
6. Elomaa, O., et al. 1995. Cloning of a novel bacteria-binding receptor structurally related to scavenger receptors and expressed in a subset of macrophages. *Cell.* **80**:603–609.
7. Arredouani, M.S., and Kobzik, L. 2004. The structure and function of marco, a macrophage class a scavenger receptor. *Cell. Mol. Biol. (Noisy-le-grand).* **50**:OL657–OL665.
8. Murphy, J.E., Tedbury, P.R., Homer-Vanniasinkam, S., Walker, J.H., and Ponnambalam, S. 2005. Biochemistry and cell biology of mammalian scavenger receptors. *Atherosclerosis.* **182**:1–15.
9. Arredouani, M., et al. 2004. The scavenger receptor MARCO is required for lung defense against pneumococcal pneumonia and inhaled particles. *J. Exp. Med.* **200**:267–272.
10. Arredouani, M.S., et al. 2005. MARCO is the major binding receptor for unopsonized particles and bacteria on human alveolar macrophages. *J. Immunol.* **175**:6058–6064.
11. Arredouani, M.S., et al. 2006. The macrophage scavenger receptor SR-AI/II and lung defense against pneumococci and particles. *Am. J. Respir. Cell Mol. Biol.* **35**:474–478.
12. Kleeberger, S.R., Reddy, S., Zhang, L.Y., and Jedlicka, A.E. 2000. Genetic susceptibility to ozone-induced lung hyperpermeability: role of toll-like receptor 4. *Am. J. Respir. Cell Mol. Biol.* **22**:620–627.
13. Mukhopadhyay, S., et al. 2006. MARCO, an innate activation marker of macrophages, is a class A scavenger receptor for Neisseria meningitidis. *Eur. J. Immunol.* **36**:940–949.
14. Montuschi, P., Nightingale, J.A., Kharitonov, S.A., and Barnes, P.J. 2002. Ozone-induced increase in exhaled 8-isoprostane in healthy subjects is resistant to inhaled budesonide. *Free Radic. Biol. Med.* **33**:1403–1408.
15. Long, N.C., et al. 2001. Ozone causes lipid peroxidation but little antioxidant depletion in exercising and nonexercising hamsters. *J. Appl. Physiol.* **91**:1694–1700.
16. Hamada, K., Goldsmith, C.A., Suzaki, Y., Goldman, A., and Kobzik, L. 2002. Airway hyperresponsiveness caused by aerosol exposure to residual oil fly ash leachate in mice. *J. Toxicol. Environ. Health A.* **65**:1351–1365.
17. Pulfer, M.K., Taube, C., Gelfand, E., and Murphy, R.C. 2005. Ozone exposure in vivo and formation of biologically active oxysterols in the lung. *J. Pharmacol. Exp. Ther.* **312**:256–264.
18. Suzuki, H., et al. 1997. A role for macrophage scavenger receptors in atherosclerosis and susceptibility to infection. *Nature.* **386**:292–296.
19. Moore, K.J., et al. 2005. Loss of receptor-mediated lipid uptake via scavenger receptor A or CD36 pathways does not ameliorate atherosclerosis in hyperlipidemic mice. *J. Clin. Invest.* **115**:2192–2201. doi:10.1172/JCI24061.
20. Babaev, V.R., Patel, M.B., Semenkovich, C.F., Fazio, S., and Linton, M.F. 2000. Macrophage lipoprotein lipase promotes foam cell formation and atherosclerosis in low density lipoprotein receptor-deficient mice. *J. Biol. Chem.* **275**:26293–26299.
21. Takahashi, K., et al. 1992. Expression of macrophage scavenger receptors in various human tissues and atherosclerotic lesions. *Clin. Biochem.* **25**:365–368.
22. Naito, M., Kodama, T., Matsumoto, A., Doi, T., and Takahashi, K. 1991. Tissue distribution, intracellular localization, and in vitro expression of bovine macrophage scavenger receptors. *Am. J. Pathol.* **139**:1411–1423.
23. Tyson, K.L., Weissberg, P.L., and Shanahan, C.M. 2002. Heterogeneity of gene expression in human atheroma unmasked using cDNA representational difference analysis. *Physiol. Genomics.* **9**:121–130.
24. Sakaguchi, H., et al. 1998. Role of macrophage scavenger receptors in diet-induced atherosclerosis in mice. *Lab. Invest.* **78**:423–434.
25. Yoshimatsu, M., et al. 2004. Induction of macrophage scavenger receptor MARCO in nonalcoholic steatohepatitis indicates possible involvement of endotoxin in its pathogenic process. *Int. J. Exp. Pathol.* **85**:335–343.
26. Pryor, W.A., Squadrito, G.L., and Friedman, M. 1995. A new mechanism for the toxicity of ozone. *Toxicol. Lett.* **82–83**:287–293.
27. Connor, L.M., Ballinger, C.A., Albrecht, T.B., and Postlethwait, E.M. 2004. Interfacial phospholipids inhibit ozone-reactive absorption-mediated cytotoxicity in vitro. *Am. J. Physiol. Lung Cell. Mol. Physiol.* **286**:L1169–L1178.
28. Notter, R.H. 2000. Lung surfactants: basic science and clinical applications. Marcel Dekker. New York, New York, USA. 130–176.
29. Postle, A.D., Heeley, E.L., and Wilton, D.C. 2001. A comparison of the molecular species compositions of mammalian lung surfactant phospholipids. *Comp. Biochem. Physiol. A. Mol. Integr. Physiol.* **129**:65–73.
30. Pryor, W.A., Bermudez, E., Cueto, R., and Squadrito, G.L. 1996. Detection of aldehydes in bronchoalveolar lavage of rats exposed to ozone. *Fundam. Appl. Toxicol.* **34**:148–156.
31. Cao, J., Fales, H.M., and Schaffner, C.P. 1995. Cellular sterol accumulation stimulated by cholesterol 5 beta,6 beta-epoxide in J774 macrophages. *Proc. Soc. Exp. Biol. Med.* **209**:195–204.
32. Lemaire-Ewing, S., et al. 2005. Comparison of the cytotoxic, pro-oxidant and pro-inflammatory characteristics of different oxysterols. *Cell Biol. Toxicol.* **21**:97–114.
33. Kafoury, R.M., et al. 1999. Induction of inflammatory mediators in human airway epithelial cells by lipid ozonation products. *Am. J. Respir. Crit. Care Med.* **160**:1934–1942.
34. Kafoury, R.M., et al. 1998. Lipid ozonation products activate phospholipases A2, C, and D. *Toxicol. Appl. Pharmacol.* **150**:338–349.
35. Leitinger, N., et al. 1999. Structurally similar oxidized phospholipids differentially regulate endothelial binding of monocytes and neutrophils. *Proc. Natl. Acad. Sci. U.S.A.* **96**:12010–12015.
36. Yeh, M., et al. 2001. Increased transcription of IL-8 in endothelial cells is differentially regulated by TNF-alpha and oxidized phospholipids. *Arterioscler. Thromb. Vasc. Biol.* **21**:1585–1591.
37. Leonarduzzi, G., et al. 2005. Oxysterol-induced upregulation of MCP-1 expression and synthesis in macrophage cells. *Free Radic. Biol. Med.* **39**:1152–1161.
38. Chang, M.M., Wu, R., Plopper, C.G., and Hyde, D.M. 1998. IL-8 is one of the major chemokines produced by monkey airway epithelium after ozone-induced injury. *Am. J. Physiol.* **275**:L524–L532.
39. Jaspers, I., Flescher, E., and Chen, L.C. 1997. Ozone-induced IL-8 expression and transcription factor binding in respiratory epithelial cells. *Am. J. Physiol.* **272**:L504–L511.
40. Ryan, L., O'Callaghan, Y.C., and O'Brien, N.M. 2004. Comparison of the apoptotic processes induced by the oxysterols 7beta-hydroxycholesterol and cholesterol-5beta,6beta-epoxide. *Cell Biol. Toxicol.* **20**:313–323.
41. Driscoll, K.E., Simpson, L., Carter, J., Hassenbein, D., and Leikauf, G.D. 1993. Ozone inhalation stimulates expression of a neutrophil chemotactic protein, macrophage inflammatory protein 2. *Toxicol. Appl. Pharmacol.* **119**:306–309.
42. Deng, H., Mason, S.N., and Auten, R.L., Jr. 2000. Lung inflammation in hyperoxia can be prevented by antichemokine treatment in newborn rats. *Am. J. Respir. Crit. Care Med.* **162**:2316–2323.
43. Ning, Y., et al. 2004. Particle-epithelial interaction: effect of priming and bystander neutrophils on interleukin-8 release. *Am. J. Respir. Cell Mol. Biol.* **30**:744–750.
44. Tao, F., and Kobzik, L. 2002. Lung macrophage-epithelial cell interactions amplify particle-medi-

ated cytokine release. *Am. J. Respir. Cell Mol. Biol.* **26**:499–505.
45. Montuschi, P., Barnes, P.J., and Roberts, L.J., 2nd. 2004. Isoprostanes: markers and mediators of oxidative stress. *FASEB J.* **18**:1791–1800.
46. Aringer, L., and Eneroth, P. 1974. Formation and metabolism in vitro of 5,6-epoxides of cholesterol and beta-sitosterol. *J. Lipid Res.* **15**:389–398.
47. Smith, C.A., and Harrison, D.J. 1997. Association between polymorphism in gene for microsomal epoxide hydrolase and susceptibility to emphysema. *Lancet.* **350**:630–633.
48. Hersh, C.P., et al. 2006. Genetic association analysis of functional impairment in chronic obstructive pulmonary disease. *Am. J. Respir. Crit. Care Med.* **173**:977–984.
49. Newman, J.W., Morisseau, C., and Hammock, B.D. 2005. Epoxide hydrolases: their roles and interactions with lipid metabolism. *Prog. Lipid Res.* **44**:1–51.
50. Petruzzelli, S., et al. 1992. Cigarette smoke inhibits cytosolic but not microsomal epoxide hydrolase of human lung. *Hum. Exp. Toxicol.* **11**:99–103.
51. Willey, J.C., et al. 1997. Quantitative RT-PCR measurement of cytochromes p450 1A1, 1B1, and 2B7, microsomal epoxide hydrolase, and NADPH oxidoreductase expression in lung cells of smokers and nonsmokers. *Am. J. Respir. Cell Mol. Biol.* **17**:114–124.
52. Savill, J. 1998. Apoptosis. Phagocytic docking without shocking. *Nature.* **392**:442–443.
53. Cho, H.Y., Reddy, S.P., Debiase, A., Yamamoto, M., and Kleeberger, S.R. 2005. Gene expression profiling of NRF2-mediated protection against oxidative injury. *Free Radic. Biol. Med.* **38**:325–343.

Respiratory Research

BioMed Central

Research

Signaling pathways required for macrophage scavenger receptor-mediated phagocytosis: analysis by scanning cytometry

Timothy H Sulahian*[1], Amy Imrich[1], Glen DeLoid[1], Aaron R Winkler[2,3] and Lester Kobzik[1]

Address: [1]Harvard School of Public Health, Molecular and Integrative Physiological Sciences Program, 655 Huntington Ave, Building II, 2nd Floor, Boston, MA 02115, USA, [2]Department of Inflammation, Wyeth Research, 35 Cambridge Park Dr., Cambridge, MA 02140, USA and [3]Department of Pharmacology and Experimental Therapeutics, Boston University School of Medicine, 715 Albany St., L-603, Boston, MA 02118, USA

Email: Timothy H Sulahian* - tsulahian@cellsignal.com; Amy Imrich - aimrich@hsph.harvard.edu; Glen DeLoid - gdeloid@hsph.harvard.edu; Aaron R Winkler - ARWinkler@wyeth.com; Lester Kobzik - lkobzik@hsph.harvard.edu

* Corresponding author

Published: 7 August 2008

Respiratory Research 2008, **9**:59 doi:10.1186/1465-9921-9-59

Received: 27 March 2008
Accepted: 7 August 2008

This article is available from: http://respiratory-research.com/content/9/1/59

Abstract

Background: Scavenger receptors are important components of the innate immune system in the lung, allowing alveolar macrophages to bind and phagocytose numerous unopsonized targets. Mice with genetic deletions of scavenger receptors, such as SR-A and MARCO, are susceptible to infection or inflammation from inhaled pathogens or dusts. However, the signaling pathways required for scavenger receptor-mediated phagocytosis of unopsonized particles have not been characterized.

Methods: We developed a scanning cytometry-based high-throughput assay of macrophage phagocytosis that quantitates bound and internalized unopsonized latex beads. This assay allowed the testing of a panel of signaling inhibitors which have previously been shown to target opsonin-dependent phagocytosis for their effect on unopsonized bead uptake by human *in vitro*-derived alveolar macrophage-like cells. The non-selective scavenger receptor inhibitor poly(I) and the actin destabilizer cytochalasin D were used to validate the assay and caused near complete abrogation of bead binding and internalization, respectively.

Results: Microtubule destabilization using nocodazole dramatically inhibited bead internalization. Internalization was also significantly reduced by inhibitors of tyrosine kinases (genistein and herbimycin A), protein kinase C (staurosporine, chelerythrine chloride and Gö 6976), phosphoinositide-3 kinase (LY294002 and wortmannin), and the JNK and ERK pathways. In contrast, inhibition of phospholipase C by U-73122 had no effect.

Conclusion: These data indicate the utility of scanning cytometry for the analysis of phagocytosis and that phagocytosis of unopsonized particles has both shared and distinct features when compared to opsonin-mediated phagocytosis.

Background

Lung infection is responsible for more disability-adjusted life years lost than any other disease [1] and high levels of inhaled dusts have been linked in several epidemiological studies to increases in ear and airway infections, cardiovascular disease, lung cancer and mortality [2-5]. Alveolar macrophages (AMs) are a first line of defense against inhaled bacteria and environmental dusts. Therefore, understanding the mechanism by which AMs defend against inhaled insults is crucial. Since contact with inhaled particles often takes place before an antibody response has occurred or with particles for which specific antibodies are not readily made, the AM relies on innate receptors to recognize inhaled particles.

Scavenger receptors (SRs) are a key component of the innate immune system. In addition to their well-known role in low-density lipoprotein metabolism, SRs play a critical role in AM clearance of inhaled particles by binding and allowing the cells to internalize unopsonized microorganisms, apoptotic bodies and environmental dusts [6,7]. General blockade of SRs using polyanionic inhibitors results in a dramatic reduction of AM uptake of residual oil fly ash, ambient air particles, diesel dust, iron oxide, titanium dioxide, silica, *Escherichia coli* *Staphylococcus aureus* 8-11]. Specific blockade and transfection of members of the SR family have shown these receptors to be capable of binding several Gram-positive and Gram-negative bacteria as well as isolated lipopolysaccharide and lipotechoic acid [12-21]. In addition, mice deficient in SR-A or MARCO demonstrate reduced bacterial clearance, increased pulmonary inflammation and increased mortality following an intranasal challenge with *Streptococcus Pneumoniae* [10,22]. Furthermore, MARCO can bind CpG DNA [23], whereas blockade of MARCO with a monoclonal antibody dramatically reduces AM uptake of titanium dioxide, iron oxide, silica and latex beads [24,22,25]. SR-A and MARCO, therefore, are clearly critical components of pulmonary host defense. However, it is important to point out that AMs also express several other less well-characterized SRs including LOX-1, SR-PSOX and SRCL [10]. These SRs are capable of binding bacteria [26-28] and might also contribute to the AM response to inhaled insults.

While it is clear that SR-initiated uptake of inhaled particles is critically important for lung defense, it is currently not known which signaling pathways are necessary for SR-mediated phagocytosis. In contrast, phagocytosis of opsonized particles (via Fc or complement receptors) has been well characterized [29]. Many characteristics of opsonin-mediated phagocytosis are shared by both Fc and complement receptors (such as signaling by tyrosine kinase, protein kinase C (PKC), phosphoinositide-3 kinase (PI-3K), mitogen activated protein kinases (MAPK) and phospholipase Cγ (PLCγ)). In contrast, some characteristics are unique to one receptor pathway (such as sensitivity of complement-mediated uptake to microtubule inhibitors) [30]. Many of these opsonin-mediated phagocytic signaling pathways have also been implicated in non-phagocytic SR-mediated responses such as cytokine production and lipoprotein endocytosis [31-38]. We hypothesized that these pathways would also be necessary for SR-mediated phagocytosis. To test this, we employed a battery of well-established signaling inhibitors and a novel high-throughput fluorescence phagocytosis assay.

AMs are known to express a wide array of SRs with overlapping ligand specificities. Therefore, it is likely that inhaled particles are simultaneously bound by multiple SR family members. Since the underlying biology of the particle-AM interaction is more complicated than a simple one ligand/one receptor interaction, we chose a target particle (latex spheres) that likewise binds multiple SRs to more closely model the true physiology of particle-AM interactions. It should be noted that the latex sphere has long been used as a model for inhaled particulates and is similar to 'real world' particles in terms of its SR-mediated uptake by AM [10,39,9,40,41,25,42].

Methods

Cell isolation, differentiation and characterization

Discarded platelet apheresis collars were obtained from the Kraft Family Blood Donor Center at the Dana-Farber Cancer Institute (Boston, MA, USA). Buffy coats were harvested from these collars and enriched for monocytes using the RosetteSep Monocyte Enrichment kit (Stem Cell Technologies, Vancouver, BC, Canada). Monocytes were then cultured in Vuelife bags (American Fluoroseal, Gaithersburg, MD, USA) for 11 days at 5% CO_2 and 37°C in RPMI/10% FBS/20 μg/ml gentamicin supplemented with 20 ng/ml human granulocyte/macrophage-colony stimulating factor (GM-CSF, Peprotech, Rocky Hill, NJ, USA). GM-CSF matured MØ (GM-MØ) were then harvested and resuspended at 1×10^6/ml in RPMI/10% FBS. 1×10^5 cells were dispensed into black-walled 96 well Micro-Clear plates (Greiner Bio-One, Monroe, NC, USA). For some experiments, the number of cells per well was altered but the volume remained constant. After plating and adherence, GM-MØ were incubated for 40–44 hours, and then used to measure particle binding and internalization.

Some GM-MØ were characterized by flow cytometry before being plated for experiments. Cells were stained with anti-PSOX (10 μg/ml, provided by Dr. Kimihisa Ichikawa, Sankyo, Tokyo, Japan), anti-LOX-1 (10 μg/ml, Cell Sciences, Inc., Canton, MA, USA), anti-SR-A (10 μg/ml, provided by Dr. Motohiro Takeya, Kumamoto University, Kumamoto, Japan), anti-CD68 (10 μg/ml, Dako,

Carpinteria, CA, USA), anti-CD14 (3.3 μg/ml), anti-HLA-DR (10 μg/ml), anti-HLA-DQ (10 μg/ml) or equal concentrations of isotype matched control antibodies (all from BD Biosciences, Rockville, MD, USA) in PBS with 2 mg/ml bovine serum albumin (BSA) and 4 mg/ml human IgG (both from Sigma, St. Louis, MO, USA). This step was followed by staining with 20 μg/ml Alexafluor 488 labeled $F(ab')_2$ goat anti-mouse antibodies (Invitrogen, Carlsbad, CA, USA) and fixation in PBS with 1% paraformaldehyde. Other cells were stained with 10 μg/ml PLK-1 (anti-MARCO [10]) or control IgG that had been biotinylated using biotin-X-NHS (Calbiochem, San Diego, CA, USA). This was followed by secondary staining with 7.5 μg/ml streptavidin-phycoerythrin (Invitrogen) and fixation as described above. Cellular fluorescence was measured using a Coulter Epics Elite flow cytometer (Beckman Coulter, Miami, FL, USA).

Cells were also evaluated for their ability to bind unopsonized latex beads in the presence or absence of SR inhibitors. One hundred microliters of GM-MØ (suspended at 2 × 10^6/ml in HBSS/0.3% BSA) were plated in each well of a low adherence 96-well plate (Corning, Corning NY, USA). One hundred microliters of 20 μg/ml polyinosinic acid (poly (I)), 20 μg/ml chondroitin sulfate (both from Sigma), 20 μg/ml PLK-1 mAb or 20 μg/ml $mIgG_3$ isotype control (eBioscience, San Diego, CA, USA) were added and cells were allowed to incubate for 10 minutes at 37°C. One hundred microliters of green fluorescent latex beads (1 μm, Invitrogen) were added at a concentration of 1 × 10^8/ml in HBSS/0.3%BSA with or without 10 μg/ml poly(I), 10 μg/ml chondroitin sulfate, 10 μg/ml PLK-1 or 10 μg/ml $mIgG_3$. This corresponds to a 50:1 bead to cell ratio. Cells were incubated for 30 minutes at 37°C, with gentle pipetting every 10 minutes to resuspend the cells and beads. After incubation, the assay was stopped by chilling cells on ice and analyzing fluorescence by flow cytometry.

For mouse studies, primary AMs were isolated from C57BL/6J mice (The Jackson Laboratory, Bar Harbor, ME, USA). Immediately before bronchialveolar lavage, mice were euthanized by an overdose of Phenobarbital. The lungs were lavaged six times with 0.8 ml of ice-cold PBS. Cell purity and yield was determined using a hemocytometer. Murine AMs were cultured in black-walled 96 well Micro-Clear plates in RPMI/10% FBS for 40–44 hours before phagocytosis assays were performed as described for GM-MØ.

Preparation of biotinylated latex beads

Biotin-BSA was generated by incubating 50 mg of tissue culture grade BSA (Sigma) with 30 mg biotin-X-NHS in 10 ml PBS for one hour at room temperature. Unconjugated biotin was removed by extensive dialysis. Green fluorescent carboxylated latex beads (1 μm, Invitrogen) were centrifuged at high speed and washed twice in 2-(N-morpholino)ethanesulfonic acid (MES, Calbiochem) buffer (19.2 mg/ml, pH 6.0). Beads were suspended at 5 × 10^9 per ml in MES buffer. Water-soluble carbodimide (WSC, Calbiochem) was freshly dissolved in MES buffer and beads were incubated at room temperature for one hour with 10 mg/ml WSC. Beads were washed twice in 0.5 × PBS and resuspended in water. An equal volume of biotin-BSA was added for a final concentration of 2 mg/ml BSA in 0.5 × PBS. Beads were incubated overnight at room temperature and then centrifuged at high speed. Beads were then resuspended in 0.5 × PBS with 40 mM glycine and incubated for one hour. Finally, beads were washed twice in PBS containing 0.2% BSA and 0.01% sodium azide and stored at 4°C.

Internalization assay

All reagents and buffers were at room temperature when added to cells and all incubations were performed in warm (37°C) humid air unless otherwise noted. All fluorescent dyes were purchased from Invitrogen. Cells were incubated with CellTracker Blue at 100 μM in HBSS with Ca^{++} and Mg^{++} (Cambrex, East Rutherford, NJ, USA) for 40 minutes followed by a 30 minute recovery period in assay buffer (HBSS/0.3% BSA). Inhibitors (Table 1) or DMSO were then added for 20 minutes. Poly(I), cytochalasin D, nocodazole, staurosporine, wortmannin and herbimycin A were purchased from Sigma. All other inhibitors were purchased from Calbiochem. GM-MØ were then incubated for 20 minutes with bead suspension (2 × 10^8 beads/ml) +/- inhibitors for bead binding and internalization. Cells were then washed 2 × 250 μl with assay buffer, covered with fresh buffer +/- inhibitors and incubated for an additional 20 minutes to allow for further bead internalization (the cells were, therefore, incubated with inhibitors for a grand total of 60 minutes). After this the cells were washed and extracellular beads were labeled on ice for 30 minutes using streptavidin-Texas Red (20 μg/ml in assay buffer). After a final wash with 250 μl assay buffer, cells were fixed with 4% paraformaldehyde in PBS. The fixative was removed after 30 minutes and cell nuclei were stained for 30 minutes with 3 μg/ml of Hoechst 33342. The Hoechst dye was then removed and wells were filled with 100 μl of 4% paraformaldehyde in PBS for storage.

Image Acquisition and Data Analysis

Images of adherent cells were collected using the Pathway HT bioimager (BD Biosciences). Cells were both illuminated through and fluorescence emission was collected from the bottom of the plate using a 20 × NA075 lens (Olympus, Center Valley, PA, USA) and a field size of approximately 300 μm square. All images were collected using flat field correction and 2 × 2 binning of pixels. Auto focus was carried out using the fluorescence emission of

Table 1: Summary of Inhibitors Tested.

Inhibitor	Target	Final Concentration	Vehicle
Poly(I)	SR binding	10 μg/ml	PBS
Cytochalasin D	filamentous actin	15 μM	DMSO
Nocodazole	microtubules	25 μM	DMSO
Staurosporine	protein kinases	1 μM	DMSO
Chelerythrine Cl	PKC	25 μM	DMSO
Gö 6976	PKC	10 μM	DMSO
Wortmannin	PI-3K	0.04 μM	DMSO
LY294002	PI-3K	200 μM	DMSO
Genistein	tyrosine kinases	100 μM	DMSO
Herbimycin A	tyrosine kinases	80 μM	DMSO
MEK inhibitor I	MEK	200 μM	DMSO
JNK inhibitor I	JNK	4 μM	PBS
JNK control	inactive analog of JNK inhibitor I	4 μM	PBS
U-73122	phospholipase C	10 μM	DMSO
U-73343	inactive analog of U-73122	10 μM	DMSO

Hoechst and CellTracker Blue, which share the same excitation and emission spectra. Confocal images of bead fluorescence (488 BP excitation, 515 LP dichroic, 515 LP emission filters), Texas Red (560 BP excitation, 595 LP dichroic, 645 LP emission filters) and Hoechst/CellTracker Blue (380 BP excitation, 400 LP dichroic, 435 LP emission filters) were collected every 1.7 μm for a total of 10 sections. The dyes were illuminated sequentially and the confocal images collected were collapsed, creating new images with clear definition of all beads within each cell.

Cell segmentation for each image was achieved using a combination of the Hoechst signal (to identify single cells) and the CellTracker Blue signal (to define the cell borders). Using the collapsed stacks of confocal images, software was developed to define the cells (blue emission image), count the number of beads per cell (green emission image) and determine if the beads are outside the cell (red emission image) using custom software developed in MATLAB (The Mathworks, Inc., Natick, MA, USA). Hoechst/CellTracker Blue images were processed to reduce noise, enhance contrast and correct for non-uniform field brightness. A gradient-facilitated watershed segmentation algorithm was used to identify and label individual cells. Cell sizes (profile areas) were calculated as the number of pixels in segmented cell objects (collapsed stack images). Cell volumes were calculated as the sum of the cell profile areas of the individual confocal images comprising collapsed stacks. Green fluorescent (all beads) and red fluorescent (external beads) images were sharpened and contrast enhanced. Watershed segmentation was used to identify and label individual bead objects. Labeled bead objects within the "all beads" image were classified as "internal" if they had less than 20% overlap with an external bead object. Bead objects sharing one or more pixel with any cell object were considered to be associated with that cell. All partial cell images along the edges of the field were omitted from analysis.

Bead binding was calculated as the average number of cell-associated beads per cell. Typically between 1200 and 1800 total cells were counted per donor per condition. Percent internalization was calculated as the number of internalized beads divided by the total number of cell-associated beads for each cell, then multiplied by 100. Significant differences were calculated for the poly(I) data using Students paired *t*-test. For the cell density data, the Spearman correlation test was performed. For all other data, significant differences were calculated using one-way ANOVA followed by Bonferroni's multiple comparison of all means. An unpaired ANOVA was used in the analysis of the protein tyrosine kinase data in Figure 8. For all other data, a paired ANOVA was used. Prism 4 for the Macintosh (Graphpad Software, San Diego, CA, USA) was used for all graphing and statistical calculations.

Results

Characterization of GM-MØ

Monocytes are typically matured into MØ *in vitro* using M-CSF. However, AM are unusual in that they require GM-CSF, but not M-CSF, for their development *in vivo* [43-47]. Therefore, we followed the GM-CSF-based differentiation protocol of Akagawa, *et al.*, designed to produce monocyte-derived MØ with a distinctly AM-like phenotype (GM-MØ) [48]. Both AM and GM-MØ have been shown to produce lower levels of H_2O_2, express higher levels of catalase and are more resistant to H_2O_2 toxicity when compared to M-CSF derived MØ. Furthermore, AM and GM-MØ (but not M-CSF derived MØ) express HLA-DQ and are resistant to HIV infection, but susceptible to *Mycobacterium tuberculosis* infection [48,49]. Finally, we are confident that GM-MØ are an appropriate model for primary AMs in that several of the inhibitors described in this

communication (genistein, herbimycin A, wortmannin, nocodazole and staurosporine) were also tested for their ability to inhibit phagocytosis of beads by primary murine AM. In all cases, the results were comparable to those obtained using GM-MØ (data not shown).

It should be noted that, unlike murine bone marrow, incubation of human monocytes with GM-CSF alone does not produce dendritic cells, as evidenced by the morphology and surface marker expression of GM-MØ. GM-MØ were harvested after 11 days of culture in GM-CSF-supplemented media and immunolabeled to measure surface expression of general macrophage markers as well as markers which can differentiate between alveolar/GM-MØ and the more traditional M-CSF matured MØ. As shown in Figure 1, greater than 90% of GM-MØ stain positive for the MØ surface proteins CD14 and HLA-DR and demonstrate a MØ-like morphology when analyzed by light microscopy, confirming their identity as MØ. These cells are also positive for both HLA-DQ and MARCO (Figure 2), a phenotype consistent with both GM-MØ and primary AMs [10,48-51,25,52]. In addition, GM-MØ were labeled for SRs known to be present on primary AMs [53,54,10]. As shown in Figure 2, GM-MØ are weakly positive for CD68 and strongly positive for MARCO, PSOX and SR-A.

Our findings also confirm that SRs are involved in the binding of unopsonized latex beads. As shown in Figures 2F and 2G, bead uptake is dramatically inhibited by either the broad SR blocker poly(I) or the MARCO-specific SR blocker mAb PLK-1. These agents reduced the fluorescent bead signal by 80% and 62% respectively, whereas their control reagents (chondroitin sulfate and mIgG3) had no effect. Taken together, these data suggest that GM-MØ accurately model primary AMs in their expression of a wide range of SRs and that their interaction with unopsonized beads involves MARCO (and likely other SRs as well).

High throughput direct measurement of phagocytosis

A high throughput phagocytosis assay was developed to provide rapid and direct measurement of both particle binding and internalization. For this assay, GM-MØ are first incubated with CellTracker Blue, which provides a uniform label of the whole cell to facilitate cytometric identification. The GM-MØ are then allowed to bind and ingest biotinylated green fluorescent latex beads, followed by incubation with streptavidin-Texas Red to label external beads. Analysis with a scanning cytometer produces images in which beads that are bound, but not internalized, are clearly distinguishable from those which are internalized. Figures 3A–D are typical examples of images produced by this technique. In Figures 3A and 3B, phagocytosis has been inhibited by cytochalasin D treatment. As a result, all of the beads are extracellular and appear as yellow, due to the colocalization of red and green fluorescence. In contrast, the cells in Figures 3C and 3D have been allowed to internalize beads. In these images, some beads are extracellular (appearing as yellow) while others have been internalized (appearing as green). The cells in these images can be automatically identified ('segmented') and the number of beads per cell counted using a combination of commercial and custom software (Figure 3B and 3D).

In order to validate this technique, GM-MØ were cultured with known inhibitors of SR binding and phagocytosis before being incubated with fluorescent beads. We observed a nearly complete (96%) reduction in the number of beads bound by cells in the presence of the SR blocker poly(I) (Figure 4A). In contrast, the actin destabilizer cytochalasin D has no effect on total bead binding, but decreases the number of beads internalized by 90% when compared to the DMSO control (Figures 4B and 4C). To compare the results of software image analysis to human quantitation of the same images, beads per cell were manually counted for 50 cells in both the control and cytochalasin D treated conditions. These results were quite similar to those obtained by software analysis and are shown in Table 2. Hence, our software quantification technique is capable of accurately counting and distinguishing between beads that have been internalized and beads that have been bound, but not internalized.

Binding and internalization are differentially affected by cell density

To determine the optimal cell concentration for this assay, we compared results using a range of cell densities. The data collected indicate that cell density affects cell size, and has considerable and opposing effects on bead binding and internalization (Figure 5). Higher plating densities are associated with reduced cell size, as measured by pixels per cell profile in collapsed stack images, ($r = -0.972$, $p < 0.001$). Comparison of cell sizes and cell volumes calculated from confocal slices confirmed that cell size accurately reflects cell volume ($n = 95$ cells, $r = 0.971$, $p < 0.0001$, data not shown). As cell density increases, the number of beads bound per cell decreases significantly ($r = -0.853$, $p < 0.001$). This could be due to reduced cell size and/or increased cell-to-cell contact, thereby reducing the cellular surface area available for bead binding. In contrast, increasing the cell density dramatically augments the percentage of bound beads that are internalized (e.g., increasing the density of the cells from 54 to 180 cells per field resulted in a 60% increase in the percentage of internalized beads ($r = 0.622$, $p < 0.05$)), an observation that cannot easily be explained by a reduction in cell size. Taken together, these data indicate that the density used for in vitro analysis of GM-MØ has a significant influence

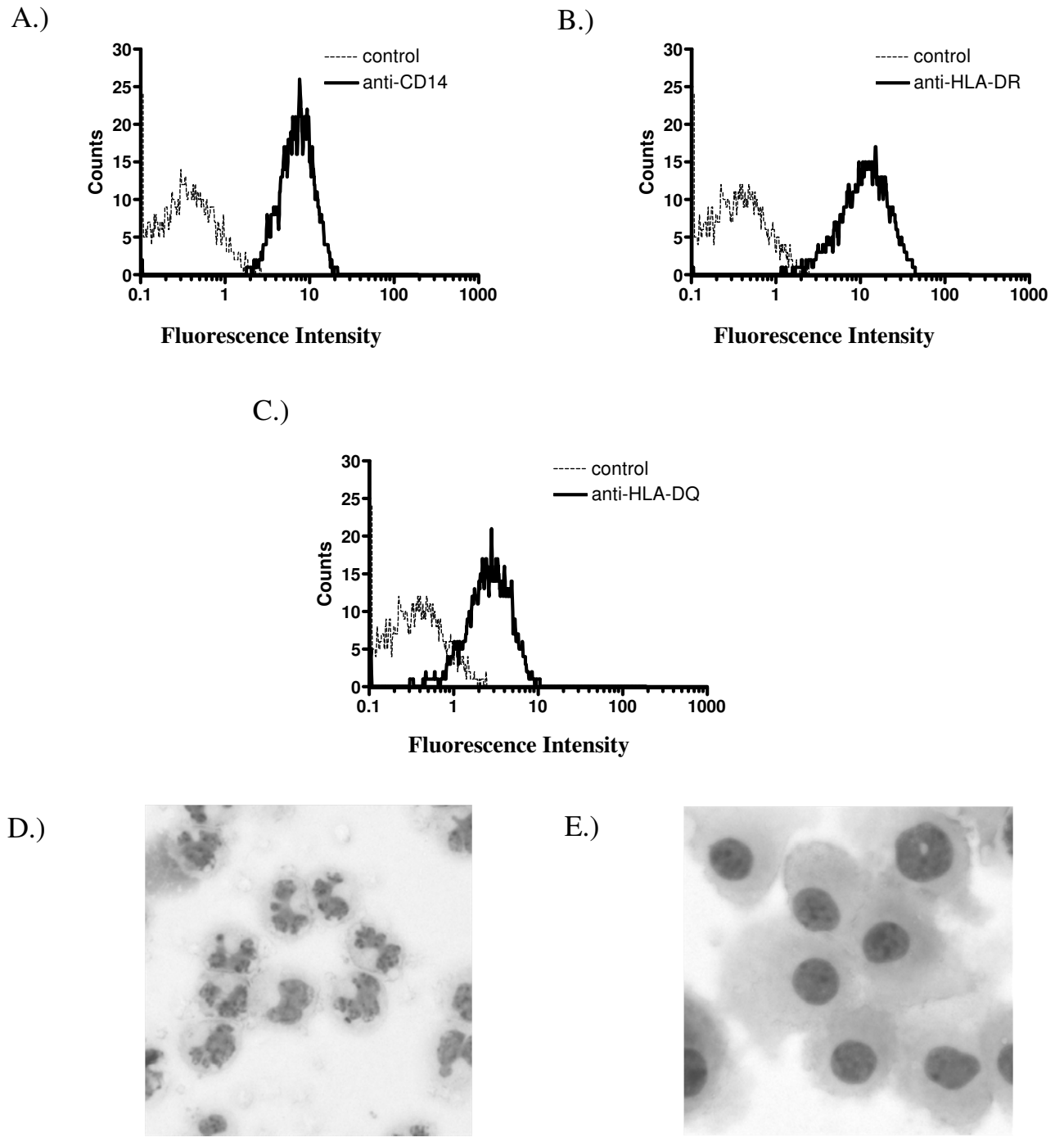

Figure 1

Characterization of GM-MØ. CD14 (A), HLA-DR (B) and HLA-DQ (C) expression were evaluated by flow cytometry. Solid lines represent the fluorescence of stained cells, while dashed lines represent the results from control antibodies. Data are representative of experiments performed on cells from three donors. Cytocentrifuge preparations illustrating monocyte and macrophage morphology before (D) and after (E) maturation with GM-CSF were captured at equal magnification (200×).

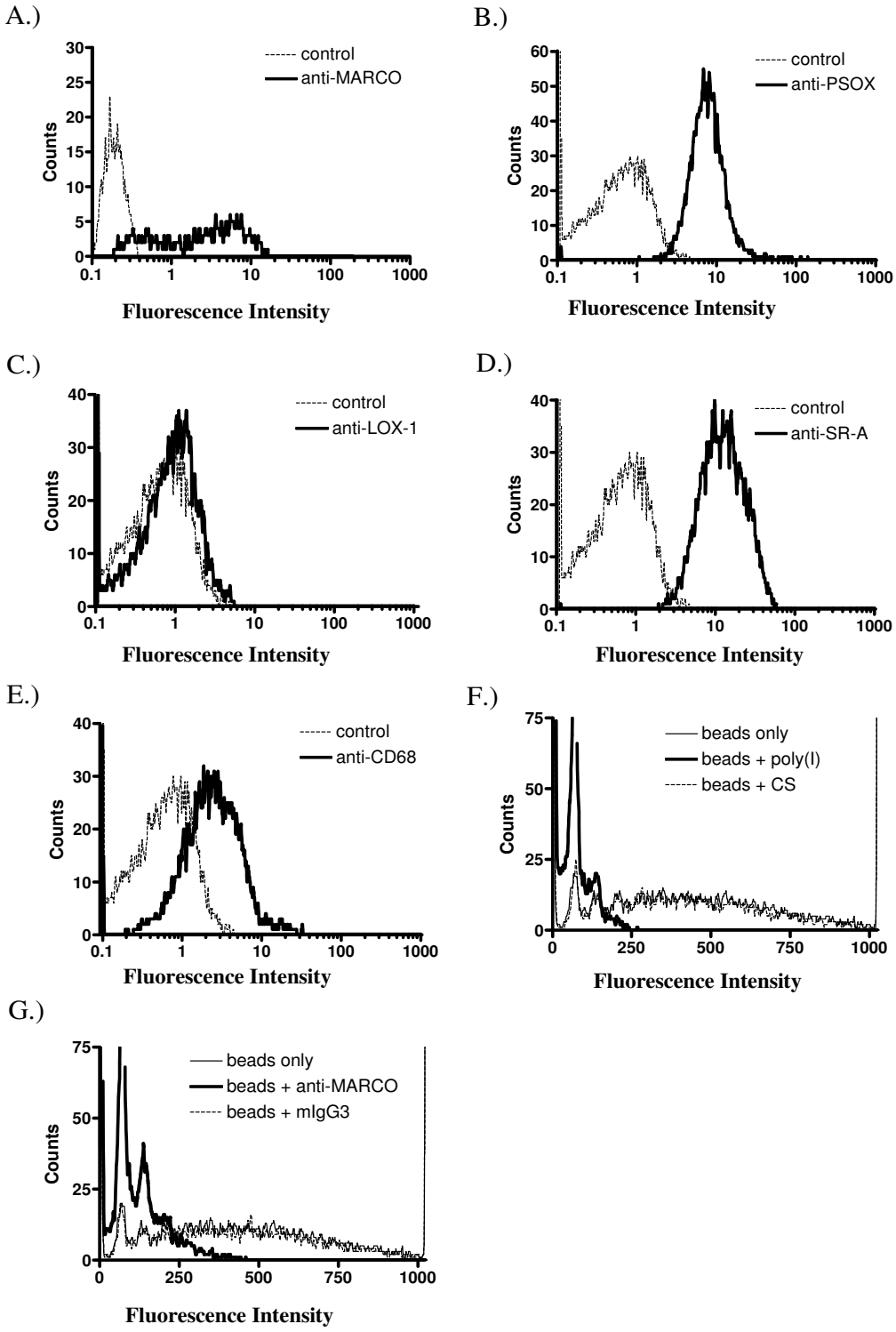

Figure 2

Characterization of SRs expressed by GM-MØ. MARCO (A), PSOX (B), LOX-1 (C), SR-A (D) and CD68 (E) expression as well as fluorescent bead binding in the presence of poly(I) (F) or an anti-MARCO mAb (G) were evaluated by flow cytometry. Data are representative of experiments performed on cells from three (A-E) or five (F and G) donors.

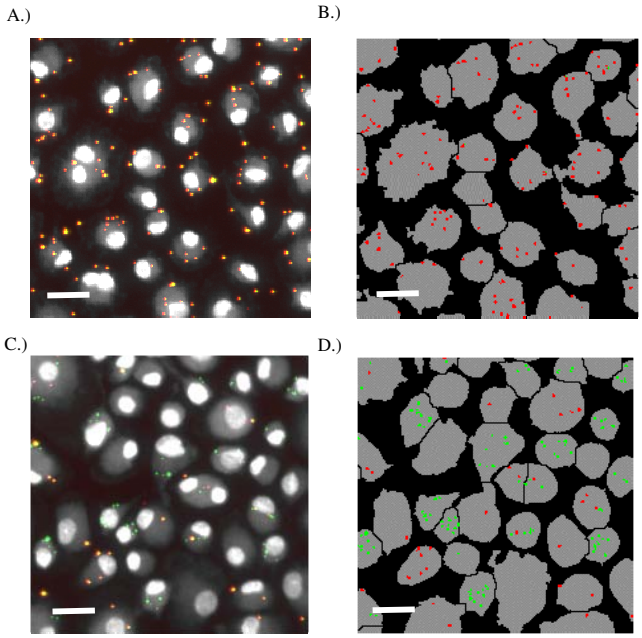

Figure 3
Binding and phagocytosis assay. Adherent GM-MØ were treated with cytochalasin D (A and B) to block internalization or vehicle control (DMSO, C and D) before incubation with biotinylated green fluorescent latex beads and labeling of extracellular beads with streptavidin-Texas Red. Images obtained by scanning cytometry show intracellular beads in green, while extracellular beads are in yellow (due to the colocalization of red and green fluorescence). Panels A and C depict the fluorescence images obtained by the scanning cytometer, while panels B and D depict the same images after automated segmenting and bead identification. Scale bars represent 20 μm.

on phagocytic parameters. For all subsequent experiments, cells were plated at 1 × 10^5 cells per well.

Microtubule destabilization inhibits SR mediated internalization

Although filamentous actin is required for phagocytosis in general, the requirement for microtubules depends upon which phagocytic receptor is involved. For example, inhibiting microtubule function blocks complement receptor-mediated, but not Fc receptor-mediated, particle

Table 2: Manual vs. Computer Enumeration of Cell-Associated Beads.

	Internalized Beads		Extracellular Beads	
	Control	Cytochalasin D	Control	Cytochalasin D
Manual	126	10	57	221
Computer	130	11	69	234

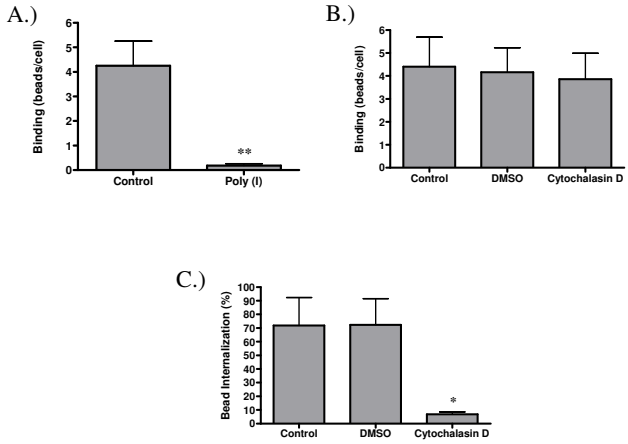

Figure 4
Quantification of bead binding and internalization. Adherent GM-MØ were pretreated with either poly(I) (A) or cytochalasin D (B and C) before incubation with fluorescent latex beads. Cells were analyzed for total bead binding (A and B) and percent internalization (C). Bars represent the means of four (A) or three (B and C) donors +/- the standard deviation. For each donor, three fields from each of three replicate wells were analyzed. *p < 0.01 **p < 0.001 when compared to either the control or DMSO conditions.

internalization [30,55]. In order to determine if SR-mediated phagocytosis requires microtubules, GM-MØ were analyzed for their ability to bind and internalize latex beads in the presence of the microtubule destabilizer nocodazole. Nocodazole treatment has no effect on the total number of beads bound per cell (data not shown), suggesting that SRs do not require microtubules for particle binding. In contrast, nocodazole treatment reduces the proportion of internalized beads by 50% when compared to the DMSO control (Figure 6). We conclude that SR-mediated internalization is similar to complement receptor-mediated phagocytosis in that they both require functional microtubules.

Effect of signaling pathway inhibitors on SR-mediated phagocytosis

A large number of signaling molecules have been implicated in MØ phagocytosis [56,57]. However, most of this work has been performed using IgG or (to a lesser extent) complement opsonized particles. Very little is known about which signaling pathways are required for SR-mediated phagocytosis. Our strategy was to analyze these pathways using a panel of relevant pharmacologic inhibitors, an approach facilitated by the high throughput assay described above.

Tyrosine kinases and PKC are both known to be involved in Fc-receptor mediated phagocytosis [57]. Therefore, we tested the effect of protein tyrosine kinase and PKC inhib-

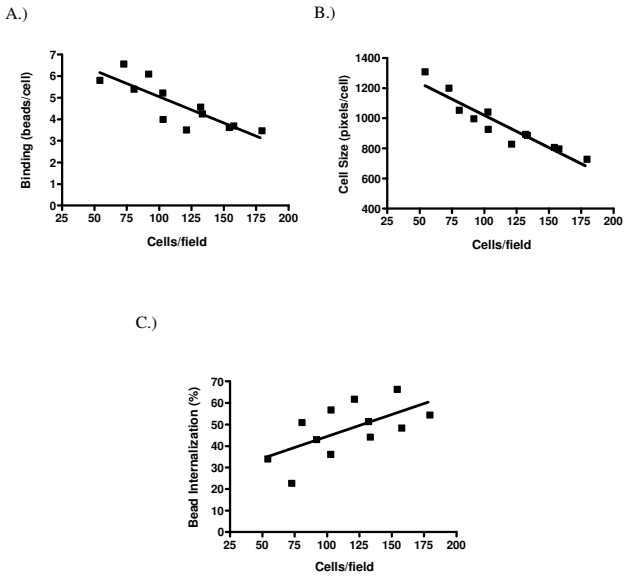

Figure 5
Bead binding and internalization are cell density dependent. GM-MØ were plated at 5 × 10^4 to 1.25 × 10^5 cells/well and cultured overnight before incubation with fluorescent latex beads. At the end of the experiment, cell density for each well was calculated as the average number of cells per field from three fields. Cells were analyzed for total bead binding (A), cell size (B) and bead internalization (C). Points represent the means of three wells each. Lines represent the best-fit linear regression. Data are pooled from three donors.

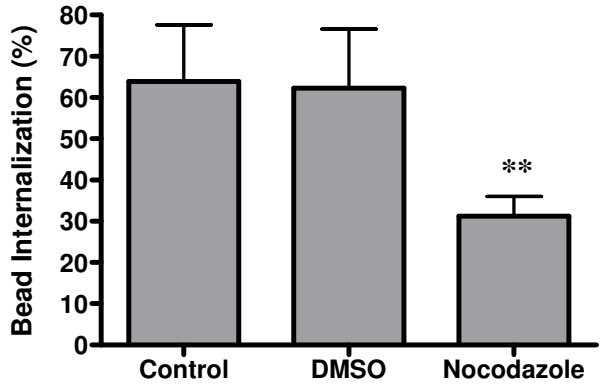

Figure 6
Microtubule destabilization inhibits SR mediated phagocytosis. Adherent GM-MØ were pretreated with nocodazole before incubation with fluorescent latex beads. Cells were analyzed for the percent internalization of bound beads. Bars represent the means of five donors +/- the standard deviation. For each donor, three fields from each of three replicate wells were analyzed. **p < 0.001 when compared to either the control or DMSO conditions.

itors on SR-mediated phagocytosis (Figures 7 and 8). Inhibition of PKC with staurosporine results in a significant reduction in the number of beads internalized. However, staurosporine is known to inhibit a number of other protein kinases in addition to PKC. In order to definitively show that PKC is required, the PKC specific inhibitors chelerythrine chloride and Gö 6976 were used. These inhibitors cause dramatic (77% and 86%, respectively) reductions in bead internalization. Similarly, treatment with the protein tyrosine kinase inhibitors genistein and herbimycin A result in a 51% and 64% reduction in internalization, respectively. These data show that PKC and tyrosine kinase activities are important for non-opsonic phagocytosis.

The MAPK family of protein kinases is critical for Fc receptor mediated phagocytosis as well as cell cycle progression and a number of other cytoskeletal processes. Since PKC and tyrosine kinases are known to stimulate MAPK [58], inhibitors of the JNK and ERK MAPK pathways were tested for their ability to inhibit SR-mediated phagocytosis. Inhibition of either of these MAPK pathways blocks internalization. The JNK inhibitor reduces bead internalization by 28% while the inactive analog used as a control does not cause a statistically significant reduction (Figure 9A). Inhibition of the ERK pathway was achieved using an inhibitor of the upstream kinase, MEK. Treatment with this inhibitor reduces phagocytosis by 42% when compared to DMSO control (Figure 9B).

In addition to the protein kinases mentioned above, the lipid modifying enzymes PI-3K and PLCγ have also been shown to play a role in MØ phagocytosis [57]. Therefore, the PI-3K inhibitors wortmannin and LY294002 and the PLCγ inhibitor U-73122 were used to block these enzymes before challenging GM-MØ with latex beads As shown in Figure 10A, wortmannin inhibits bead internalization by 59%, while LY294002 causes an even greater inhibition (78%) (Figure 10B). These data demonstrate that PI-3K is required for optimal SR-mediated phagocytosis. However, unlike PI-3K, PLCγ does not appear to be necessary, as U-73122 is unable to block internalization at the concentration tested (Figure 11).

Interestingly, while most of the inhibitors shown in Figures 7, 8, 9, 10, 11 block internalization, none of them have a significant effect on particle binding, cell size or the number of cells per field (data not shown). This indicates that SRs do not require PKC, tyrosine kinase, MAPK, PI-3K or PLCγ signaling to effectively bind unopsonized particles. In addition, the fact that cell size and number are unaffected by the inhibitors used demonstrates that these inhibitors did not affect cell viability. This is confirmed by

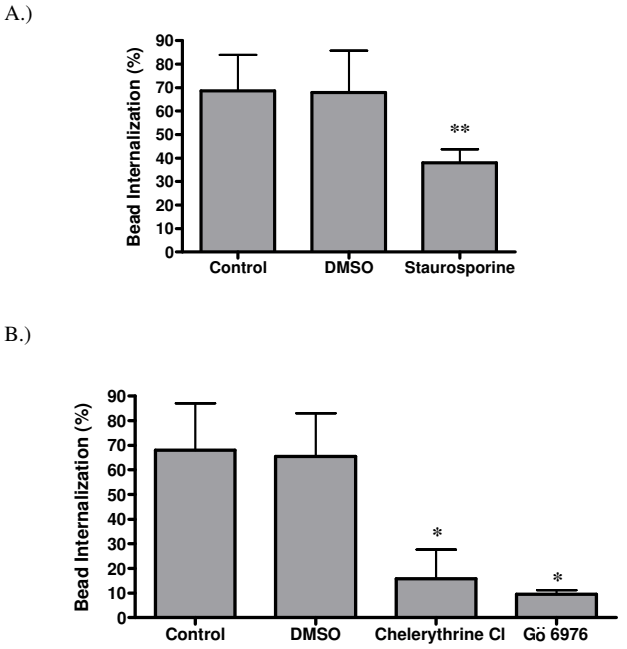

Figure 7
Protein kinase C blockers inhibit SR mediated phagocytosis. Adherent GM-MØ were pretreated with either staurosporine (A), chelerythryine chloride or Gö 6976 (B) before incubation with fluorescent latex beads. Cells were analyzed for the percent internalization of bound beads. Bars represent the means of five (A) or three (B) donors +/- the standard deviation. For each donor, three fields from each of three replicate wells were analyzed. *p < 0.01 and **p < 0.001 when compared to either the control or DMSO conditions.

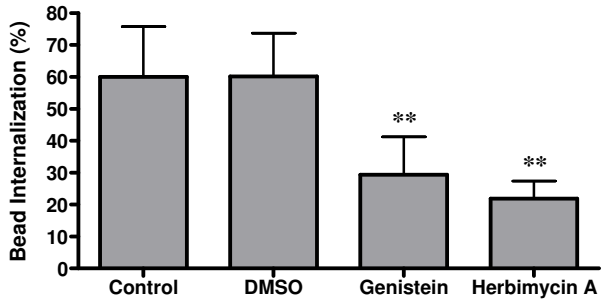

Figure 8
Protein tyrosine kinase blockers inhibit SR mediated phagocytosis. Adherent GM-MØ were pretreated with either genistein or herbimycin A before incubation with fluorescent latex beads. Cells were analyzed for the percent internalization of bound beads. Bars represent the means of at least four donors +/- the standard deviation. For each donor, three fields from each of three replicate wells were analyzed. **p < 0.001 when compared to either the control or DMSO conditions.

the observation that the inhibitors used do not alter cellular morphology or increase staining with propidium iodide (data not shown).

Discussion

While the ligand binding characteristics of SRs have been characterized [6], very little is known about the signaling pathways utilized during SR-mediated phagocytosis. In order to address this, we developed a high-throughput phagocytosis assay capable of distinguishing between internalized and non-internalized cell-associated particles. Using this assay, we tested a battery of signaling inhibitors that are known to block opsonin-mediated phagocytosis for their effect on opsonin-independent phagocytosis. We found that microtubules, PKC, tyrosine kinases, MAPKs and PI-3K are required for optimal SR-mediated phagocytosis. Furthermore, cell density has a significant impact on both particle binding and internalization.

As primary human AM are difficult to obtain in large quantities, we took advantage of a previously published *in vitro* human monocyte differentiation scheme that produces MØ that are phenotypically and physiologically similar to human AM. In order to confirm our findings, we tested a subset of inhibitors (genistein, herbimycin A, wortmannin, nocodazole and staurosporine) for their effect on bead phagocytosis by primary murine AMs. Every inhibitor tested significantly decreased bead internalization. This demonstrates that, at the very least, protein tyrosine kinases, PKC, PI-3K and microtubules are necessary for bead phagocytosis by primary murine AM. These findings are identical to those obtained using GM-MØ and further establish these cells as a useful model of primary AM.

Most currently available phagocytosis assays rely on subtracting the number of particles associated with cells in which internalization has been blocked from the number of particles associated with cells in which internalization has not been blocked. The agents used to block phagocytosis are typically cytoskeletal or mitochondrial poisons such as cytochalasin D or sodium azide (although incubation at low temperature has also been used) [59-61]. Built into these indirect techniques is the assumption that the agent used to block internalization is effective in the particular cells being studied, yet does not alter the number of bound extracellular beads.

In some cases (particularly for receptors of unopsonized targets), this assumption is erroneous, resulting in either an under- or overestimation of particle internalization.

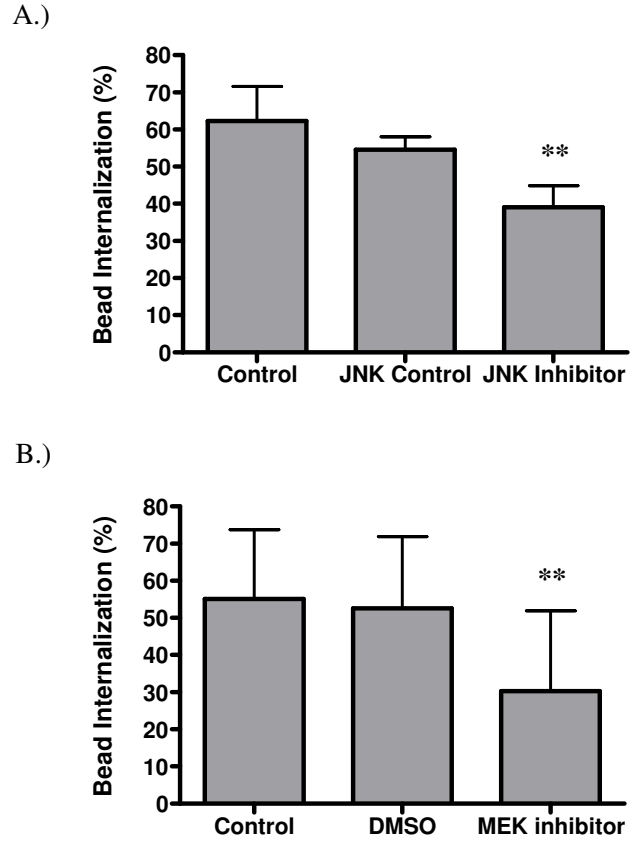

Figure 9
MAPK blockers inhibit SR mediated phagocytosis. Adherent GM-MØ were pretreated with inhibitors of either JNK (A) or MEK (B) before incubation with fluorescent latex beads. Cells were analyzed for the percent internalization of bound beads. Bars represent the means of five (A) or six (B) donors +/- the standard deviation. For each donor, three fields from each of three replicate wells were analyzed. **p < 0.001 when compared to either the control, JNK control or DMSO conditions.

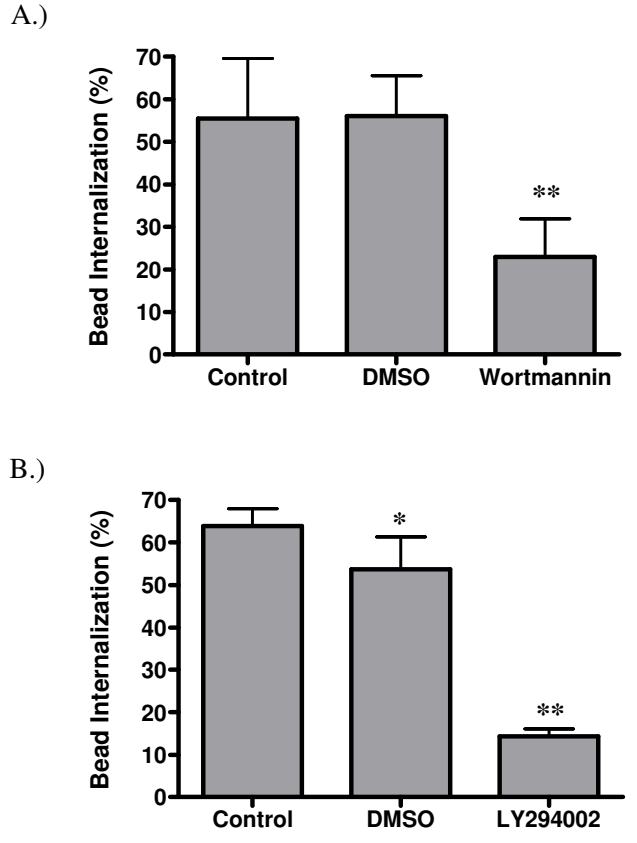

Figure 10
Effect of PI-3K inhibitors on SR mediated phagocytosis. Adherent GM-MØ were pretreated with wortmannin (A) or LY294002 (B) before being fed fluorescent latex beads. Cells were analyzed for the percent internalization of bound beads. Bars represent the means of five (A) or three (B) donors +/- the standard deviation. For each donor, three fields from each of three replicate wells were analyzed. **p < 0.001 when compared to either the control or DMSO conditions. *p < 0.05 when compared to the control condition.

For example, our two-color direct approach definitively demonstrates that cytochalasin D is an extremely effective blocker of phagocytosis in GM-MØ (Figure 3D). However, it does not alter the total number of cell-associated beads (Figure 3C). Since the total number of cell-associated beads is the sum of the internalized beads and the beads that have been bound but not internalized, these data indicate that cytochalasin D treatment *does indeed* alter the number of bound extracellular beads under our experimental conditions. In this case, using the indirect single-color technique would have led to a dramatic underestimation of bead internalization by the untreated cells. The opposite problem would have been encountered if a low temperature incubation had been used to block internalization. This is because, unlike opsonized particles, the binding of unopsonized beads is temperature dependent ([42] and our unpublished results).

Given the limitations of the indirect assays mentioned above, we chose to utilize a direct phagocytosis assay based on previously developed two-color fluorescence assays [62,42]. These assays use one intrinsic fluorescent dye to identify all particles and a second non-cell permeable stain applied after internalization to identify particles that have not been internalized. These techniques allow the investigator to distinguish between internalized and extracellular particles without relying on interventions that alter the biology of the cell. While these assays overcome the pitfalls of the indirect assays, they introduce new difficulties for data collection. For example, analysis by

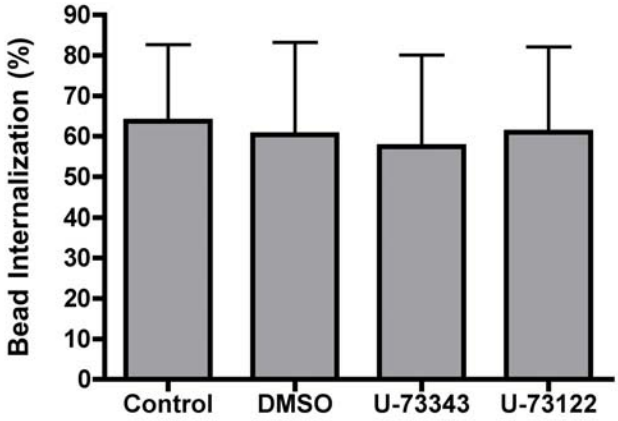

Figure 11
Effect of a PLCγ inhibitor on SR mediated phagocytosis. Adherent GM-MØ were pretreated with U-73122 or the inactive analog U-73343 before being fed fluorescent latex beads. Cells were analyzed for the percent internalization of bound beads. Bars represent the means of four donors +/- the standard deviation. For each donor, three fields from each of three replicate wells were analyzed.

flow cytometry can provide exact bead per cell counts for up to three (or perhaps four) cell-associated beads per cell. This is due to the high intensity and low bead-to-bead variability of the intrinsic fluorescent dye. However, at higher bead loads, the absolute number of beads per cell cannot be determined, as the fluorescent peaks begin to overlap [63]. Furthermore, the higher variability and lower intensity of staining with the extracellular dye precludes precise bead per cell counts at even very low bead loads (our unpublished data). As a result of these issues, results are typically reported as a ratio of fluorescence intensities (not absolute bead number) when flow cytometry is used as a read out. The alternative to flow cytometry (counting beads by eye using a fluorescent microscope) is tedious and incompatible with high throughput.

In order to overcome these limitations, we developed a system using scanning cytometer technology that can automatically count the number of beads associated with any given cell and distinguish between internalized and extracellular beads. This system allows the investigator to express his or her data as the number of beads per cell and not simply as fluorescence intensity, even for cells with high bead loads. While this assay is similar in many respects to one recently developed by Steinberg and colleagues for analysis of opsonized phagocytosis [64], it differs in that our method involves collecting a set of confocal images spanning the entire thickness of the cell that are then collapsed into a single image for analysis. This technique allows all of the cell-associated beads to be in focus for the final analysis. In contrast, we have found that using conventional fluorescence microscopy does not allow all of the cell-associated beads to remain in focus simultaneously and therefore excludes some beads from analysis (data not shown).

The confocal-based phagocytosis assay described in this report was used to test the hypothesis that SR-mediated phagocytosis is similar to complement-mediated phagocytosis in respect to its sensitivity to a microtubule inhibitor. Phagocytosis of opsonized particles by Fc or complement receptors share a number of characteristics, including dependence on actin filaments and the accumulation of signaling and actin binding proteins at the site of the forming phagosome [56]. However, fundamental differences exist between these two modes of phagocytosis [65,66,55,67,68]. These differences have led some to characterize them as type I (Fc receptor-mediated) and type II (complement receptor-mediated). Microtubule poisons such as nocodazole paralyze complement-mediated, but not Fc receptor-mediated, particle internalization [55,30]. In this report we present the first evidence that SR-mediated phagocytosis exhibits a characteristic of type II phagocytosis in that nocodazole significantly inhibits internalization.

This report is also the first to show that tyrosine kinases, PKC, PI-3K and MAPKs are necessary for SR-mediated phagocytosis by MØ. The requirement for PI-3K and tyrosine kinases is consistent with a recent report showing that PI-3K and the Src kinase Lyn are both required for SR-A-mediated MØ spreading [69]. Furthermore, treatment of MØ cell lines with soluble SR ligands results in the tyrosine phosphorylation of Src kinases, PLCγ and PI-3K as well as a tyrosine kinase dependant activation of PKC [34,33,31,32], suggesting that tyrosine kinase activation may occur relatively early in the SR signaling cascade. Consistent with the inhibition of phagocytosis reported here, inhibition of tyrosine kinases blocks the induction of urokinase-type plasminogen activator (uPA) and IL-1 expression by THP-1 cells in response to SR ligands [31,32]. Similarly, pharmacological blockade of PKC inhibits SR-mediated increases in uPA expression, myelin endocytosis, prostaglandin E2 release and ERK activation [32,36,35].

It is surprising to note that the PLCγ inhibitor U-73122 does not affect bead internalization, as U-71322 has previously been shown to inhibit myelin endocytosis by CR3$^{-/-}$ microglia [35] and PKC activation in response to oxidized LDL (oxLDL) [33]. However, the experimental conditions in these reports differ greatly from those described here as the authors use either primary murine microglia or LPS primed P388D$_1$ cells. The signaling pathways and receptors utilized by these murine cells could be quite different from those utilized by our primary unprimed

human GM-MØ. Furthermore, while PLCγ is an important activator of conventional PKC, atypical PLCγ-independent PKC isoenzymes have been shown to be important in a number of immune cell functions [70]. Our finding that PKC blockers inhibit internalization, but a PLCγ blocker does not, raises the possibility that GM-MØ utilize atypical PKC isoenzymes as second messenger signals for SR-mediated phagocytosis. While this has yet to be formally demonstrated, it is supported by our finding that an inhibitor of the atypical PKC isoenzyme activator PI-3K [70] blocks internalization.

Finally, the MAPK family of proteins are known to play an important role in MØ phagocytosis and have been implicated as downstream signaling molecules for SRs. Stimulation of SRs with fucoidan, oxLDL or poly(I) results in the activation of JNK and ERK MAPK pathways [37,31,38]. Furthermore, Lamprou and colleagues reported that inhibition of these pathways results in a reduction of latex bead internalization by medfly hemocytes [71,72]. The results of our experiments are consistent with these reports in that the inhibition of JNK and ERK pathways results in a reduction of bead internalization. This suggests that some of the pathways utilized during SR-mediated phagocytosis are conserved across a broad spectrum of species.

It is important to note that none of the signaling inhibitors tested in this report had any measurable effect on cell viability, size, density or bead binding. It is known that SR-A-mediated acetylated low density lipoprotein binding and cell adhesion require G proteins [73,74]. This, combined with the previous observation that particle binding by SRs is highly temperature dependent, suggests that it contains an active component. However, our data suggests that this active binding mechanism does not require actin filaments, microtubules, PKC, PI-3K, tyrosine kinases, MAPKs or PLCγ even though many of these pathways are necessary for internalization. Our finding that cytochalasin D has no effect on bead binding stands in contrast to the report of Post, *et al.* in which cytochalasin D was shown to inhibit SR-A-mediated cell attachment by 35% [73]. This discrepancy may reflect the differences between the cytoskeletal requirements for particle binding vs. firm anchorage to a substrate.

Conclusion

We have developed a novel high-throughput assay for particle phagocytosis that we used to test the signaling pathways and cytoskeletal components required for unopsonized phagocytosis by human monocyte-derived MØ. We found that filamentous actin, microtubules, PKC, tyrosine kinases, PI-3K, MEK and JNK are required for optimal particle internalization while an inhibitor of PLCγ has no effect.

Competing interests

The authors declare that they have no competing interests.

Authors' contributions

THS conceived and designed the experiments, generated the biotin-conjugated beads and authored the manuscript. AI participated in experimental design and manuscript authoring and carried out the binding and phagocytosis assays. GD developed the custom data analysis software and participated in manuscript authoring. ARW generated the GM-MØ protocol and participated in manuscript revision. LK contributed to the conception and design of the experiments and played a significant role in the revision of the manuscript. All authors read and approved the final manuscript.

Acknowledgements

The authors would like to thank Jean Lai for her assistance with scanning cytometry. This study was supported by grants from the National Institutes of Health (P30ES000002, R01ES011008, S10RR021132, R01ES011903 and F32ES013689).

References

1. Mizgerd JP: **Lung infection--a public health priority.** *PLoS Med* 2006, **3(2):**e76.
2. Abbey DE, Nishino N, McDonnell WF, Burchette RJ, Knutsen SF, Lawrence Beeson W, Yang JX: **Long-term inhalable particles and other air pollutants related to mortality in nonsmokers.** *Am J Respir Crit Care Med* 1999, **159(2):**373-382.
3. Pope CA, Burnett RT, Thun MJ, Calle EE, Krewski D, Ito K, Thurston GD: **Lung cancer, cardiopulmonary mortality, and long-term exposure to fine particulate air pollution.** *JAMA* 2002, **287(9):**1132-1141.
4. Dockery DW, Pope CA, Xu X, Spengler JD, Ware JH, Fay ME, Ferris BG Jr., Speizer FE: **An association between air pollution and mortality in six U.S. cities.** *N Engl J Med* 1993, **329(24):**1753-1759.
5. Heinrich J: **Nonallergic respiratory morbidity improved along with a decline of traditional air pollution levels: a review.** *Eur Respir J Suppl* 2003, **40:**64s-69s.
6. Peiser L, Mukhopadhyay S, Gordon S: **Scavenger receptors in innate immunity.** *Curr Opin Immunol* 2002, **14(1):**123-128.
7. Palecanda A, Kobzik L: **Receptors for unopsonized particles: the role of alveolar macrophage scavenger receptors.** *Curr Mol Med* 2001, **1(5):**589-595.
8. Goldsmith CA, Frevert C, Imrich A, Sioutas C, Kobzik L: **Alveolar macrophage interaction with air pollution particulates.** *Environ Health Perspect* 1997, **105 Suppl 5:**1191-1195.
9. Kobzik L: **Lung macrophage uptake of unopsonized environmental particulates. Role of scavenger-type receptors.** *J Immunol* 1995, **155(1):**367-376.
10. Arredouani MS, Palecanda A, Koziel H, Huang YC, Imrich A, Sulahian TH, Ning YY, Yang Z, Pikkarainen T, Sankala M, Vargas SO, Takeya M, Tryggvason K, Kobzik L: **MARCO is the major binding receptor for unopsonized particles and bacteria on human alveolar macrophages.** *J Immunol* 2005, **175(9):**6058-6064.
11. Iyer R, Hamilton RF, Li L, Holian A: **Silica-induced apoptosis mediated via scavenger receptor in human alveolar macrophages.** *Toxicol Appl Pharmacol* 1996, **141(1):**84-92.
12. Dunne DW, Resnick D, Greenberg J, Krieger M, Joiner KA: **The type I macrophage scavenger receptor binds to gram-positive bacteria and recognizes lipoteichoic acid.** *Proc Natl Acad Sci U S A* 1994, **91(5):**1863-1867.
13. Hampton RY, Golenbock DT, Penman M, Krieger M, Raetz CR: **Recognition and plasma clearance of endotoxin by scavenger receptors.** *Nature* 1991, **352(6333):**342-344.
14. Peiser L, De Winther MP, Makepeace K, Hollinshead M, Coull P, Plested J, Kodama T, Moxon ER, Gordon S: **The class A macro-**

phage scavenger receptor is a major pattern recognition receptor for Neisseria meningitidis which is independent of lipopolysaccharide and not required for secretory responses. *Infect Immun* 2002, **70(10):**5346-5354.
15. Peiser L, Gough PJ, Kodama T, Gordon S: **Macrophage class A scavenger receptor-mediated phagocytosis of Escherichia coli: role of cell heterogeneity, microbial strain, and culture conditions *in vitro*.** *Infect Immun* 2000, **68(4):**1953-1963.
16. Thomas CA, Li Y, Kodama T, Suzuki H, Silverstein SC, El Khoury J: **Protection from lethal gram-positive infection by macrophage scavenger receptor-dependent phagocytosis.** *J Exp Med* 2000, **191(1):**147-156.
17. Elshourbagy NA, Li X, Terrett J, Vanhorn S, Gross MS, Adamou JE, Anderson KM, Webb CL, Lysko PG: **Molecular characterization of a human scavenger receptor, human MARCO.** *Eur J Biochem* 2000, **267(3):**919-926.
18. Mukhopadhyay S, Chen Y, Sankala M, Peiser L, Pikkarainen T, Kraal G, Tryggvason K, Gordon S: **MARCO, an innate activation marker of macrophages, is a class A scavenger receptor for Neisseria meningitidis.** *Eur J Immunol* 2006, **36(4):**940-949.
19. van der Laan LJ, Dopp EA, Haworth R, Pikkarainen T, Kangas M, Elomaa O, Dijkstra CD, Gordon S, Tryggvason K, Kraal G: **Regulation and functional involvement of macrophage scavenger receptor MARCO in clearance of bacteria *in vivo*.** *J Immunol* 1999, **162(2):**939-947.
20. van der Laan LJ, Kangas M, Dopp EA, Broug-Holub E, Elomaa O, Tryggvason K, Kraal G: **Macrophage scavenger receptor MARCO: *in vitro* and *in vivo* regulation and involvement in the antibacterial host defense.** *Immunol Lett* 1997, **57(1-3):**203-208.
21. Peiser L, Makepeace K, Pluddemann A, Savino S, Wright JC, Pizza M, Rappuoli R, Moxon ER, Gordon S: **Identification of Neisseria meningitidis nonlipopolysaccharide ligands for class A macrophage scavenger receptor by using a novel assay.** *Infect Immun* 2006, **74(9):**5191-5199.
22. Arredouani M, Yang Z, Ning Y, Qin G, Soininen R, Tryggvason K, Kobzik L: **The scavenger receptor MARCO is required for lung defense against pneumococcal pneumonia and inhaled particles.** *J Exp Med* 2004, **200(2):**267-272.
23. Jozefowski S, Sulahian TH, Arredouani M, Kobzik L: **Role of scavenger receptor MARCO in macrophage responses to CpG oligodeoxynucleotides.** *J Leukoc Biol* 2006, **80(4):**870-879.
24. Hamilton RF, Thakur SA, Mayfair JK, Holian A: **MARCO mediates silica uptake and toxicity in alveolar macrophages from C57BL/6 mice.** *J Biol Chem* 2006, **281(45):**34218-34226.
25. Palecanda A, Paulauskis J, Al-Mutairi E, Imrich A, Qin G, Suzuki H, Kodama T, Tryggvason K, Koziel H, Kobzik L: **Role of the scavenger receptor MARCO in alveolar macrophage binding of unopsonized environmental particles.** *J Exp Med* 1999, **189(9):**1497-1506.
26. Nakamura K, Funakoshi H, Miyamoto K, Tokunaga F, Nakamura T: **Molecular cloning and functional characterization of a human scavenger receptor with C-type lectin (SRCL), a novel member of a scavenger receptor family.** *Biochem Biophys Res Commun* 2001, **280(4):**1028-1035.
27. Shimaoka T, Kume N, Minami M, Hayashida K, Sawamura T, Kita T, Yonehara S: **LOX-1 supports adhesion of Gram-positive and Gram-negative bacteria.** *J Immunol* 2001, **166(8):**5108-5114.
28. Shimaoka T, Nakayama T, Kume N, Takahashi S, Yamaguchi J, Minami M, Hayashida K, Kita T, Ohsumi J, Yoshie O, Yonehara S: **SR-PSOX/CXC chemokine ligand 16 mediates bacterial phagocytosis by APCs through its chemokine domain.** *J Immunol* 2003, **171(4):**1647-1651.
29. García-García E, Rosales C: **Signal transduction during Fc receptor-mediated phagocytosis.** *J Leukoc Biol* 2002, **72(6):**1092-1108.
30. Newman SL, Mikus LK, Tucci MA: **Differential requirements for cellular cytoskeleton in human macrophage complement receptor- and Fc receptor-mediated phagocytosis.** *J Immunol* 1991, **146(3):**967-974.
31. Hsu HY, Chiu SL, Wen MH, Chen KY, Hua KF: **Ligands of macrophage scavenger receptor induce cytokine expression via differential modulation of protein kinase signaling pathways.** *J Biol Chem* 2001, **276(31):**28719-28730.
32. Hsu HY, Hajjar DP, Khan KM, Falcone DJ: **Ligand binding to macrophage scavenger receptor-A induces urokinase-type plasminogen activator expression by a protein kinase-dependent signaling pathway.** *J Biol Chem* 1998, **273(2):**1240-1246.
33. Claus R, Fyrnys B, Deigner HP, Wolf G: **Oxidized low-density lipoprotein stimulates protein kinase C (PKC) and induces expression of PKC-isotypes via prostaglandin-H-synthase in P388D1 macrophage-like cells.** *Biochemistry* 1996, **35(15):**4911-4922.
34. Miki S, Tsukada S, Nakamura Y, Aimoto S, Hojo H, Sato B, Yamamoto M, Miki Y: **Functional and possible physical association of scavenger receptor with cytoplasmic tyrosine kinase Lyn in monocytic THP-1-derived macrophages.** *FEBS Lett* 1996, **399(3):**241-244.
35. Cohen G, Makranz C, Spira M, Kodama T, Reichert F, Rotshenker S: **Non-PKC DAG/phorbol-ester receptor(s) inhibit complement receptor-3 and nPKC inhibit scavenger receptor-AI/II-mediated myelin phagocytosis but cPKC, PI3k, and PLCgamma activate myelin phagocytosis by both.** *Glia* 2006, **53(5):**538-550.
36. Falcone DJ, McCaffrey TA, Vergilio JA: **Stimulation of macrophage urokinase expression by polyanions is protein kinase C-dependent and requires protein and RNA synthesis.** *J Biol Chem* 1991, **266(33):**22726-22732.
37. Campa VM, Iglesias JM, Carcedo MT, Rodriguez R, Riera J, Ramos S, Lazo PS: **Polyinosinic acid induces TNF and NO production as well as NF-kappaB and AP-1 transcriptional activation in the monocytemacrophage cell line RAW 264.7.** *Inflamm Res* 2005, **54(8):**328-337.
38. Ricci R, Sumara G, Sumara I, Rozenberg I, Kurrer M, Akhmedov A, Hersberger M, Eriksson U, Eberli FR, Becher B, Boren J, Chen M, Cybulsky MI, Moore KJ, Freeman MW, Wagner EF, Matter CM, Luscher TF: **Requirement of JNK2 for scavenger receptor A-mediated foam cell formation in atherogenesis.** *Science* 2004, **306(5701):**1558-1561.
39. Kenoyer JL, Phalen RF, Davis JR: **Particle clearance from the respiratory tract as a test of toxicity: effect of ozone on short and long term clearance.** *Exp Lung Res* 1981/05/01 edition. 1981, **2(2):**111-120.
40. Lehnert BE, Tech C: **Quantitative evaluation of opsonin-independent phagocytosis by alveolar macrophages in monolayer using polystyrene microspheres.** *J Immunol Methods* 1985/04/22 edition. 1985, **78(2):**337-344.
41. Lehnert BE, Valdez YE, Bomalaski SH: **Lung and pleural "free-cell responses" to the intrapulmonary deposition of particles in the rat.** *J Toxicol Environ Health* 1985/01/01 edition. 1985, **16(6):**823-839.
42. Parod RJ, Brain JD: **Immune opsonin-independent phagocytosis by pulmonary macrophages.** *J Immunol* 1986, **136(6):**2041-2047.
43. Akagawa KS, Kamoshita K, Tokunaga T: **Effects of granulocyte-macrophage colony-stimulating factor and colony-stimulating factor-1 on the proliferation and differentiation of murine alveolar macrophages.** *J Immunol* 1988, **141(10):**3383-3390.
44. Dranoff G, Crawford AD, Sadelain M, Ream B, Rashid A, Bronson RT, Dickersin GR, Bachurski CJ, Mark EL, Whitsett JA, Mulligan RC: **Involvement of granulocyte-macrophage colony-stimulating factor in pulmonary homeostasis.** *Science* 1994, **264(5159):**713-716.
45. Robb L, Drinkwater CC, Metcalf D, Li R, Kontgen F, Nicola NA, Begley CG: **Hematopoietic and lung abnormalities in mice with a null mutation of the common beta subunit of the receptors for granulocyte-macrophage colony-stimulating factor and interleukins 3 and 5.** *Proc Natl Acad Sci U S A* 1995, **92(21):**9565-9569.
46. Witmer-Pack MD, Hughes DA, Schuler G, Lawson L, McWilliam A, Inaba K, Steinman RM, Gordon S: **Identification of macrophages and dendritic cells in the osteopetrotic (op/op) mouse.** *J Cell Sci* 1993, **104 (Pt 4):**1021-1029.
47. Zsengeller ZK, Reed JA, Bachurski CJ, LeVine AM, Forry-Schaudies S, Hirsch R, Whitsett JA: **Adenovirus-mediated granulocyte-macrophage colony-stimulating factor improves lung pathology of pulmonary alveolar proteinosis in granulocyte-macrophage colony-stimulating factor-deficient mice.** *Hum Gene Ther* 1998, **9(14):**2101-2109.
48. Akagawa KS: **Functional heterogeneity of colony-stimulating factor-induced human monocyte-derived macrophages.** *Int J Hematol* 2002, **76(1):**27-34.
49. Akagawa KS, Komuro I, Kanazawa H, Yamazaki T, Mochida K, Kishi F: **Functional heterogeneity of colony-stimulating factor-**

induced human monocyte-derived macrophages. *Respirology* 2006, **11 Suppl:**S32-6.
50. Granucci F, Petralia F, Urbano M, Citterio S, Di Tota F, Santambrogio L, Ricciardi-Castagnoli P: **The scavenger receptor MARCO mediates cytoskeleton rearrangements in dendritic cells and microglia.** *Blood* 2003, **102(8):**2940-2947.
51. Jozefowski S, Arredouani M, Sulahian T, Kobzik L: **Disparate regulation and function of the class A scavenger receptors SR-AI/II and MARCO.** *J Immunol* 2005, **175(12):**8032-8041.
52. Re F, Belyanskaya SL, Riese RJ, Cipriani B, Fischer FR, Granucci F, Ricciardi-Castagnoli P, Brosnan C, Stern LJ, Strominger JL, Santambrogio L: **Granulocyte-macrophage colony-stimulating factor induces an expression program in neonatal microglia that primes them for antigen presentation.** *J Immunol* 2002, **169(5):**2264-2273.
53. Stanton LA, Fenhalls G, Lucas A, Gough P, Greaves DR, Mahoney JA, Helden P, Gordon S: **Immunophenotyping of macrophages in human pulmonary tuberculosis and sarcoidosis.** *Int J Exp Pathol* 2003, **84(6):**289-304.
54. Tomokiyo R, Jinnouchi K, Honda M, Wada Y, Hanada N, Hiraoka T, Suzuki H, Kodama T, Takahashi K, Takeya M: **Production, characterization, and interspecies reactivities of monoclonal antibodies against human class A macrophage scavenger receptors.** *Atherosclerosis* 2002, **161(1):**123-132.
55. Allen LA, Aderem A: **Molecular definition of distinct cytoskeletal structures involved in complement- and Fc receptor-mediated phagocytosis in macrophages.** *J Exp Med* 1996, **184(2):**627-637.
56. Aderem A, Underhill DM: **Mechanisms of phagocytosis in macrophages.** *Annu Rev Immunol* 1999, **17:**593-623.
57. Swanson JA, Hoppe AD: **The coordination of signaling during Fc receptor-mediated phagocytosis.** *J Leukoc Biol* 2004, **76(6):**1093-1103.
58. Liebmann C: **Regulation of MAP kinase activity by peptide receptor signalling pathway: paradigms of multiplicity.** *Cell Signal* 2001, **13(11):**777-785.
59. Oda T, Maeda H: **A new simple fluorometric assay for phagocytosis.** *J Immunol Methods* 1986, **88(2):**175-183.
60. Steinkamp JA, Wilson JS, Saunders GC, Stewart CC: **Phagocytosis: flow cytometric quantitation with fluorescent microspheres.** *Science* 1982, **215(4528):**64-66.
61. Santos JL, Montes MJ, Gutierrez F, Ruiz C: **Evaluation of phagocytic capacity with a modified flow cytometry technique.** *Immunol Lett* 1995, **45(1-2):**1-4.
62. Ogle JD, Noel JG, Sramkoski RM, Ogle CK, Alexander JW: **Phagocytosis of opsonized fluorescent microspheres by human neutrophils. A two-color flow cytometric method for the determination of attachment and ingestion.** *J Immunol Methods* 1988, **115(1):**17-29.
63. Rassias AJ, Givan AL, Marrin CA, Whalen K, Pahl J, Yeager MP: **Insulin increases neutrophil count and phagocytic capacity after cardiac surgery.** *Anesth Analg* 2002, **94(5):**1113-9, table of contents.
64. Steinberg BE, Scott CC, Grinstein S: **High-throughput assays of phagocytosis, phagosome maturation, and bacterial invasion.** *Am J Physiol Cell Physiol* 2007, **292(2):**C945-52.
65. Caron E, Hall A: **Identification of two distinct mechanisms of phagocytosis controlled by different Rho GTPases.** *Science* 1998, **282(5394):**1717-1721.
66. Hall AB, Gakidis MA, Glogauer M, Wilsbacher JL, Gao S, Swat W, Brugge JS: **Requirements for Vav guanine nucleotide exchange factors and Rho GTPases in FcgammaR- and complement-mediated phagocytosis.** *Immunity* 2006, **24(3):**305-316.
67. May RC, Caron E, Hall A, Machesky LM: **Involvement of the Arp2/3 complex in phagocytosis mediated by FcgammaR or CR3.** *Nat Cell Biol* 2000, **2(4):**246-248.
68. Olazabal IM, Caron E, May RC, Schilling K, Knecht DA, Machesky LM: **Rho-kinase and myosin-II control phagocytic cup formation during CR, but not FcgammaR, phagocytosis.** *Curr Biol* 2002, **12(16):**1413-1418.
69. Nikolic DM, Cholewa J, Gass C, Gong MC, Post SR: **Class A scavenger receptor-mediated cell adhesion requires the sequential activation of Lyn and PI3-kinase.** *Am J Physiol Cell Physiol* 2007, **292(4):**C1450-8.
70. Tan SL, Parker PJ: **Emerging and diverse roles of protein kinase C in immune cell signalling.** *Biochem J* 2003, **376(Pt 3):**545-552.
71. Lamprou I, Tsakas S, Theodorou GL, Karakantza M, Lampropoulou M, Marmaras VJ: **Uptake of LPS/*E. coli*/latex beads via distinct signalling pathways in medfly hemocytes: the role of MAP kinases activation and protein secretion.** *Biochim Biophys Acta* 2005, **1744(1):**1-10.
72. Lamprou I, Mamali I, Dallas K, Fertakis V, Lampropoulou M, Marmaras VJ: **Distinct signalling pathways promote phagocytosis of bacteria, latex beads and lipopolysaccharide in medfly haemocytes.** *Immunology* 2007, **121(3):**314-327.
73. Post SR, Gass C, Rice S, Nikolic D, Crump H, Post GR: **Class A scavenger receptors mediate cell adhesion via activation of G(i/o) and formation of focal adhesion complexes.** *J Lipid Res* 2002, **43(11):**1829-1836.
74. Whitman SC, Daugherty A, Post SR: **Regulation of acetylated low density lipoprotein uptake in macrophages by pertussis toxin-sensitive G proteins.** *J Lipid Res* 2000, **41(5):**807-813.